Submarine mass wasting processes along the continental slope of the Middle America Trench

DISSERTATION

ZUR ERLANGUNG DES DOKTORGRADES AN DER
MATHEMATISCH-NATURWISSENSCHAFTLICHEN FAKULTÄT
DER CHRISTIAN-ALBRECHTS- UNVIVERSITÄT

vorgelegt von

Rieka Karoline Harders

Kiel, 2011

Referent**:**	Prof. Dr. Jan Hinrich Behrmann
Korreferent:	Prof. Dr. Christian Berndt
	Dr. Ingo Grevemeyer
Tag der mündlichen Prüfung:	4.10.2011
Zum Druck genehmigt:	
	Der Dekan

Hiermit erkläre ich an Eides statt, dass ich die vorliegende Doktorarbeit selbständig erstellt und keine weiteren als die angegebenen Hilfsmittel verwendet habe. Des Weiteren habe ich weder diese noch eine ähnliche Arbeit an anderer statt im Rahmen eines Prüfungsverfahrens vorgelegt, veröffentlicht oder zur Veröffentlichung eingereicht.

Abstract

This Thesis work presents a regional-scale study of submarine mass-wasting phenomena of the continental slope of a subduction zone. The nature of the study makes it a new, outstanding contribution for two main reasons: 1) The large-scale and interdisciplinary characters of the study conform a comprehensive investigation - unmatched by any other previous study- of land sliding processes along the slope of a tectonically-active convergent margin. 2) The investigation is also unique because it looks into the processes at a subduction zone dominated by tectonic erosion. This type of geological setting represents about 50% of the world subduction zone systems, but it has been overlooked in previous studies of mass wasting processes.

The study region is located along a segment of the Middle America Trench (MAT) that extends about 1500 km from the Costa Rica - Panama border to the Guatemala - Mexico boundary. The study investigates the structures of the continental slope of the Pacific-Ocean-side of Central America and the trench-region of the incoming oceanic Cocos plate. We have investigated the distribution of submarine slope failures and their deposits, the type of failures, and their seafloor morphology. We have also investigated possible preconditioning and triggering mechanisms, and the relationship of those mechanisms and the variability in failure type to the tectonic processes of this particular geological setting. Finally, we have made some inferences of the significance of mass wasting processes in the long-term evolution of the slope, compared to other geological settings.

The Central America subduction zone has been the locus of intense, continued geo-scientific investigation since the late 1970s that culminated with the selection of the region as the focus site for the US-Margins program and the German SFB574 during the first decade of the 21st century. Those two programs included research in a broad range of topics that attempted to advance our understanding of the entire subduction zone system. As a result numerous projects from both communities have benefited from close collaborations. This PhD work is integrated within the research project SFB 574, financed by the DFG, that has as main research goal investigations on “Volatiles and fluids in subduction zones and their impact on climate feedback and trigger mechanisms for natural disasters”.

We have analyzed a database containing a compilation of multibeam bathymetry of 7 research cruises, 3 cruises of side-scan sonar imagery and core samples of a dedicated

cruise. The database has been assembled in a collaborative effort between both US-Margins and SFB 574 communities.

Based on seafloor morphology and backscatter imagery, and seismic images we have mapped and classified 147 submarine slope failures in the region. Slope failures vary in their type, abundance and distribution along and across the slope to define six distinct segments along the MAT. The lateral extent of the six segments correlates well with similar along-trench segmentation in the character of the incoming ocean plate, expressed as changes in its relief, age and crustal thickness.

We have also found that the six along-margin segments display changes in the across-slope structuring of the different geological elements, including changes in the morphological expression of upper, middle and lower slope, total slope width, and slope dip angle. This structuring of the elements of the slope appears to be related to a long-term evolution caused by the tectonic processes associated to subduction erosion.

One segment covers the area of under-thrusting of Cocos Ridge under the shelf-slope offshore Osa Peninsula (southern Costa Rica). Here, 1-km-high narrow, sharp ridges and small conical seamounts festooning Cocos Ridge cause slumps often with rock and debris avalanches from a short, steep continental slope. A second segment occurs offshore central Costa Rica, where large conical seamounts and ridges of 1-3 km high and 40 km wide under-thrust the continental slope causing large re-entries of the slope toe, and furrows across the slope formed by collapse, of previously uplifted upper plate, along steep headwalls behind the under-thrusting seamounts. Failures have generated large slumps, debris flows and rock avalanches containing blocks up to 500 m in diameter. In contrast at a third segment in northern Costa Rica, offshore the North Nicoya Peninsula, a smooth incoming plate is parallel opposite by a continental slope lacking relevant mass wasting structures. The contiguous fourth segment offshore Nicaragua displays a steep middle slope with large translational slides opposite an ocean plate with numerous 1-km-tall seamounts and 100s-meter-high horst and graben relief. Under the fifth segment, offshore El Salvador, subducts a well developed horst and graben relief, but somewhat surprising the segment displays a generally failure-free slope, and only the uppermost slope displays a series of small translation slides The plate under-thrusting the sixth segment offshore Guatemala is similarly characterized by a horst and graben terrain. However, here a steeper slope exhibits frequent, small-scale failures, a few km wide, across the entire segment.

We conclude that the distribution and type of mass wasting phenomena is modulated by the interaction of long-term tectonics that precondition the slope with a shorter-term scale due to the local activity of morphological features on the under-thrusting oceanic plate. The slope sediment appears to be fairly similar along the region and do not seem to play a role in the segmentation. We acknowledge that other factors not analyzed in this work, like changes in earthquake character or intensity among segments could play an unforeseen role in the mass wasting. We however propose that the type of earthquakes available in historical records appear to occur at a considerably shorter recurrence time than the development of failures detectable with our data. To evaluate potential preconditioning or trigger mechanisms for translational sliding we carried out a series of sedimentological and geotechnical analyses on specific core samples collected at and near slides to obtain index properties of the sediment and to test mechanical behaviors of distinct layers. We inspected in detail the lithology and sediment properties of a gravity core that penetrated through the detachment plane of a translational slide. The analyses showed an anomalous density, pore water alkalinity, and shear strength profile at and below a few-centimeters-thick volcanic tephra layer, which indicates that the ash layer acted as slide plane. The tephra was correlated to the San Antonio tephra (SAT), erupted 6000 years ago from Masaya-Caldera (Nicaragua) and sampled in several other cores along the MAT. Grain size analysis and layer thickness comparisons with other sites indicated the removal of 80-95% of the layer during sliding. Direct shear test experiments on the SAT and on other ash samples from Middle American showed a surprisingly high volume reduction during shearing. Grain size distribution curve-estimations revealed that the SAT is highly hydraulic conductive with values between 10^{-4} and 10^{-5}. These results indicated that tephra layers might be able to significantly reduce their volume under undrained conditions and become a weak layer for sliding. This mechanism implies a build up of high pore pressures between marine clays and within a tephra layer to reduce the effective stress and promote failure.

We speculate that qualitatively important mass wasting processes have contributed in an essential manner to define the evolution of the slope region of the MAT. From this work we conclude that the fundamental influence of mass wasting processes on the long-term continental slope evolution at subduction erosive margins has been previously overlooked.

Kurzfassung

Die vorliegende Doktorarbeit stellt eine Studie regionaler Größenordnung über submarine Massenumlagerungserscheinungen am Kontinentalhang einer Subduktionszone dar. Die besondere Beschaffenheit der Arbeit macht sie aus zweierlei Gründen zu einem neuen und herausragenden Beitrag 1.) Die mit interdisziplinärem Charakter und in großem Rahmen angelegte Studie fügt sich zu einer umfassenden Untersuchung von Rutschungsprozessen entlang des Hanges eines tektonisch aktiven Kontinentalrandes zusammen, an dem zuvor noch keine vergleichbaren Hangrutschungsarbeiten vorgenommen wurden. 2.) Die Untersuchung ist außerdem einzigartig, weil sie die Prozesse innerhalb einer von tektonischer Erosion dominierten Subduktionszone beleuchtet. Dieser besondere geologische Schauplatz repräsentiert etwa 50% der Subduktionszonen weltweit, aber er wurde als solcher in Bezug auf submarine Rutschungen in vorausgegangenen Arbeiten übersehen.

Die Studienregion liegt entlang eines Teils des Mittelamerikanischen Grabens. Das Arbeitsgebiet beläuft sich auf eine Ausdehnung von etwa 1500 km und erstreckt sich von der Grenze zwischen Costa Rica und Panama bis zur Grenze zwischen Guatemala und Mexiko. Die Arbeit untersucht auf der pazifischen Ozeanseite vor Zentral Amerika die Struktur des Kontinentalhanges in der Grabenregion und die Beziehungen zu den morphologischen Elementen der eingehenden ozeanischen Cocos Platte. Es wurde die Verteilung von submarinen Rutschungen am Kontinentalhang sowie die Rutschungsablagerungen in der gesamten Grabenregion untersucht. Der Hangversagungstyp wurde spezifiziert und die oberflächliche Meeresbodenmorphologie des Hanges sowie der eingehenden ozeanischen Platte untersucht. Außerdem wurden mögliche Präkonditionierungen und Auslösemechanismen für das Hangversagen untersucht sowie die Abhängigkeit der Variabilität unter den Rutschungstypen zu den dominanten tektonischen Prozessen innerhalb der geologisch spezifischen Umgebung dieses Plattenrandes. Letztlich wurden Schlüsse über die Signifikanz von Massenumlagerungsprozessen auf die langfristige Hangentwicklung gezogen und mit anderen geologisch ähnlichen Umgebungen verglichen.

Die Subduktionszone Zentralamerikas ist seit den späten 1970ger Jahren Ort intensiver, kontinuierlicher Untersuchungen gewesen. Diese vorausgegangenen Untersuchungen kumulierten im ersten Jahrzehnt des 21sten Jahrhunderts in der Auswahl der Region als Schwerpunktgebiet für das Programm „Margins“ der USA und

dem deutschen und DFG geförderten Sonderforschungsbereich SFB 574. Beide Programme beinhalten die Forschung an einer großen Bandbreite von Themen mit dem Bestreben, das Verständnis des Systems „Subduktionszone“ voranzutreiben. Viele Einzelprojekte haben von der engen Zusammenarbeit beider Forschungsgemeinschaften dieser Länder profitiert. Diese Doktorarbeit entspringt selbst dem SFB 574, der sich als oberstes Forschungsziel gesetzt hat, Volatile und Fluide in Subduktionszonen und deren rückwirkende Wirkung auf das Klima zu untersuchen und den Auslösemechanismen von Naturkatastrophen nachzugehen.

Dieser Arbeit liegt eine Datenbasis zugrunde, die aus einer Zusammenstellung von Fächerlotdaten aus 7 Forschungsausfahrten sowie Seitensichtsonardaten aus 3 Ausfahrten und Sedimentkernproben einer speziell gewidmeten Ausfahrt besteht. Diese Datenbasis wurde durch ein kollaboriertes Bemühen beider Forschungsgemeinschaften, dem Margins-Programm der USA und dem SFB 574 zusammengeführt. Aufgrund der Meeresbodenmorphologie und Bildern von Rückstreuungsdaten sowie seismischen Abbildungen konnten 147 submarine Rutschungserscheinungen in der Region kartiert und klassifiziert werden. Die Hangversagungen variieren in ihrem Typus, ihrer Häufigkeit und der Verteilung entlang und quer des Hanges in einer Art und Weise, dass sich sechs Segmente entlang des Mittelamerikanischen Grabens herausbilden. Die laterale Ausdehnung der sechs Segmente korreliert gut mit einer ähnlichen Segmentation entlang des Grabens, die sich wiederum über den Charakter der eingehenden Ozeanplatte, die Veränderungen des Oberflächenreliefs, des Plattenalters und der Krustendicke äußert.

Außerdem wurde in der Arbeit herausgefunden, dass die sechs Segmente ebenfalls die quer zum Hang verlaufenden Strukturveränderungen verschiedener geologischer Elemente abdecken, wie etwa die Veränderung der Morphologie des oberen,- mittleren und unteren Kontinentalhanges, die Gesamtweite und variierende Neigungswinkel des Hanges. Diese Gestaltung der geologischen Hangelemente scheint an eine langfristige Entwicklung gebunden zu sein, die durch tektonische Prozesse bei Subduktionserosion hervorgerufen wird.

Eines der Segmente deckt die Fläche ab, unter der der Cocos-Bergrücken der ozeanischen Platte unter den Schelf und den Hang der südcostarikanischen Halbinsel Osa geschoben wird. Hier rufen 1-km-hohe, schmale und scharfe Firste und kleine konische unterseeische Berge des Cocos Bergrückens Abschiebungen und Gesteinslawinen am kurzen und steilen Kontinentalhang hervor.

Ein anderes Segment entsteht seewärts vor Zentral Costa Rica. Hier werden große, konische, unterseeische und 1-3 km breite Berge und Firste unter den Kontinentalhang geschoben und hinterlassen dabei weite Eintrittsmarken am Hangfuß. Es bilden sich hier tiefe Senken am Hang durch Einstürze der zuvor angehobenen oberen Platte entlang steiler Abbruchkanten, die sich hinter den sich unterschiebenden unterseeischen Bergen bildeten. Die meisten Hangversagungen sind große Abschiebungen, Muren und Gesteinslawinen mit Blöcken bis zu 500 m Durchmesser.

Im Gegensatz dazu steht ein drittes Segment im nördlichen Teil seewärts vor Costa Rica, nördlich der Halbinsel Nicoya. Hier steht eine eingehende, relativ eben erscheinende ozeanische Platte einem ebenso glatt erscheinenden Kontinentalhang gegenüber, dem es an Hangrutschungen fehlt.

Das angrenzende vierte Segment seewärts vor Nicaragua zeigt hingegen einen steilen Mittelhang mit beträchtlichen translationalen Rutschungen. Diesem Hang steht eine mit zahlreichen 1-km-hohen unterseeischen Bergen und eine mit einem 100-meter hohen Horst- und Grabenrelief bestückte Ozeanplatte gegenüber.

Unter das fünfte Segment, seewärts vor El Salvador gelegen, subduziert ein gut entwickeltes Horst- und Grabenrelief, doch erschient es überraschend, dass das Segment nahezu hangversagungsfrei ist und nur am obersten Hang einige kleine translationale Rutschungen aufweist.

Die sich unterschiebende Platte des sechsten Segments, seewärts vor Guatemala gelegen, lässt sich ähnlich durch ein ausgeprägtes Horst- und Grabengelände charakterisieren. Allerdings weist hier ein steilerer Hang eine Häufung kleinerer Hangrutschungen, etwa einige km breit, entlang des gesamten Segmentes auf.

Wir schließen daraus, dass die Verteilung und der sich herausbildende spezifische Hangrutschungstyp ein Ergebnis der Interaktion zwischen präkonditionierender Langzeittektonik und kurzfristiger Stressausübung durch die sich unterschiebenden lokalen morphologischen Besonderheiten der ozeanischen Platte ist.

Da sich die Hangsedimente nicht auffallend entlang des Gebietes unterscheiden, scheinen sie keine Rolle bei der Herausbildung der Segmente zu spielen. Hierbei muss aber eingeräumt werden, dass andere Faktoren, wie Unterschiede in den Erdbebeneigenschaften oder deren Intensitäten pro Segment, die wir in dieser Arebit nicht untersuchten, eine unerwartete Rolle bei Massenumlagerungserscheinungen spielen könnten. Allerdings kann dem gegenübergestellt werden, dass der Erdbebentyp, der über die historischen Aufzeichnungen zugängig ist, in einer bedeutend kürzeren

Rekurrenzzeit auftritt, als es die hier erfassten Hangrutschungen tun. Um potentielle Präkonditionierungsfaktoren und Auslösemechanismen für translationale Rutschungen zu untersuchen wurde innerhalb dieser Arbeit eine Serie von sedimentologischen und geotechnischen Analysen an spezifischen Sedimentkenrproben unternommen, die aus und aus der Nähe von Rutschungen entstammen. So sollten Indexeigenschaften des Sediments bestimmt und das mechanische Verhalten individueller Lagen getestet werden. Dazu wurde im Detail Lithologie und Sedimenteigenschaften an Proben eines Schwerelotkernes untersucht, der die Scherfläche einer translationalen Rutschung durchstoßen hat. Die Analysen zeigten anormale Dichte-, Porenwasseralkalinitäts- und Scherkraft- Profile innerhalb und unter einer wenige Zentimeter dicken Vulkanischen Tephralage. Damit wurde deutlich, dass die Aschelage als Rutschfläche diente. Diese Tephra korreliert chemisch mit der San Antonio Tephra (SAT), die vor 6000 Jahren aus der Masaya-Caldera (Nicaragua) ausbrach und in vielen anderen Kernproben wieder gefunden wurde.

Korngrössenanalysen und Vergleiche der Lagendicke mit solchen in Kernen anderer Kernlokalitäten deuteten darauf hin, dass 80%-95% der Lage während des Abrutschens entfernt wurde.

Direkte Scherfersuche an der SAT und an anderen Ascheproben von Mittelamerika zeigten eine überraschend hohe Volumenabnahme während des Scherens an. Graphische Abschätzungen an Korngrössenvertilungskurven brachten hervor, dass die SAT eine hohe hydraulische Leitfähigkeit zwischen 10^{-4} und 10^{-5} besitzt. Diese Ergebnisse deuteten darauf hin, dass Tephralagen in der Lage sein könnten, unter undrainierten Bedingungen ihr Lagenvolumen so zu verringern, dass sie eine Schwächezone bilden, an der Abrutschungen statt finden könnten. Dieser Mechanismus setzt voraus, dass sich ein hoher Porendruck zwischen den marinen Tonen und innerhalb der Tephralage bildet, um den effektiven Stress zwischen den Lagen zu verringern und das Hangversagen zu begünstigen.

Es wird daher in dieser Arbeit spekuliert, dass qualitativ wichtige Massenumlagerungsprozesse essentiell dazu beitragen, die Entwicklung der Hangregion am Mittelamerikanischen Graben zu bestimmen. Aus dieser Arbeit schließen wir, dass der fundamentale Einfluss von Massenumlagerungsprozessen auf die langfristige Hangentwicklung im Vorfeld übersehen wurde.

List of Figures

Chapter 1:

Chapter 2:

Chapter 3:

relation to the incoming plate relief domains. The margins displays rotational slumps and scars from seamount subduction. Close ups of representative structures and their interpretation are shown in the figures marked by the black boxes.

Figure 5. Sidescan sonar imagery of the region of Nicoya slump (location in Figure 4). The complex morphology of the > 60 km wide slump probably developed when the slope failed over two subducting seamounts. A large seamount is located the SE causing the Rio Bongo uplift, and a smaller seamount is located under the headwall near the middle region of the slump structure, indicated by crown-shaped cracks and associated fractures. The headwall and deposits of the northwestern part of the slump differ from the morphology of the slump in its southeastern area. Blocky deposits and high headwalls represent a slump with a disintegrative character that developed rock avalanches in the southeast, down-slope of the Rio Bongo uplift. The northwestern two-thirds of the slump shows a more cohesive translational character. d = debris flow, da= debris avalanche, ra= rock avalanche.

Figure 6. Perspective view of sidescan sonar imagery draped on multibeam bathymetry of the region of Costa Rica deformed by subducting seamounts. Two under-thrusting seamounts are currently located under the so-called Jaco and Parrita scars (region location in Figure 4). The grooves in the slope bounded by sidewall faults mark the trajectory of the under-thrusting seamounts, and contain the deposits of a series of successive rotational failures produced as the seamounts subduct deeper under the overriding plate. The seamounts uplift and fracture an area considerably larger than the area that fails in their wake. d = debris flow, ra = rock avalanche.

Figure 7. Northern-most embayment offshore Costa Rica. a) multibeam bathymetry map, b) slope angle. The NW flank is sculptured by several headwalls and sidewalls of retrogressive translational slides. Slides developed on the inner wall of the embayment and the failed material followed canyon paths to build planar sediment bodies in the embayment's floor.

Figure 8. Perspective view of sidescan sonar imagery draped on multibeam bathymetry of the cohesive, translational Quepos slide related to uplift of the uppermost slope due to subduction of a ridge offshore Central Costa Rica. Numbers 1-4 indicates four failure events that spatially overlap and possibly represent a time evolution (1 oldest and 4 youngest) in the development of the slide caused by the southeast oblique subducting of a ridge (location of region in Figure 4).

Figure 9. The Cabo Blanco slide, related to uplift of the uppermost slope due to subduction of a seamount, located southeast of Nicoya Peninsula. a) Shaded-relief bathymetric map (location of region in Figure 4). b) Perspective view of sidescan sonar imagery draped on multibeam bathymetry of the upper portion of Cabo Blanco slide. Location of b is marked a. The slide is a cohesive, translational type with detached, coherent blocks in the upper area, slid blocks in the middle portion and compressional ridges in the lower segment.

Figure 10. Shaded-relief bathymetric map of the BGR and Geomar slides located in the uppermost slope offshore Costa Rica. The scars are small developed between

500 and 700m water depth and do not appear related to deformation associated to currently subducting seamounts.

Figure 11. Perspective view of sidescan sonar imagery draped on multibeam bathymetry of the Sirena slump in the lower slope offshore Osa Peninsula and associated run out deposits, including large blocks, that reach the ocean plate (location in Figure 4). The slope scar is 12 km wide, with a 1 km high headwall that dips 30º-51º. The avalanche is related to subduction of a sharp ridge -cresting Cocos Ridge- clearly visible in the images. Southeast of the scar, high-backscatter slope-sub-parallel structures may be incipient headwalls (marked in red). Down-slope of them, tongue-shaped bodies bounded by slope-normal structures (marked in yellow) might indicate developing gravity-related deformation.

Figure 12. Perspective view of sidescan sonar imagery draped on multibeam bathymetry of the deformation and slope failures caused by ridges and associated seamount groups on the Cocos Ridge in the forearc SW of Osa Peninsula (location in Figure 4). Numerous slope-parallel fractures in the slope occur up-slope of the headwalls of slumps. Apparently failures are disintegrative slumps that develop into rock avalanches..

Figure 13. The North Nicoya segment (location in Figure 1a). a) Shaded-relief bathymetric map of the segment. The incoming plate displays the smoothest segment along the study area. The oceanic plate contains few seamounts compared to the SE segment of Costa Rica, and some small-to-middle-size normal faults compared to the segments towards the NW. The continental slope contains comparatively few failures (delineated in white). b) Shaded-relief bathymetric map of a type example of failure: The translational Hermosa slide. Red squares mark location of sediment cores M66-151, 152, 153 described in detail by Harders et al. (2010). Numerous scarps parallel to the slope strike indicate that abundant normal faults cut across the area.

Figure 14. Perspective view of sidescan sonar imagery draped on multibeam bathymetry of a region of the middle slope of the North Nicoya segment (location in Figure 13). The image shows the Hermosa slide and 4 neighboring slide scars. The slides have formed near the mouth of canyons and where normal faults cut the slope, clearly visible in the northwest part of the headwall of Hermosa slide. Slid blocks are visible on top of the slide plane.

Figure 15. Seafloor maps of the NW region of the North Nicoya segment. a) Shaded-relief bathymetric map showing an uplifted area and, located down-slope, a failure scar showing no clear slide sidewalls. Further down-slope occur possible compressional ridges that might indicate slow deformation. b) Perspective view of sidescan sonar imagery draped on multibeam bathymetry of the middle to upper slope (location in a). The image shows the group of radial fractures clustered on the uplifted area and associated headwall. Scarps of discrete normal faults cut the slope at numerous locations.

Figure 16. Shaded-relief bathymetric map of the Nicaragua segment. a) The segment displays large translational slides on the middle continental slope, and seamounts on the ocean plate that are comparatively smaller than in the Seamounts - Central Costa Rica segment Cocos Ridge – Osa Peninsula

Segment. b) Close-up of middle-slope translational Masaya slide showing the slide scar and overlying slid blocks. Failure deposits are missing at the base of the scar. The scar toe converges into a channel that may have been formed by the mass wasting transport processes. c) Close-up of middle-slope translational slide scars with overlying slid blocks and channel initiating at the scar toe. d) Close-up of middle-to-lower-slope small rotation slumps possibly associated to failure induced by small-scale relief of the incoming oceanic plate.

Figure 17. Shaded-relief bathymetric map of the El Salvador segment. a) The segment is characterized by the best-developed upper-middle slope canyon system of the study area that possibly implies a comparatively more stable slope. In accord, the segment contains the fewest slope failures of all segments. Typically, these are small translational slides in the upper slope. A few rotational failures seem to initiate at normal fault scarps in the middle to lower slope. A well developed bending-related normal fault system with large offsets characterizes the incoming ocean plate, but no seamounts are present. b) Close-up of upper-slope small translational slides that represent the most abundant type and typically occur at canyon walls.

Figure 18. Seafloor maps of the Guatemala segment. a) Shaded-relief bathymetric map of the segment. It displays the greatest variability of types of mass wasting structures of all segments. b) Local slope angle. The image displays numerous normal fault scarps. Normal faulting initiates in the upper part of the middle slope, indicated by red arrows, and develops across the middle-lower slope, affecting the development and shape of slope failures. The rough topography of the slope possibly indicates a comparatively high frequency of slope failure. c) Close-up of the lower slope translational slides, which are oriented along fault scarps indicated by arrows. d) Close-up of the middle slope. Rotational failures with irregular shapes start at or near normal fault scarps indicated by arrows and are difficult to distinguish from faulting scarps.

Chapter 4:

Figure 1. Tectonic plates of the subduction system of Central America. The plate subducting along the Middle America Trench was formed at the Cocos-Nazca Spreading Center in the southeastern and at the East Pacific Rise in the north. Isochrones are marked by dashed-lines, with age in million years. The semi-transparent box marks study region with segments discussed in the text.

Figure 2. Artificially illuminated, perspective view of Cocos Ridge, continental slope, and Osa Peninsula (3x vertical exaggeration [v.e.]). The image is 130 km wide along the trench axis. Ridge topography is elevated 1-2 km compared to the plate to the north. Trench axis depth is 1950 m at SE edge of figure and 2920 m at NW edge. The plate is ornamented with ridges up to ~1 km above surrounding seafloor and groups of small seamounts.

Figure 3. Artificially illuminated, perspective view of the relief of the seamount segment and slope off Central Costa Rica (3x v.e.). The image is 270 km wide along the trench axis. Trench axis depth is 2000 m at SE edge of figure

and 4200 m at NW edge. The ocean plate is festooned with 2-3 km tall seamounts and guyots and 0.5-1.0 km high ridges.

Figure 4. Artificially illuminated, perspective view of the relief of the ocean plate and continental slope offshore North Nicoya Peninsula and Nicaragua (3x v.e.). (a) The comparatively smooth ocean plate and tectonically little-disturbed offshore North Nicoya Peninsula. The image is 120 km wide along the trench axis, depth along trench axis is 4200 m at SE edge and 5100 m at NW edge). (b) The heavily faulted ocean plate with numerous seamounts. The image is 130 km wide along the trench axis. Trench axis depth is 5000 m at SE edge and 5400 m at NW edge. The middle continental slope is strongly fractured, cut by extensional faults and has many translational landslide scars.

Figure 5. Artificially illuminated, perspective view of the ocean plate and continental slope offshore El Salvador and Guatemala (3x v.e.). (a) Relief of the strongly faulted ocean plate and tectonically disturbed slope offshore El Salvador. The image is 200 km wide along the trench axis. Trench axis depth is 5300 m at SE edge and 5800 m at NW edge. (b) Relief of the ocean plate and rugged slope offshore Guatemala. The image is 164 km wide along the trench axis. Trench axis depth is 6100 m at SE edge and 6500 m at NW edge.

Chapter 5:

Figure 1. Shaded relief map offshore Central America. Bathymetry data are color coded from pale blue to dark blue. Numbers refer to cores taken with German research vessel Meteor cruises M54 and M66 and German research vessel Sonne cruise SO 107. Cores 131–133 were taken at Masaya slide, a big slide scar of 12 km × 6 km. Numbers 151–153 refer to cores taken at the medium-sized Hermosa slide (scar of 3 km × 7 km), with core 151 discussed in section 3.2.

Figure 2. Shaded relief map offshore Costa Rica showing Hermosa slide (scar of 3 km × 7 km), with core locations (red squares) M66/151 to M66/153 in the northwest of the upper slide scarp.

Figure 3. Shaded relief map offshore Nicaragua, showing core locations M66/131 to M66/133, taken at Masaya slide (slide scar 12 km × 6 km).

Figure 4. Multibeam bathymetry map of Hermosa slide with contour lines every 10 m. The slide and a near by similar feature are delineated by white filled black circles. Locations of gravity cores M66/151, M66/152, and M66/153 are marked with red squares. Subbottom seismic profiler parasound track is indicated by lines across the headwall (M1–M4 are navigation waypoints). The seismic image from the red track is shown in Figure 6. Black dashed box shows the location of side scan sonar data shown in Figure 5.

Figure 5. TOBI side scan data of the upper region of the Hermosa slide. Dots (black, encircled in white) mark the outline of the slide. Arrows point to the retrogressive character of the headwall and slid blocks on the slide plane as well as to normal fault scarps in the slopes sediment. Core position M66/151 (marked as red square) is located where slide plane and headwall merge. The location of the Parasound profile (Figure 6) is marked as a black dashed line. Location is shown in Figure 4 as black dashed box.

Figure 6. Parasound subbottom seismic profiler image and line interpretation across the headwall of Hermosa slide (see profile location in Figure 4 marked as red line). In spite of interferences with the signal of other instruments shown as black stripes in the image the strata and headwall scarp are clearly visible. Five minutes of UTC time ~375 m on x-axis.

Figure 7. Multisensor core logger data and analog measurements of density, porosity, shear strength, and pore water alkalinity as well as lithology from core M66/151 of Hermosa slide.

Figure 8. Description and analog data of density and shear strength of core M66/167. The SAT ash layer is marked at 95–104 cm bsf, showing a higher initial shear strength compared to the clay. Note that the overall "normal" trend of the data (increase of shear strength and density with increasing core depth) and peaks in density and shear strength are due to overconsolidated clay clasts or overconsolidated material extruded by the mud mound (Mound Culebra [see also Kutterolf et al., 2008d]).

Figure 9. Multisensor core logger data of density and location of ash layers (highlighted in gray) of core M54/11-2 taken from the ocean plate (see also Figure 1 for core location). The SAT ash layer is marked at 12– 29 cm bsf (locations of ash layers taken from Kutterolf et al. [2007a, Figure 4]).

Figure 10. Cumulative grain size distribution curve showing the entire SAT layer of samples M66/151 (grain size <32 not analyzed), M66/167, and M54/11-2. All samples are coarse silt to middle sand (20–600 mm). The kf values were calculated after Hazen [1892], using these curves to determine d10 and d60 if U < 5 with the formula kf = 0.0116 * (d10)2 and with U = d60/d10 and dy with the value (%) at the grain size (mm) defined along the curve.

Fugure 11. Cyclic direct shear tests showing total volume change in % of mafic and felsic ashes and quartz grains of 0.063–0.125 mm grain size. Shearing went from left to right, continued until no further volume changes were recorded, and sheared back to the left (arrows). For each sample four cycles of shearing were conducted (effective vertical stress is 40 kPa ~7 m below seafloor, and shear velocity is 0.5 mm/min).

Figure 12. Cumulative grain size distribution of the coarser part of the SAT layer from cores M66/167 and M54/11-2, using the same method for kf-calculation described in Figure 10.

List of Tables

List of Abbreviations

MAT: Middle America Trench

DTS1: Deep Towed Sidescan Sonar 1

TOBI: Towed Ocean Bottom Instrument

M_w: Moment Magnitude

M_s: Surface Wave Magnitude

SF: Factor of safety

ODP: Ocean Drilling Project

GMT: Generic Mapping Tools

CTD: Conductivity, Temperature, Depth

GPS: Global Positioning System

MSCL: Multi Sensor Core Logger

EMP: Electro Microprope

La-ICP-MS: Laser Ablation - Inductively Coupled Plasma - Mass Spectrometry

SAT: San Antonio Tephra

FTZ: Fracture Zone Trace

Contents

Chapter 1

1. Introduction

1.1 Submarine landslides

Many regions of the world have experienced landslide activity. Large onshore landslides have attracted our attention because people were put in danger, or killed, and properties have been damaged. The geo-hazard of on-land landslides is publically well known, and most regions where they occur are directly accessible to study. In contrast characterization and location of submarine mass wasting around the worlds slopes are comparatively far less known, because they are often in uncharted or recently mapped areas and are more difficult to access. Therefore the knowledge of submarine landslide risk assessment is lagging behind from what has been already achieved for on-land landslide risk assessment (Locat and Lee 2002). The highest threat for life and property from submarine mass wasting is often named to be either from tsunamis (e.g. Synolakis et al., 2002; Garcia et al., 2003; Fine et al., 2005; Bondevik and Svendsen, 1994), or the destruction of submarine infrastructures by moving sediment mass (Heezen and Ewing, 1952; Heezen and Hollister, (1971); Klaucke and Cochonat, 1999). During the last 60 years an increasing amount of research had been made to answer the questions of where, how and why submarine landslides occur and how frequent they are at different locations.

The now classical review of occurrence, frequency, causes and mechanisms of submarine landslides is that by Hampton and Lee (1996), where the most important findings since the early 1950's are summarized. Since oil industry has been moving exploration of hydrocarbons into deeper waters, a variety of slides have been found to occur in offshore oil provinces like along the Norwegian margin, in the Gulf of Mexico, in the Caspian Sea and in the Gulf of Guinea (Barley, 1999). The largest slide of the world, the Storegga Slide, was discovered over one of the largest gas fields of the world, offshore Norway (Bryn et al. 2003). The slide affected an area of c. 95.000 km^2 with a volume of 2.400-3.200 km^3 (Haflidason et al., 2004) and probably triggered a tsunami of which sediments have be found at the adjacent land areas of Britain and north Europe (Dawson et al., 1993). Today it is known that seafloor failures are a widespread phenomenon at the world's continental margins, and an accompanying

process during the sedimentary basin formation and slope evolution (Camerlenghi and Pini, 2009). Submarine landslides has been described to occur at 4 general tectonic settings: 1) Passive margins, 2) Active rift and transform margins 3) Convergent margins, and 4) Flanks of volcanoes.

1.1.2 Submarine landslides at passive margins

In the past most modern studies on the spatial occurrence, architecture and development of submarine slope failures were conducted at the passive Atlantic margin (Weaver et al. 2000; Canals et al., 2004; Hühnerbach and Masson, 2004; Chaytor et al., 2009 and Lee, 2009), where slope evolution is sediment dominated. In this setting Hampton et al. (1996) and Lee (2009) describe that most submarine slides occur in active river deltas, submarine canyon-fan systems, and on the open continental slope. These are locations where a sloping seafloor is covered by thick sediment deposits and different environmental stresses are high (Hampton et al., 1996), e.g. earthquakes due to isostatic rebound (ten Brink et al., 2009) or high pore pressures due to rapid unconsolidated sedimentation (Dugan and Flemmings, 2000). Studies along the U.S. coast of the Atlantic margin indicate that submarine landslides are most frequent on the glacially influenced segment of the margin. Mean values of the slide dimensions are 71-107 km in length, 15-30 km in width and with headwall heights of 647 to 118 m (Twitchel et al., 2009). The sediments involved in sliding are quaternary glacially- or fluviatile-derived, and deposited by river systems, as fan deltas, or by bottom currents (Chaytor et al., 2009). Slope angles of the margin where slides occur are generally low, with mean values between 3 and 6.8º although they reach up to 11º at canyon walls (Twitchel et al., 2009). Seismic activity due to isostatic rebound is typically assumed to trigger most of the slides, because slope angles are often less than 5º and the slopes should be stable otherwise (Lee et al., 1993).

Offshore Europe, along the passive Atlantic margin there are fewer, but larger submarine landslides, compared with the counter part off Canada and the US coast in the western North Atlantic (Hühnerbach and Masson, 2004). Weaver et al. (2000) divided the European and north African margin into 3 sections, with different spatial and frequent distributions of submarine landslides: The glaciated margin north of 56º N, the glacially-influenced margin between 26º N and 56ª N and a non-glaciated margin south of 26º N. Whereas mass movements are frequent along the glaciated margin, the glacially-influenced margin shows fewer submarine landslides but instead canyons of

turbidities. In the southern most section large-scale submarine slides are frequent and instability is preconditioned by fast sediment accumulation rates due to upwelling of organic matter (Weaver et al., 2000).

1.1.3 Submarine landslides at active margins

In active margins, slope evolution is fundamentally controlled by the interplay of sediment dynamics and tectonic processes. In contrast to investigations on passive margins, there have been fewer studies on mass wasting on active margins. There are three main types of active margins: 1) Rift and strike-slip margins (they could be separated in two but they seem to share several traits), 2) Convergent margins with accretionary prisms, and 3) Convergent margins dominated by tectonic erosion.

1.1.3.1 Submarine landslides at strike-slip margins

Off Central California, along the strike-slip fault-dominated margin, mass movements are associated with incised canyons and typically originate from the steep canyon sidewalls. The slides show similar features like slides on passive margins with long run out distances (mean values 15.8 km), often disintegrated into debris flows (McAdoo et al., 2000).

1.1.3.2 Submarine landslides at convergent margins with accretionary prisms

This type of margin is influenced by compressional tectonics related to the accretionary processes. Here, preconditioning of slope failure and the architectures of slides are different from passive margins. Orange and Breen (1999) investigated the curious existence of headless canyons offshore Oregon. They could explain the slope instability and failure mechanisms occurring on the steep seaward and landward-verging thrusts of the accretionary prism by seepage forces developed during the compression-driven compaction of accreted sediment. McAdoo et al. (2000) found that compared to most other margin types around the US, slope failures offshore Oregon originate at steeper slope angles (mean value of 16.3ª), but have relatively short run out distances (5km). Head scarps are steep and high with mean values of 177.6m and up to 410 m. He noted that the steep headwall angles might indicate that the material involved in sliding is cohesive and consolidated due to the compaction during accretionary processes. In spite of frequent earthquake shaking, submarine landslides occur less frequent compared to other margins around the USA and the slope appears to be stable in many areas (McAdoo et al., 2000).

1.1.3.3 Submarine landslides at convergent margins with subduction erosion:

There are no previous large-scale investigations on mass wasting along convergent margins dominated by subduction erosion, although slope failures had been previously recognized in this type of systems. Since the late 70´s there have been studies aiming at understanding the tectonic differences of a subduction zone with accretion and those with non-accretion but tectonic erosion. In convergent erosive margins the interaction with the down-going plate is eroding the base of the upper plate. This tectonic process affects the margin and leads to its subsidence, oversteepening and extensional faulting across the continental slope. For instance, the continental slope offshore Costa Rica has subsided 3-5 km during the Neogene time (Vannucchi et al. 2003). Compared to other continental margins, mass wasting imprints and deposits on erosional convergent margins are possibly faster modified. In contrast, younger sediments would cover slide imprints at passive margins. Examples of subduction erosion margins are the MAT, offshore Ecuador and Peru, along the Chilean margin and along the Japan Kuril trench (von Huene et al., 2004 and references therein).

1.1.4 Approaches to study submarine landslides

The study of submarine mass wasting concerns the detailed characterization of an event. Depending on the data type and quality the main characteristics of a landslide have to be determined, such as the external slide morphology, internal structure of the failure and resulting deposits, geometry of its slip plane, run-out distances, transport mechanisms and flow pathways. Based on these findings the type of mass wasting may be specified using a classification scheme.

Suggestions for suitable classifications of offshore mass movements have been proposed by various authors in the past, such as Carter (1975), Moore (1978), Lowe (1979), Nardin et al. (1979), Prior and Coleman (1979), Cook and Mullins (1983), Moore et al. (1989), Mulder and Cochonat (1996) and Locat and Lee (2002). Since the earlier studies on submarine mass movements in the late 1960` (Dott, 1963, Morgenstern 1967) classification criteria have progressively changed because new imaging capabilities provided by improved techniques enabled an in-depth analysis and revised some aspects of the older classification systems (Canals et al., 2004). Based on state-of-the-art tools like swath bathymetry, deep-tow side scan sonar and 3D seismic reflection, the most modern and widely accepted classification scheme was suggested

by Mulder and Cochonat (1996) and modified by Locat and Lee (2002).

The evaluation of possible trigger and preconditioning factors that may have contributed to the instability is an important approach for risk assessment of landslides. Sultan et al., (2004) emphasized the importance of analyzing and distinguishing trigger and preconditioning factors. They defined preconditioning factors as those that contribute to the initiation, but do not trigger a submarine slide. Thus, preconditioning factors may be related to the overall tectonic history, sediment properties, and fluid flow regime. These factors include the overall stress history of repeated earthquake cycles, slope angle, type of sediment, grain size distribution, degree of saturation, prior straining, and gas hydrate dissolution and dissociation. In contrast the trigger mechanisms of a slide are defined as the external stimulus that initiates slope instability (Sultan et al., 2004), and includes a range of processes like slope over-steepening, seismic loading, storm-wave loading. At fast rates some preconditioning factors may become trigger mechanism like sediment accumulation and under consolidation, gas charging, gas hydrate dissociation, low tides, seepage and glacial loading (Locat and Lee, 2002). In cases it is inferred that a combination of trigger mechanisms induced slope failure of sediments that had been weakened by a set of preconditioning factors (Canals et al. 2004).

1.2 Objectives and outline of thesis

This PhD work is part of the research program SFB (Sonderforschungsbereich) 574, financed by the German Research Association "DFG" (Deutsche Forschungsgemeinschaft) and later financed by IFM-GEOMAR. The SFB 574 investigates pathways and fluxes of fluids and volatiles at subduction zones to understand the processes of subduction recycling. Since July 2001 the SFB focused on pacific Central America, a type of margin that offers unique features and has attracted researchers since the late 1950's. After the nomenclature of Gutenberg and Richter (1954) the convergent margin between Guatemala and Panama would be classified as representative of the "Pacific Margin" type. Investigations in the past revealed that forearc tectonics, submarine sliding, arc magmatism and interplate seismicity differ in segments along the MAT (Ranero et al., 2007).

After 100% coverage of multibeam bathymetry data was achieved along 1300 km of the MAT, a first large-scale study of mass wasting along the active convergent margin of the Pacific coast was possible. Although submarine mass wasting was detected and studied before in the region, the analyses were focused on a limited number of structures. This PhD work comprises for the first time an inventory of all mass wasting structures observed between Guatemala and Costa Rica. The work incorporates tectonic, geologic and geotechnical observations to analyze the origin and style of mass wasting, as well as slide mechanisms.

The work is structured in 6 chapters from which chapters 3, 4 and 5 are standing-alone studies with their own individual introduction, methodology, discussion and conclusion that have been published in peer review articles listed in the Science Citation Index.

Chapter 1 provides an overview of the study area by introducing the tectonic and geological setting. The chapter summarizes relevant achievements of former studies in the area.

Chapter 2 explains the methodology and data sets used in this work.

Chapter 3 is a study of:

Submarine slope failures along the convergent continental margin of the Middle America Trench

Authors: Rieka Harders, César R. Ranero, Wilhelm Weinrebe and J. H. Behrmann

Status: published 2011 in Geochemistry, Geophysics, Geosystems. 2011, Volume 12, No. 6, Q05S32, doi:10.1029/2010GC003401, ISSN:1525-2027

The chapter has an independent introduction, methodology, discussion and conclusion part. The work comprises an inventory of mass wasting structures distributed along 1300 km of the continental slope of the Middle America Trench and represents the first comprehensive study of submarine failures along a convergent margin dominated by subduction erosion. An integrated data set of full coverage of bathymetry data, sidescan sonar images and seismic data along this type of margin was the basis for the mapping of 147 submarine landslides. The study reveals first indices to a relation of long-term tectonic processes, the effect of subduction of high ocean plate features and the distribution and style of submarine mass wasting.

I contributed to this work by mapping all structures, interpreting and classifying the failures, and speculating of the preconditioning and trigger mechanisms in the region. I wrote the article with contributions of the co-authors.

Chapter 4 is a study presenting:

An Overview of the Role of Long-Term Tectonics and Incoming Plate Structure on Segmentation of Submarine Mass Wasting Phenomena Along the Middle America Trench

Authors Rieka Harders, César R. Ranero and Wilhelm Weinrebe

Status in press as Chapter 35 in: Y. Yamada et al. (eds.), Submarine Mass Movements and Their Consequences, Advances in Natural and Technological Hazards Research 31, DOI 10.1007/978-94-007-2162-3_35, © Springer Science+Business Media B.V. 2012

This chapter has an independent introduction, methodology, discussion and conclusion part. In this study, submarine mass wasting is related to long-term tectonic processes associated to subduction erosion. The work shows that the structural segmentation of the ocean plate between Guatemala to Costa Rica matches the segmentation of the

distribution and variability of mass wasting along the continental slope. Underthrusting of ocean-plate features of large relief, and subduction erosion processes seem to control the evolution of the slope and the abundance and style of submarine landslides. Long-term preconditioning of the slope by tectonic processes interacts with short-term under-thrusting of high-relief features of the ocean plate to trigger gravitational collapse of different intensity along the Middle America Trench.

I contributed to this work by analyzing the data, interpreting the structures, putting them into the context of long-term slope evolution and writing the article with contribution of co-authors.

Chapter 5 is a study analyzing:

Tephra layers: A controlling factor on submarine translational sliding?

Autohrs: Rieka Harders, Steffen Kutterolf, Christian Hensen, Tobias Mörz and Warner Brückmann

Status: published 2010 in Geochemistry, Geophysics, Geosystems. Volume 11, No.5, Q05S23, doi:10.1029/2009GC002844, ISSN: 1525-2027.

This chapter has an independent introduction, methodology, discussion and conclusion part. The study investigates a trigger mechanism that would induce translational sliding by a partly liquefied tephra layer, which is sandwiched in-between clayey sediment. The mechanism implies that ground shaking by large earthquakes induces rearrangement of ash shards causing sudden compaction (volume reduction) to produce a rapid accumulation of water in the upper part of the layer. Undrained conditions cause overpressure and effective shear strength is reduced within the ash layer. Sliding along the weak layer would then be promoted. The hypothetical mechanism is based on results from geotechnical measurements and sedimentary laboratory work on sediment cores recovered during a dedicated cruise offshore Costa Rica and Nicaragua.

I contributed to this work by planning and collecting the core data during the cruise, conducting geotechnical measurements and sedimentary work, and writing the article with contributions from co-authors.

Chapter 6 gives an outlook for each chapter, stressing the numerous venues of future research that this PhD work has opened.

1.3 Tectonic and geological setting

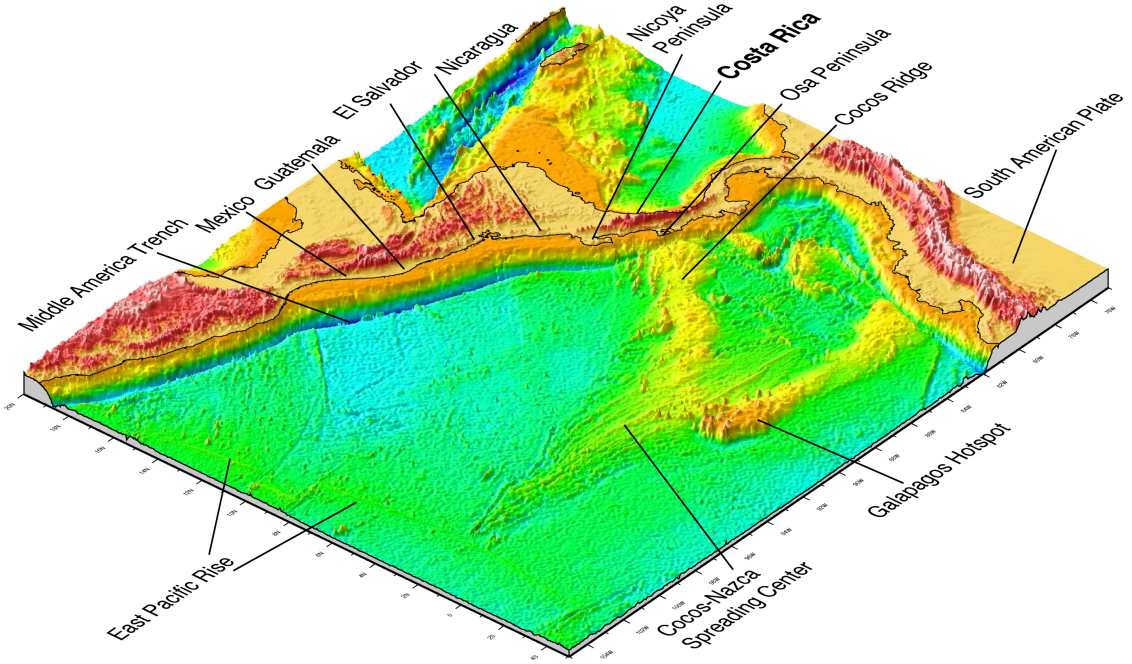

Figure 1.1: Overview of the geographical, tectonic and geological setting. Countries, plate boundaries, tectonic features as well as topography of Cocos,- and Caribbean Plate and parts of Nazca Plate.

Since late Oligocene/ early Miocene the oceanic Cocos Plate subducts beneath the continental Caribbean Plate along the Middle America Trench (Fig.1.1 and Fig. 1.2) (Barckhausen et al., 2008), currently at a rate of 85 mm/a in the region of interest (DeMets, 2001). The trench axis of the MAT deepens from Costa Rica to Guatemala, and the continental slope narrows towards Costa Rica, and widens towards Guatemala (von Huene et al., 2000). The lithosphere of the oceanic Cocos plate is formed at the Cocos-Nazca Spreading Center, strongly affected by the Galapagos Hot Spot, and at the East Pacific Rise (Barckhausen et al. 2001). This complex origin generated a variable and segmented oceanic plate character, with different morphologies and topographies along trench. The subduction of this complex plate structure drives the along-trench diversity in tectonic processes of the upper Caribbean Plate. A fracture zone trace marks the boundary between the two oceanic lithospheres, currently entering the subduction zone offshore Nicoya Peninsula (Barckhausen et al. 2001).

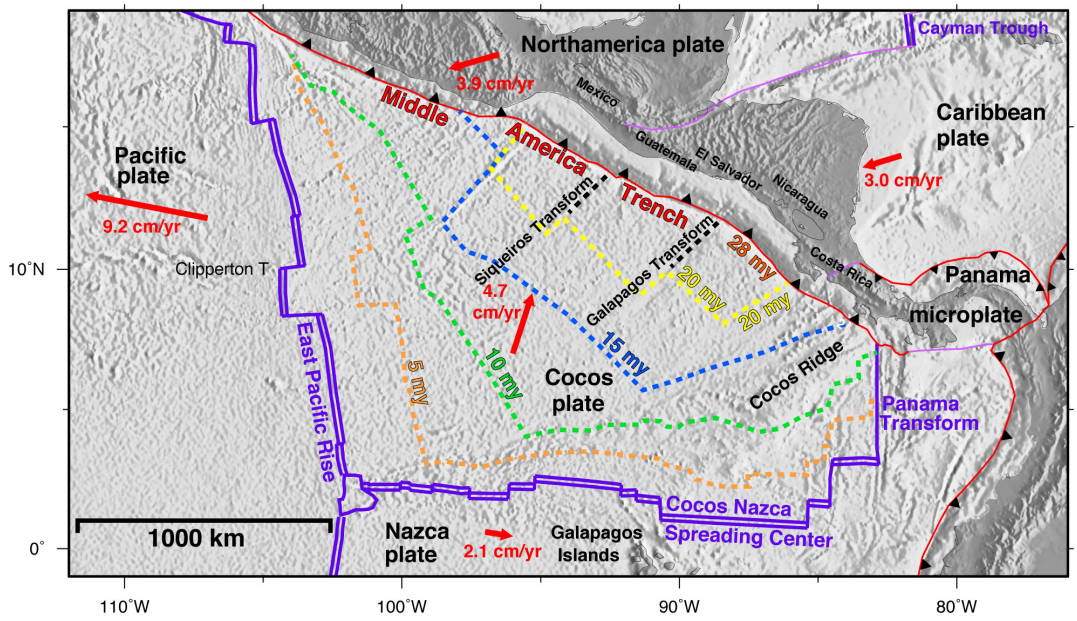

Figure 1.2: Main tectonic elements of the Central America subduction zone along the Middle America Trench. The study region extends from the locus of subduction of the Siqueiros Transform fault to the area of subduction near the Panama transform zone. Tectonic elements: Subduction zone (marked as a red line with triangles), spreading centers (marked in deep purple), convergence rates (red numbers with arrows) and plate ages of Cocos Plate (dotted lines with numbers).

1.3.1 The tectonic model of the MAT

There has been a long debate on the tectonic process that dominates the margin between offshore Costa Rica and Guatemala. Although the margin offshore Guatemala had been for long interpreted as non-accretionary or erosional (see review in Ranero et al., 2007), until late 90's early 21st century, the margin offshore Costa Rica was interpreted to be accretionary (Shipley et al 1986, 1990; Silver et al. 1985). Analysis of magnetic data (Barckhausen et al., 1998), seismic refraction data (Ye et al., 1996) and multichannel seismic reflection sections (Hinz et al., 1996), and results of ODP Leg 170 (Kimura et al. 1997) showed however that the margin is non-accretionary and sediments of the ocean plate are under-thrusted rather than accreted. Drilling showed that the small frontal sediment prism is made up of re-worked sediment of the continental slope (Kimura et al. 1997). An alternative model was proposed where active basal erosion and seamounts tunneling beneath the margin wedge was interpreted based on seismic images and subsidence records (Ranero and von Huene, 2000; Ranero et al., 2000, Vannuchi et al., 2003). Erosive tectonic processes lead to subsidence of the entire MAT between Guatemala (Vannuchi et al., 2004) to Costa Rica during the Neogene. Offshore Costa Rica subsidence and upper plate extension was interpreted from cores of DSDP

leg 84, ODP leg 170 where it was shown, that a large mass was missing (Vannuchi et al., 2003), as well as seismic images documented upper plate extension (McIntosh et al., 1993; Ranero et al., 2000). It was shown that upper plate extension was the response of basal erosion, leading to subsidence of the margin offshore Costa Rica (von Huene et al., 2000; Ranero et al, 2000). Similarly, an independent study indicated that the beginning of long term subsidence due to basal erosion of the upper plate offshore Nicaragua was determined to occur in the Late Oligocene/ Early Miocene (Ranero et al., 2000). Subsidence of the Guatemala margin is also supposed to have started during Late Oligocene/ Early Miocene and the record of vertical tectonism showed that the margin subsidence is migrating towards the continent (Vannuchi et al., 2004). Between Guatemala and Costa Rica there is the 9-15 km thick sediment accumulation under the shelf, the Sandino forearc basin, which is subsiding at its center since Late Cretaceous (Ladd et al., 1985; Ranero et al., 2000). It was suggested that the initial subduction began at ca. 75 Ma and that the subsidence of the Sandino basin was triggered by sinking of the slab into the mantle, because subduction initiation is associated with rapid subsidence 150- 200 km from the trench (Ranero et al., 2000).

1.3.2 Seismicity along the MAT

Earthquakes along the MAT clearly define a Wadati-Benioff Zone of landward dipping seismicity where the Cocos Plate subducts beneath the Caribbean Plate (Protti et al., 1994). From Guatemala to Costa Rica the region is regularly stroke by earthquakes of Mw >6 and up to Mw 7.9. The report by the United States Geological Survey (USGS, http://earthquake.usgs.gov/earthquakes/world/historical_country.php#costa_rica) indicates that since 1902 there have been between Guatemala and Costa Rica 20 earthquakes with Mw > 5.5 and up to 7.9 causing a total loss of 37.141 human lives . From this number it has to be taken into account that about 60 % of all casualties occurred as a consequence of the Mw 7.5 earthquake in the overriding plate along the Motagua strike-slip fault in Guatemala 1976. Historical records indicate ~15 earthquakes of Ms > 7 have occurred in the last 100 years only offshore Costa Rica and Nicaragua (Ambraseys and Adams, 1996).

1.3.3 The volcanic arc of Central America

The explosive volcano chains between Guatemala and Costa Rica belong to the Central American Volcanic Arc (CAVA) and result from subduction of the Cocos Plate beneath

the Caribbean Plate. The CAVA holds one of the highest densities of volcanoes around the world. Volcano styles range from strombolian through violently surtesyan to plinian eruptions and include the formation of ignimbrites (Kutterolf et al., 2007). The volcanism is closely related to the subduction of fluids within the oceanic lithosphere. Bending related faulting of the oceanic plate at the MAT creates pervasive fractures in the oceanic plate through which fluids are transported downwards. This process changes the geochemical and mechanical properties of the oceanic lithosphere and upper mantle. The fluids migrate downwards along at least 20 km deep cutting faults and react with the peridotites of the upper mantle creating serpentinite (Ranero et al., 2003). Further subduction induces the metamorphic dehydration of the slab and fluids are released upwards into the mantle wedge of the continental plate, contributing to the highly explosive volcansim (Ruepke et al., 2002). The volcanic front shifted westwards with time and reached its present position about 8 Ma ago (Ehrenborg, 1996). Volcano eruptions along the CAVA can create buoyant columns reaching up to 40 km into the stratosphere. The prevailing westerly winds cause dispersal of the felsic and mafic ashes towards the Pacific Ocean (Kutterolf et al., 2007). It was estimated that 10-13 km^3/a of volcanoclasitc sediments are produced per km along the arc (Straub and Schmincke 1998).

1.3.4 Sediments on the continental slope and ocean plate

The offshore sediments along the MAT are made up by land-derived andesitic and rhyolitic detritus derived from Central America and are frequently intercalated by tephra layers (volcanic ash, volcanic glass) from the CAVA (Helm, 1984; Kutterlof et al., 2008a, Harders et al., 2010). The first 150m -200m sediments of the continental slope between Guatemala and Costa Rica are made up by Pliocene and Pleistocene gray to olive-green terrigenous clay, comprising dioctahedral smectite that shows a clear increase in crystallinity with sediment age (Helm, 1984). Offshore Nicaragua sediments covering the ocean crust are in general 250-300m thick and increase to a thickness near Leg 170 of 400m (von Huene et al., 2000). Offshore Costa Rica the oceanic crust is covered by ~380 m thick sediments consisting of around 220 hemipelagic carbonate clays, beneath ~160m of siliceous hemipelagic sediments, which are interbedded by diatomaceous ooze ash layers (Saffer et al., 2000).

1.4 References

Ambraseys, N. N., and R. D. Adams (1996) Large-magnitude Central American earthquakes, 1898–1994, Geophys. J. Int., 127, 665–692, doi:10.1111/j.1365-246X.1996.tb04046.x.

Barckhausen, U., Ranero, C.R., von Huene, R., Cande, S.C., Roeser, H.A. (2001) Revised tectonic boundaries in the Cocos Plate off Costa Rica: Implications for the segmentation of the convergent margin and for plate tectonic models. J. Geophys. Res. 106, (B9), 19207-19220.

Barckhausen, U., Roeser, H.A., von Huene, R. (1998) Magnetic signature of upper plate structures and subducting seamounts at the convergent margin off Costa Rica. J. Geophys. Res. 103 (B4), 7079-7093.

Barley, B., (1999) Deepwater problems around the world. Lead. Edge 18 (4), 488– 494.

Bondevik, S., Svendsen, J.I. (1994) Annales Geophysicae, European Geophys. Soc.: 1. Solid Earth Geophysics and Natural Hazards, Suppl. 1 vol. 12, pp. C207.

Bryn, P., Berg, K., Lien, R., Solheim, A., Forsberg, K.F. (2003a) How we conclude on the Storegga Slide risk, COSTA. Continental Slope Stability Workshop 4, 10–13 Febr. 2003, Bologna, Italy, Abstr. Vol. 4 pp.

Canals, M., G. Lastras, R. Urgeles, J. L. Casamor, J. Mienert, A. Cattaneo, M. De Batist, H. Haflidason, Y. Imbo, J.S. Laberg, J. Locat, D. Long, O. Longva, D. G. Masson, N. Sultan, F. Trincardi, P. Bryn (2004) Slope failure dynamics and impacts from seafloor and shallow sub-seafloor geophysical data: case studies from the COSTA project. Mar. Geol. 213, 9–72.

Chaytor, J. D., ten Brink, U. S., Solow, A. R., Andrews, B. D. (2009) Size distribution of submarine landslides along the U.S. Atlantic margin, Mar. Geol. 264, 16-27.

Carter, R.M. (1975) A discussion and classification of subaqueous mass-transport with particular application to grain flow and fluxoturbidites. Earth-Sci. Rev. 11, 145–177.

Cook, H.E., Mullins, H.T., 1983. Basin margin environment. AAPG Mem. 33, 540–617.

Dott, R.H., 1963. Dynamics of subaqueous gravity depositional processes. AAPG Bull. 47 (1), 104– 128.

Dugan, B., P.B. Flemmings (2000), Overpressure and Fluid Flow int he New Jersey Continental Slope: Implications for Slope Failure and Cold Seeps, Science, 289, 288-291

Camerlenghi, A., Pini, G.A., 2009. Mud volcanoes, olistostromes and Argille scagliose in the Mediterranean region, Sedimentology, v. 56, issue 1, pp. 319-365

Dawson, A.G., Long, D., Smith, D.E., Shi, S., Foster, I.D.L., 1993. Tsunamis in the Norwegian Sea caused by the Storegga submarine landslides. In: Tinti, S. (Ed.), Tsunamis in the World. Kluwer Acad. Publ., The Netherlands, pp. 31– 42.

DeMets, C., 2001. A new estimate for present –day Cocos-Caribbean plate motion: Implications for slip along the Central America volcanic arc. Geophysical Research Letters 28 (21), 4043-4046.

Ehrenborg, J., 1996. A new stratigraphy for the Tertiary volcanic rocks of the Nicaraguan highland. Geol. Soc. Amer. Bull. 108, 830–842.

Fine, I.V., Rabinovich, A.B., Bornhold, B.D., Thomson, R.E., Kulikov, E.A., 2005. The Grand Banks landslide-generated tsunami of November 18, 1929: preliminary analysis and numerical modeling. Mar. Geol. 215, 45–57.

Gracia, E., Dañobeitia, J. J., PARSIFAL Team, 2003. Mapping active faults offshore Portugal (368N–388N): implications for seismic hazard assessment along the southwest Iberian margin. Geology 31 (1), 83– 86.

Gutenberg, B. & Richter, C.F.: Seismicity of the Earth and Associated Phenomena, 2nd edition. Princeton Univ. Press, New Jersey, 1954.

Haflidason, H., Sejrup, H.P., Nygard, A., Bryn, P., Lien, R., Berg, K., Masson, D.G., Forsberg, C.F., 2004. Architecture, geometry and slide development of the Storegga Slide. Mar. Geol. 213. 201–234.

Hampton, M.A., Lee, H.J., Locat, J., (1996). Submarine landslides. Rev. Geophys. 34, 33–59.

Harders, R., S. Kutterolf, C. Hensen, T. Moerz, and W. Brueckmann (2010), Tephra layers: A controlling factor on submarine translational sliding?, Geochem. Geophys. Geosyst., 11, Q05S23, doi:10.1029/2009GC002844.

Heezen, B.C., Ewing, M., 1952. Turbidity currents and submarine slumps, and the 1929 Grand Banks earthquake. Am. J. Sci. 250, 849–873.

Heezen, B.C., Hollister, C.D. (1971) The face of the deep. Oxford Univ. Press, New York, London, and Toronto.

Helm, R. (1984), Mineralogy and diagenesis of slope sediments offshore Guatemala and Costa Rica, Leg 84, Proc. Deep Sea Drill. Program Initial Rep., 15, 571-594

Hinz, K., von Huene, R., Ranero, C.R. & the PACOMAR Working Group: Tectonic structure of the convergent Pacific margin offshore Costa Rica from multichannel seismic reflection data. Tectonics 15 (1996), pp.54–66.

Hühnerbach, V. and D. G. Masson (2004), Landslides in the North Atlantic and its adjacent seas: an analysis of their morphology, setting and behavior, Mar. Geol., 213, 343-362

Kimura, G., Silver, E., Blum, P. et al., 1997. Proceedings of the ocean drilling program, 170, 458 pp.

Klaucke, I., Cochonat, P., 1999. Analysis of past seafloor failures on the continental slope off Nice (SE France). Geo Mar. Lett. 19, 245– 253.

Kutterolf, S., Freundt, A., Pérez, W., Wehrmann, H., Schmincke, H.-U. (2007), Late Pleistocene to Holocene temporal succession and magnitudes of highly-explosive volcanic eruptions in west-central Nicaragua. Journal of Volcanology and Geothermal Research, 163, 55-82.

Kutterolf, S., A. Freundt, W. Perèz, T. Moerz, U. Schacht, H. Wehrmann, H.-U. Schmincke (2008), The Pacific offshore record of Plinian arc volcanism in Central America: 1. Along-arc correlations: Geochemistry Geophysics Geosystems, 9, no. 2, doi:10.1029/2007GC00163

Ladd, J. W., & Schroder, S. (1985) Seismic stratigraphy of the continental shelf offshore Guatemala implications for vertical tectonics related to subduction, Deep Sea Drilling Project Leg 84:Initial Reports of the Deep Sea Drilling Project 84: Washington, U.S. Govt. Printing Office, pp.879–894.

Lee, H.J., W. C. Schwab, J.S. Booth (1993), Submarine landslides: an introduction. In: Schwab, W.C., Lee, H.J., Twitchell, D.C. (Eds.) (2002), Submarine Landslides: Selected Studies in the US Exclusive Economic Zone, US Geological Survey Bulletin, 158–166.

Lee, H. (2009), Timing of occurrence of large submarine landslide on the Atlantic Ocean margin, Mar. Geol. 264, 53-64.

Locat, J., Lee, H.J., 2002. Submarine landslides: advances and challenges. Can. Geotech. J. 39, 193– 212.

Lowe, D.R., 1979. Sediment gravity flows: their classification and some problems of application to natural flows and deposits. Spec. Publ. SEPM 27, 75– 82.

McAdoo, B. G., L. F. Pratson, D. L. Orange (2000), Submarine landslide geomorphology, US continental slope, Mar. Geol. 169, 103-136

McIntosh, K., Silver, E. & Shipley, T.: Evidence and mechanisms for forearc extension at the accretionary Costa Rica convergent margin. Tectonics. 12 (1993), pp.1380–1392.

Moore, D.G., 1978. Submarine slides. In: Voight, B. (Ed.), Rockslides and Avalanches: 1. Natural Phenomena. Elsevier, Amsterdam, pp. 563– 604.

Moore, J.G., Clague, D.A., Holcomb, R.T., Lipman, P.W., Normark, W.R., Toressan, M.E., 1989. Prodigious submarine landslides on the Hawaiian Ridge. J. Geophys. Res. 94, 14465– 14484.

Mulder, T., Cochonat, P., 1996. Classification of offshore mass movements. J. Sediment. Res. 66 (1), 43– 57.

Morgenstern, N., 1967. Submarine slumping and the initiation of turbidity currents. In: Richards, A.F. (Ed.), Marine Geotechnique. Univ. Illinois Press, Urbana, pp. 189–220.

Nardin, T.R., Hein, F.J., Gorsline, D.S., Edwards, B.D., 1979. A review of mass movement processes and acoustic characteristics and contrasts in slope and base-of-slope systems versus canyon-fan-basin systems. Spec. Publ.-Soc. Econ. Paleontol. Mineral 27, 61– 73.

Prior, D.B., Coleman, J.M., 1979. Submarine landslides: geometry and nomenclature. Z. Geomorphol. (N. F.) 23, 415–426.

Protti, M., Guendel, F., McNally, K. 1994. The geometry of the Wadati-Benioff zone under southern Central America and its tectonic significance: results from a high-resolution local seismographic network, Physics of the Earth and Planetary Interiors, Volume 84, Issues 1-4, Pages 271-287, ISSN 0031-9201, DOI: 10.1016/0031-9201(94)90046-9.

Ranero, C.R. & von Huene, R. (2000), Subduction erosion along the Middle America convergent margin. Nature 404, pp.748–752.

Ranero, C. R.; von Huene, R.; Flueh, E., Duarte, M. Baca, D., and K. McIntosh. 2000. A cross section of the forearc Sandino Basin, Pacific Margin of Nicaragua. Tectonic*s*, vol.19, 335-357.

Ranero, C.R., Morgan, J.P., McIntosh, K., Reichert, C. (2003), Bending-related faulting and mantle serpentinization at the Middle America Trench. Nature, 425, 367-373.

Ranero, C. R.; von Huene, R.; Weinrebe, W. and Barckhausen, U., (2007) Convergent margin tectonics of Middle America: A marine perspective. In: Central America, Geology, Hazards and Resources, pp. 239-265. Ed. G. Alvarado and J. Bundschu, A. A. Balkema Publisher

Ruepke, L.H., Phipps Morgan, J., Hort, M. & Connolly, J.A.D. (2002), Are the regional variations in Central American arc lavas due to differing basaltic versus peridotitic slab sources of fluids? Geology 30 pp. 1035–1038.

Saffer, D.M., Silver, E.A., Fisher, A.T., Tobin, H. and Moran, K., 2000. Inferred pore pressure at the Costa Rica subduction zone: implications for dewatering processes. Earth and Planetary Science Letters, 177: 193-207.

Shipley, T.H. & G.F. Moore (1986), Sediment accretion, subduction, and dewatering at the base of the trench slope off Costa Rica: A seismic reflection view of the décollement, J. Geophys. Res. 91, pp.2019–2028.

Shipley, T.H., Stoffa, P.L. &. Dean, D.F. (1990), Underthrust sediments, fluid migration paths, and mud volcanoes associated with the accretionary wedge off Costa Rica: Middle America Trench. J. Geophys. Res. 95 pp.8743–8752.

Silver, E.A., Ellis, M.J., Breen, N.A. & Shipley, T.H. (1985), Comments on the growth of accretionary wedges. Geology 13, pp.6–9.

Straub S. and Schmincke H. (1998) Evaluating the tephra input into Pacific c Ocean sediments: Distribution in space and time. Geologische Rundschau 87(3), 461- 476.

Sultan, N. P. Cochonat, M. Canals, A. Cattaneo, B. Dennielou, H. Haflidason, J.S. Laberg, D. Long, J. Mienert, F. Trincardi, R. Urgeles, T.O. Vorren, C. Wilson (2004), Triggering mechanisms of slope instability processes and sediment failures on continental margins: a geotechnical approach. Mar. Geol., 213, 291-321, doi:10.1016/j.margeo.2004.10.011

Synolakis, C.E., Bardet, J.-P., Borrero, J.C., Davies, H.L., Okal, E.A., Silver, E.A., Sweet, S., Heezen, B.C., Hollister, C.D., 1971. The Face of the Deep. Oxford Univ. Press, New York, USA. 659 pp.

Twitchel, D.C., Chaytor, J.D., ten Brink, U.S., Buczkowski, B. (2009). Morphology of late Quaternary submarine landslides along the U.S. Atlantic continental margin. Mar. Geol. v. 264, pp. 4-15, doi:10.1016/j.margeo.2009.01.009

ten Brink, U. S., E. L. Geist, B. D. Andrews (2006), Size distribution of submarine landslides and its implication to tsunami hazard in Puerto Rico, Geophys. Res. Letters, 33, L11307, doi:10.1029/2006GL026125.

Vannucchi, P., C.R. Ranero, S. Galeotti, S.M. Straub, D.W. Scholl and D. McDougall-Ried (2003), Fast rates of subduction erosion along the Costa Rica Pacific margin: Implications for nonsteady rates of crustal recycling at subduction zones: Journal of Geophysical Research,108, no. B11, 2511, doi: 10.1029/2002JB002207.

Vannucchi, P., Galeotti, S., Clift, P., Ranero, C. R.,. von Huene, R. , 2004. Long-term subduction erosion along the Middle America Trench offshore Guatemala. Geology 32, 617–620.

von Huene, R., Ranero, C.R., Weinrebe, W. 2000, Quartenary convergent margin tectonics of Costa Rica, segmentation of the Cocos Plate, and Central American volcanism. Tectonics, 19 (2), 314-334.

von Huene, R., C.R. Ranero, P.Watts (2004), Tsunamigenic slope failure along the Middle America Trench in two tectonic settings, Marine Geology, 203, 303-31

Weaver, P. P. E., R. B. Wynn, N. H. Kenyon, J. Evans (2000), Continental margin sedimentation, with special reference to the north-east Atlantic margin, Sedimentology, 47 (Suppl. 1), 239–256.

Ye, S., Bialas, J., Flueh, E.R.; Stavenhagen, A., von Huene, R., Leandro, G., & Hinz, K: Crustal structure of the Middle American Trench off Costa Rica from wide-angle seismic data. Tectonics 15 (1996), pp.1006–1021

Chapter 2

2. Methodology

2.1 Data and Material

The mutlibeam bathymetry data that imaged the seafloor along the MAT were acquired during German R/V Sonne cruises SO76, 81, 107, 144, 150, 163-1 and US R/V M. Ewing cruises 0005 and 01404 with the Atlas Hydrosweep system, Sonne 13 cruise with the SIMRAD EM-120-system from Kongsberg. During cruise SO144, SO163 and SO173 sidescan sonar data were collected with the "deep-towed side-scan sonar system" (DTS-1) and the "Towed Ocean Bottom Instrument" (TOBI) system. Parasound data were obtained during cruise M66-3. These cruises were a series of cruises from 1991-2003 into the area of Central America funded by the "Bundesministerium für Bildung und Forschung" (BMBF) and the Deutsche Forschungsgemeinschaft (DFG).

Sediment core data were collected during cruises SO173, M54/11 and M66-3 between 2002 and 2005. Grain size data of sediment samples from the collected core data were achieved, by using both a laser particle analyzer or by wet sieving. Ash beds were chemically investigated by electron microprobe (EMP) for major and minor elements and correlated to dated onshore tephra deposits. Pore water was tested for alkalinity by pressure infiltration through a pore water squeezer and a following titration. Sediment samples of the cores were taken for determination of index properties, such as bulk density and magnetic susceptibility by a GEOTEK Ltd. (UK) multi sensor whole core logger (MSCL). Shear strength values of the sediments were tested by a cone-penetrometer "Strassentest". As well as moisture content, mineral density were obtained through volume determinations. Geotechnical shear tests on dry and sieved ashes were conducted with a shear box to obtain total compaction and peak shear strength values under a specific load and shear momentum.

2.1.2 Acoustic data acquisition

The principle of hydro acoustic methods is to transmit an acoustic signal that is reflected at body, received by a hydrophone and transformed into a digital signal. The

received signals differ because of the different travel times of the compressional waves propagating through the medium. They also differ because of the specific energy loss when they hit the reflector (object). The shorter time taken for the sound pulse to return to the ship the shallower is the water. Noise and speckle are the most disturbing elements for the data quality. The noise is generated by the water itself and in the deep ocean it is mostly caused by thermal agitation like the Brownian motion of the water molecules.

2.1.3 Multibeam Bathymetry

The Atlas Hydrosweep DS Deep Sea Multibeam echo sounder is a system developed for deep ocean water, based on a sound frequency of 14.5-16 kHz. It uses 59 beams across a 90º swath. The along track and across track beam resolution is 1º or 2º and working with standard accuracy in water depth up to 11000m. The bathymetry coverage across track is 6 times the water depth to up to an absolute value of 20 km. The transducers obtain up to 395 soundings per ping, with a ping rate of approx. 10Hz. The mean sound velocity through water is automatically determined. The maximum resolution is 6.1cm with a maximum output sample rate of 12.2 kHz. The system is installed with the transducers fixed to the ships hall.

Figure 2.1: The swath of the Hydrosweep DS system from Atlas. Foto taken from: http://www.atlashydro.atlas-elektronik.com/typo3/index.php?id=2072

The multibeam swath bathymetry echo sounder EM120 from Kongsberg Simrad works with a fan of 191 sound beams measuring water depths of up to 11.000m with accuracy. The acoustic signal is transmitted and received by two transducers fixed at the ships underside. The acoustic signals are send in a range of 11.25-12.75 kHz with a maximum ping rate of 5 Hz. The data are obtained by successive emission-reception cycles of the acoustic signal. The beam coverage is 150º perpendicular to the ships travel direction and 2º in direction of the ships track. The beam spacing can be set to equidistant or equiangular. The water depth is calculated perpendicular to the ships travel direction for each of the 191 beams by the signals two-way travel time, and under consideration of sound speed variations in the water (sound wave velocity in water approx. 1500 m/s^2) and the angle of each beam. To guarantee a good data quality the ship speed during the data collection of this work was set to 3 knots. In addition the signals amplitude can be used not only to determine the water depth but also to give information about the seafloor texture (Flueh et al., 2004).

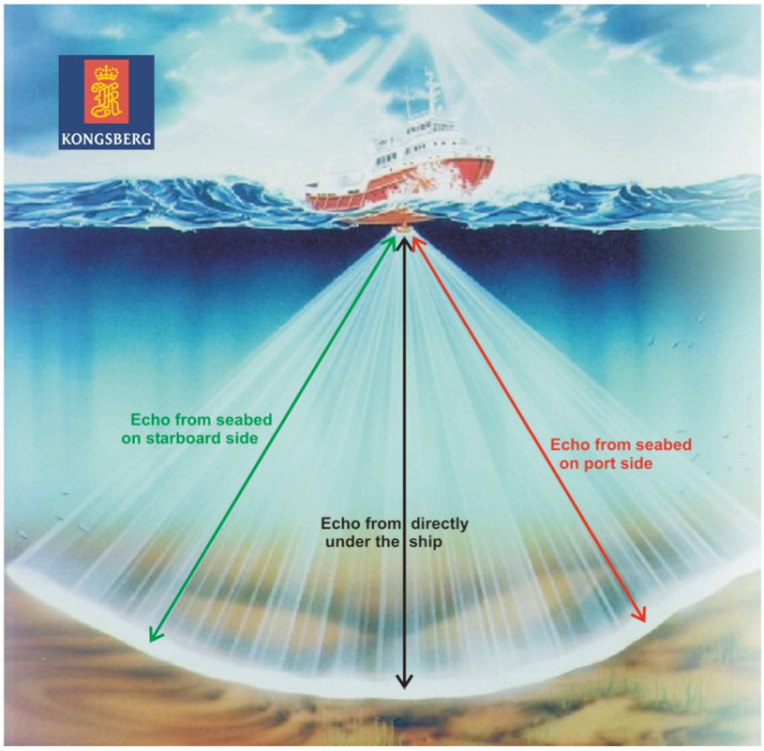

Figure 2.2: The swath of the Kongsberg system, working with 191 beams altogether. Figure taken from: http://www.antarctica.ac.uk/bas_research/instruments/swathbathymetry.php

2.1.4 TOBI Sidescan Sonar System

Sidescan sonar systems use sound waves to identify textures and changes in the type of sediment present on the seafloor. The Towed Ocean Bottom Instrument (TOBI) system is a work station that comprises a two-sided 30kHz sidescan sonar, a 7.5kHz sub-bottom profiling sonar, a set of scientific instruments (magnetometer and CTD), and a range of vehicle attitude sensors (pitch, roll, and heading from a gyro-compass). The underwater vehicle is towed with a 200 m umbilical behind a depressor weight. The depressor is attached to the surface ship via the main 0.68" armored coax cable. This towing method prevents ship induced heave influencing the vehicle.

Figure 2.3: The TOBI system is towed behind a research vessel, emitting sound waves to the seafloor and penetrate the top few cm of the seafloor sediments. Figure taken from: http://www.noc.soton.ac.uk/shmg/mapping-themes/deep-water-habitats

The vehicle is usually 'flown' at heights of between 200 to 500 m above the seabed. All signals to and from the vehicle are sent via the single coax conductor. Signals are processed on the ship and logged onto magneto-optical disks. The system can work in water depth of up to 6.000m. The system uses a frequency of 30-32 kHz and a pulse length of 2.8ms. It has a maximum range to each side of the instrument of 3000m and a footprint size of 8 x 3.5m along track and 43 x 2.1m across track.

2.1.5 Data Processing

Processing of multibeam bathymetry data with the help of special software includes cleaning from noise and the creation of a mosaic derived from the amplitude measurements, to obtain information about the lithological properties of the seafloor. Other software is used for the processing of sidescan sonar data, where the data tracks of the sidescan sonar have to be georeferenced and then put together into a mosaic.

2.1.6 Processing of Atlas Hydrosweep DS and Sounder EM120 data

The Hydrosweep bathymetry data were cleaned and converted to depth soundings with the MBsystem [Caress and Chayes, 1996] and gridded with GMT [Wessel and Smith,1998] at 0.001 degrees node spacing. The sound velocity of the water column was obtained by CTD measurements. The EM120 have been processed with the software package CARAIBES from IFREMER, Brest (France), with water velocities taken from CTD measurements. The data were iteratively gridded and cleaned from noise in each step. The final grid of 50 x 50m was exported to GMT and merged with bathymetry data of former cruises.

2.1.7 Processing of sidescan sonar data

Processing of the sidescan sonar data was done with the software PRISM (Le Bas et al., 1999 and Le Bas 2002) and the commercial ERADS Imaging package. Processing includes in a first step data conversion into NetCDF format (Network Common Data Format) Rew and Davis, 1990). PRISM picks the vehicle elevation automatically during conversion. The NetCDF data are then quality checked with several rout lines within the PRISM package. Depending on the size of the data set it is recommended to separate a large dataset into several map sheets. The best suitable size for a map sheet is proposed by the program. Then options available on PRISM can be chosen for the suitable processing, including navigation merging, slant-range correction, various filters and a shading correction. The final image is an ERDAS file, created for each map sheet and can be further processed with the software package of ERDAS. Within PRISM multi-band images are generated, if tracks are overlapping. These images can then be stencillised in ERDAS. Afterwards all map sheets can be merged into one mosaic. ERDAS creates a geo.tif, which can then be imported into IVS Fledermaus or ESRI ArcGIS for draping it over bathymetry data, and further detailed analysis.

2.1.8 The Parasound System

The parasound system (Gerriets et al., 2003) is a sediment echo sounder that provides a vertical view into the sediment succession for approx. the first 200m below seafloor. It uses the parametric effect, which is the non-linear acoustic interaction of finite amplitude waves. This effect is generated when two sound waves of different frequencies but high amplitude are emitted simultaneously. The transducers of the system send out 18kHz and 22kHz, creating a signal of 4 kHz with duration of 250 µs. Pulses are emitted every 400ms until a first echo arrives, while the length of the reception window is 266ms, which accounts for the depth window of 200m. The footprint of the systems is 7% of the water depth. During data collection on cruise M66-3 the ships velocity was set to a speed between 2 to 4 knots. The data were stored as ps3 files and plotted with the software SENT from University of Bremen.

2.1.9 Core location and positioning

Processed Multibeam bathymetry data were displayed with „IVS 3D Fledermaus“ enabling exploration of the virtual 3D data space. Different illuminations were applied to identify the slides morphology and define their geographical location. Parasound profiles of ~ 1 nautical mile length were shot perpendicular to slide headwalls starting from the upper slide plane along the headwall into the undisturbed sediments. Core positions were planned for translational slides of specific interest. For each slide two to three cores were placed into the slide plane, close to the headwall, and one core placed outside the slide into undisturbed sediment. Core positioning during coring was controlled by simultaneously taken Parasound data. Due to great water depths (> 1000m-3000m) the rope tension of the gravity device may have lead to derivations of the core at the seafloor, leading to a possible shift of the position within a radius of up to ~250m relative to the hook on the crane where the rope is fixed to (pers. com. Eric Stehn 2006, technical assistant R/V Meteor cruise M66/3a).

2.1.10 Gravity core recovery

Sediment cores of 6 and 9 m lengths were taken by gravity coring during the cruise. The coring device composed of a 1.5-t-weight on top of a 6 or 9m long steel tube coated with an inner PVC liner. The outer liner diameters are 12.5 cm and average liner

thickness is around 2.5 mm. As soon as the cores arrived on board they were cut into 1 m long segments, locked at both sides and stored in a cooled (4°C) room, waiting for Multi Sensor Core Logger (MSCL) measurements soon after (< 1hour).

2.1.11 Core logging

Each segment end was sampled for gas-analysis with syringes and afterwards prepared for geotechnical logging with the GEOTEK Ltd. (UK) multi sensor whole core logger (MSCL). 4 parameters were measured directly: wet bulk density, magnetic susceptibility, p-wave velocity and temperature. [Blum 1997, Tittman and Wahl 1965, Evans 1965]. After geotechnical core logging the cores were cut lengthwise to sample the sediment for pore water chemistry, moisture content, mineral density, undrained shear strength and for subsequent description including core photography.

2.1.12 Geochemistry

The pore water was retrieved by pressure filtration in a pore water squeezer that operated with argon at a pressure up to 5bar. Absolute values for Alkalinity [mmol(eq) l^{-1}], H2S [µmol l^{-1}], NH4 [µmol l^{-1}], PO4 [µmol l^{-1}], Cl [mmol l^{-1}], Si [µmol l^{-1}] and CH4 [mmol l^{-1}] were obtained. For further information see http://www.ifm-geomar.de/index.php?id=mg_analytik.

2.1.13 Geotechnical index properties

Moisture content and mineral density were determined through mass and volume determinations [Blum 1997, DIN]. For this purpose core specimens of exactly 10 cm3 were extruded from the cores with an open-ended stainless steel cylinder. Moisture content was determined by measuring the specimen's mass before and after removal of interstitial pore fluid through oven drying for 24 hours at temperatures varying from 90° to 110°C. Moisture content, porosity, and void ratio are defined by the mass or volume of extracted water, corrected for the mass and volume of salt evaporated during the drying process [ASTM 1990]. The mass and volume of the evaporated pore-water salts are calculated for a standard seawater salinity (35), seawater density at laboratory conditions (1.024 g cm^{-3}), and an average seawater salt density of 2.20g cm^{-3} following ODP procedures described in Blum [1997]. We used two different ways to determine index properties: Wet-bulk volume was measured with the 10cm^3 volume sampler and

consequent determination of the grain density using the penta-gaspygnometer from Quantachrom with Helium 4.6 as a measuring gas. In order to assess the geotechnical properties of sediments from the slide locations off Costa Rica and Nicaragua the undrained shear strength "cu" was determined using a fall-cone method. The fall-cone testing was conducted with a "Strassentest" Kegelfallpenetrometer (fall cone tester). The cone has an angle of 60° and a mass of 85g. The cone was lowered carefully to the surface of the sediment and than fell free and rested in the sediment for five seconds until no further movement could be expected. Finally the depth of penetration was measured with a dial gauge. The undrained shear strength was determined with the equation of Hansbo [1957] with the coefficients from Houlsby [1982]:

$cu = k*M*h^{-2}$

where k is an empirical Factor determined by the cone angle, M is the mass of the cone and h is the penetration depth of the cone.

2.1.14 Grain size analysis

Ashes were taken out of the cores to determine their grain sizes by wet sieving. The samples were cleaned from organic and carbonate matter with H_2O_2 and acetic acid, dried in the oven for 24 hours at 105°C and weighed afterwards. Samples were then filled with distilled water and put into an ultra sonic sound bath for 5 minutes. Afterwards they were wet sieved with ASTM sieves of 63µm, 120µm, 250µm and, 500 µm mesh size, dried at 105 °C and each fraction weighed.

2.1.15 Shear tests

Sieved dry ash was loosely put into a shear box for the direct shear test. We sheared mono grain size ashes and combinations of different grain sizes. The box was filled with a volume of around 100cm³ dry ash. The box was loaded with a 16 kg weight, producing an effective vertical stress of 40 kPa, which is similar to vertical stresses existing in 7 m depths bsf. The shear velocity was put to very low values of 0.5 mm min^{-1} going in one direction until residual shear strength was reached. With the same velocity the direction was changed to get back to the starting position. For each grain size and the grain size combinations at least 4 rounds were sheared until no significant changes in peak shear strengths were detected when compared with the previous round. Total displacement, shear strengths and total compaction were measured. The direct

shear test was done following the suggestions given by the DIN 18137-3 (Deutsches Institut für Normung) (2002).

2.1.16 Dating and correlation of ash beds

For age determination offshore volcanic ash samples were chemically correlated with deposits on land (Kutterolf et al., 2008). The charcoal contents of onshore samples were analyzed at the Leibniz Laboratory for Radiometric Dating and Isotope Research at the University of Kiel. The selected samples were mechanically cleaned under the microscope, afterwards sieved, and dark organic-looking material < 250 µm was selected for further treatment. The residual material was then extracted with 1 % HCl and 1 % NaOH at 60°C and again with 1 % HCl. The alkali extraction of the organic fraction (humic acid fraction) was precipitated with HCl, washed, and dried. The combustion to CO_2 of all fractions was performed in a closed quartz tube together with CuO and silver wool at 900°C. The C^{14} concentration of the samples was measured by comparing the simultaneously collected C^{14}, C^{13}, and C^{12} beams of each sample with those of Oxalic Acid standard CO_2 and coal background material. The C^{14} ages were calculated according to Stuiver and Polach (1977) with a δC^{13} correction for isotopic fractionation based on the 13C/12C ratio measured by the AMS system simultaneously with the C^{14}/C^{12} ratio.

Marine ash beds and matrix glass were analyzed by electron microprobe (EMP) for major and minor elements. EMP analyses were conducted on epoxy embedded samples with a CAMECA SX 50 wavelength dispersive electron microprobe at IFM-GEOMAR, Kiel. Major element compositions were determined at 15 kV accelerating voltage and a beam current of 10 nA for basaltic glass and 6 nA for felsic glass. Peak counting times were 30 to 60 s for most major elements and 60 to 100 s for the trace elements and backgrounds. The beam was defocused to 10 µm to minimize analytical Na loss. Natural and synthetic glasses and minerals were used as standards for calibration. Standard deviation is less than 2% for major elements and <10% for tracer elements. All analyses have been normalized to 100% to eliminate the effects of variable post-depositional hydration from the comparison between marine and/or on-land tephras.

2.2 References

Blum, P. (1997), Physical properties handbook: A guide to the shipboard measurement of physical properties of deep-sea cores. ODP Tech. Note, 26. available from http://www-odp.tamu.edu/publications/tnotes/tn26/INDEX.HTM.

Caress, D. W., and D. N. Chayes (1996), Improved processing of Hydrosweep DS multibeam data on the R/V Maurice Ewing, Mar. Geophys. Res., 18, 631–650, doi:10.1007/ BF00313878.

DIN 18137-3 (Deutsches Institut für Normung e.V.) (2002), Soil, investigation and testing - Determination of shear strength - Part 3: Direct shear test

Flueh. E., Söding, E., Suess, E. (Eds.), 2004. RV SONNE Cruise Report SO173/1, 3&4-Suubduction II: The Central American Continental Margin. Vol. 115 of GEOMAR Report. GEOMAR, Kiel.

Gerriets, A., von Lom-Keil, H., Spiess, V., Zwanzig, C., Bruns, R., 2003. A major upgrade of the sediment echosounder ATLAS PARASOUND and the digital acquisition software ParaDigMA for high-resolution seafloor studies. EGS – AGU – EUG Joint Assembly, Abstracts from the meeting held in Nice, France, 6-11 April 2003, 11720.

Hansbo, S. (1957), A new approach to the determination of the shear strength of clay by the fall-cone test.: Proceedings of the Royal Swedish Geotechnical Institute, 14, 5-47

Houlsby, G.T. (1982), Theoretical analysis of the fall cone test: Géotechnique, 32, 111-119.

Kutterolf, S., A. Freundt, W. Perèz, T. Moerz, U. Schacht, H. Wehrmann, H.-U. Schmincke (2008), The Pacific offshore record of Plinian arc volcanism in Central America: 1. Along-arc correlations: Geochemistry Geophysics Geosystems, 9, no. 2, doi:10.1029/2007GC00163

Le Bas, T., Hühnerbach, V., (1999). PRISM processing of remoteley-sensed imagery for seafloor maping, version 3.1. International Rtepor. Southampton Oceanography Centre.

Le Bas, T., 2002. P.R.I.S.M.- Processing of Remote –sensed Imagery for Seafloor Mapping. A collection of software for the processing, analysis and enhancememt of side-scan sonar imagery using geometric corrections for seafloor characterisation and mapping.

Rew, R., Davis, G., (1990). Netcdf: an interface for scientific data access. Computer Graphics and Applications, IEEE 10 (4), 76-82, Unidata Progam Center, Boulder, CO.

3

Submarine slope failures along the convergent continental margin of the Middle America Trench

R. Harders, C. Ranero, W. Weinrebe, J.H. Behrmann

Published in G^3, Volume 12, Number 6, June 2011, Q05S32,
doi:10.1029/2010GC003401 ISSN: 1525-2027

Geochemistry Geophysics Geosystems G3

Article
Volume 12, Number 6
24 June 2011
Q05S32, doi:10.1029/2010GC003401
ISSN: 1525-2027

Published by AGU and the Geochemical Society

Submarine slope failures along the convergent continental margin of the Middle America Trench

Rieka Harders
SFB 574, Leibniz-Institut für Meereswissenschaften an der Universität Kiel (IFM-GEOMAR), Wischhofstrasse 1-3, D-24148 Kiel, Germany (rharders@ifm-geomar.de)

César R. Ranero
Barcelona Center for Subsurface Imaging, ICREA, Instituto de Ciencias del Mar, CSIC, Pg. Marítim de la Barceloneta 37-49, E-08003 Barcelona, Spain (cranero@icm.csic.es)

Wilhelm Weinrebe and Jan H. Behrmann
SFB 574, Leibniz-Institut für Meereswissenschaften an der Universität Kiel (IFM-GEOMAR), Wischhofstrasse 1-3, D-24148 Kiel, Germany (wweinrebe@ifm-geomar.de; jbehrmann@ifm-geomar.de)

[1] We present the first comprehensive study of mass wasting processes in the continental slope of a convergent margin of a subduction zone where tectonic processes are dominated by subduction erosion. We have used multibeam bathymetry along ~1300 km of the Middle America Trench of the Central America Subduction Zone and deep-towed side-scan sonar data. We found abundant evidence of large-scale slope failures that were mostly previously unmapped. The features are classified into a variety of slope failure types, creating an inventory of 147 slope failure structures. Their type distribution and abundance define a segmentation of the continental slope in six sectors. The segmentation in slope stability processes does not appear to be related to slope preconditioning due to changes in physical properties of sediment, presence/absence of gas hydrates, or apparent changes in the hydrogeological system. The segmentation appears to be better explained by changes in slope preconditioning due to variations in tectonic processes. The region is an optimal setting to study how tectonic processes related to variations in intensity of subduction erosion and changes in relief of the underthrusting plate affect mass wasting processes of the continental slope. The largest slope failures occur offshore Costa Rica. There, subducting ridges and seamounts produce failures with up to hundreds of meters high headwalls, with detachment planes that penetrate deep into the continental margin, in some cases reaching the plate boundary. Offshore northern Costa Rica a smooth oceanic seafloor underthrusts the least disturbed continental slope. Offshore Nicaragua, the ocean plate is ornamented with smaller seamounts and horst and graben topography of variable intensity. Here mass wasting structures are numerous and comparatively smaller, but when combined, they affect a large part of the margin segment. Farther north, offshore El Salvador and Guatemala the downgoing plate has no large seamounts but well-defined horst and graben topography. Off El Salvador slope failure is least developed and mainly occurs in the uppermost continental slope at canyon walls. Off Guatemala mass wasting is abundant and possibly related to normal faulting across the slope. Collapse in the wake of subducting ocean plate topography is a likely failure trigger of slumps. Rapid oversteepening above subducting relief may trigger translational slides in the middle Nicaraguan upper Costa Rican slope. Earthquake shaking may be a trigger, but we interpret that slope failure rate is lower than recurrence time of large earthquakes in the region. Generally, our analysis indicates that the importance of mass wasting processes in the evolution of margins dominated by subduction erosion and its role in sediment dynamics may have been previously underestimated.

Components: 11,500 words, 18 figures, 1 table.

Keywords: convergent margin; landslides; slope failure; subduction erosion; submarine mass wasting; tectonics.

Index Terms: 3060 Marine Geology and Geophysics: Subduction zone processes (1031, 3613, 8170, 8413); 3070 Marine Geology and Geophysics: Submarine landslides.

Received 18 October 2010; **Accepted** 12 April 2011; **Published** 24 June 2011.

Harders, R., C. R. Ranero, W. Weinrebe, and J. H. Behrmann (2011), Submarine slope failures along the convergent continental margin of the Middle America Trench, *Geochem. Geophys. Geosyst.*, *12*, Q05S32, doi:10.1029/2010GC003401.

Theme: Central American Subduction System
Guest Editors: G. Alvarado, K. Hoernle, and E. Silver

1. Introduction

[2] Submarine landslides are a geohazard that threatens life, property near or at the seashore, and industrial investments offshore. Tsunamis generated by submarine landslides strike populated coastlines, like off Papua New Guinea at the Sissano Lagoon in 1998 [*Tappin et al.*, 2001], and can destroy offshore infrastructures [e.g., *Fine et al.*, 2005]. To evaluate their occurrence and advance a global understanding of the generation of submarine mass movements, the style, size, frequency, and relation to underlying tectonic and hydrogeological processes need to be studied.

[3] Large-scale studies of different tectonic settings are important to understand how tectonic and sedimentary processes relate potential regional preconditioning factors, and trigger mechanisms for slope instability. Here we present a comprehensive inventory of mass wasting structures along more than 1300 km of the convergent margin of the Middle America Trench (MAT), including the region studied by *von Huene et al.* [2004a] and *Hühnerbach et al.* [2005] (Figure 1). We use expanded and higher-resolution bathymetric coverage, and evaluate additional side-scan sonar data, collected in selected areas after inspection of seafloor relief maps. We describe the spatial occurrence and style of the different slope failure structures from the border of Mexico and Guatemala to southernmost Costa Rica at the border with Panama, and discuss their relation to the tectonically segmented margin, review possible preconditioning factors, and infer potential triggers.

[4] This study represents the first comprehensive study of mass wasting processes along a convergent margin that is dominated by tectonic erosion processes [*Ranero and von Huene*, 2000]. The data show that changes in style and abundance of slope failures define a segmentation along the slope of the margin (Figures 1 and 2). Similarly, different failure types typically characterize the lower, middle and upper slope sectors of every segment. We interpret that the along margin segmentation, and across slope changes reflect variations in the intensity and style of the tectonic processes related to subduction erosion. In turn, the style and intensity of tectonic erosion along the subduction zone is possibly related to a first degree to changes in volcanic construction relief (ridges and seamounts) and topography formed by bending-related deformation (horst and graben), and age of the incoming oceanic plate. The changes in character of the incoming ocean plate define a segmentation that spatially corresponds to the continental slope segmentation opposite.

1.1. Previous Work on Slope Failure at Subduction Zones

[5] Only one similarly large-scale study of mass wasting processes at a subduction zone has been previously carried out [*McAdoo et al.*, 2000]. *McAdoo et al.* [2000] investigated the accretionary prism offshore Oregon, where failures are attributed to tectonic oversteepening of the prism, and are possibly triggered by seepage forces [*Orange and Breen*, 1992]. In contrast, no previous comprehensive studies of submarine mass movements at active erosive margins exist. At erosional margins, works describe single or a few landslides, for example at the Peru margin [*von Huene et al.*, 1989], offshore Costa Rica and Nicaragua [*von Huene et al.*, 2004a; *Hühnerbach et al.*, 2005] and along the slope off New Zealand [*Kukowski et al.*, 2010]. A larger-scale investigation offshore Ecuador focused on the nature and distribution of turbiditic deposits,

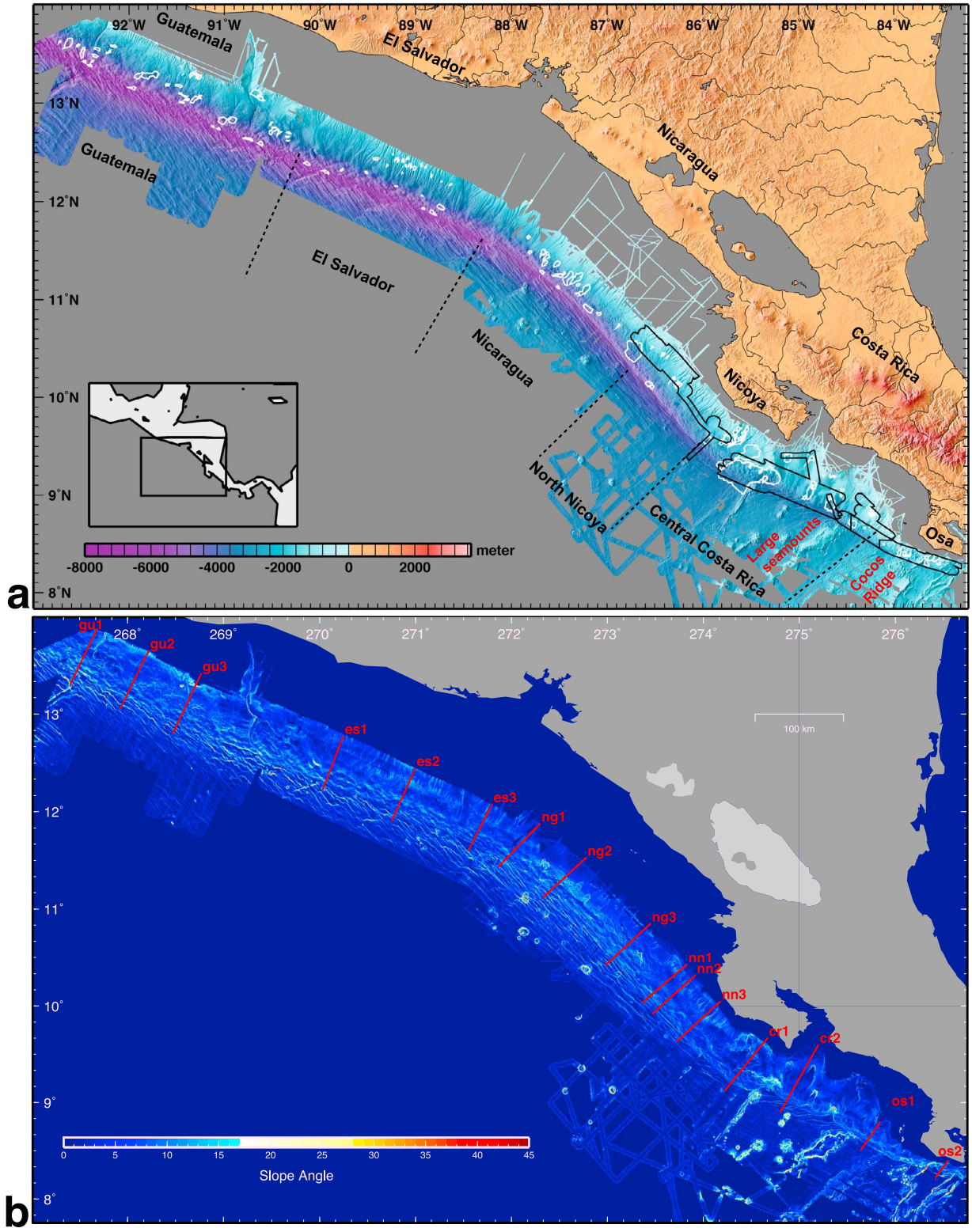

Figure 1. Data coverage along the study area of the Middle America Trench from the border of Mexico-Guatemala to the border of Costa Rica–Panama. (a) Color-coded, shaded relief digital terrain elevation of the ocean and continental plates along the MAT. The black polygons mark areas mapped with side-scan sonar. The inventory of failures includes 147 mass wasting structures (white polygons). The distribution of failures appears to be grouped in six slope segments that are delimited by black dashed lines. (b) Local slope angle used with the relief data and side-scan sonar data to map failures. Lines indicate location of profiles in Figure 2.

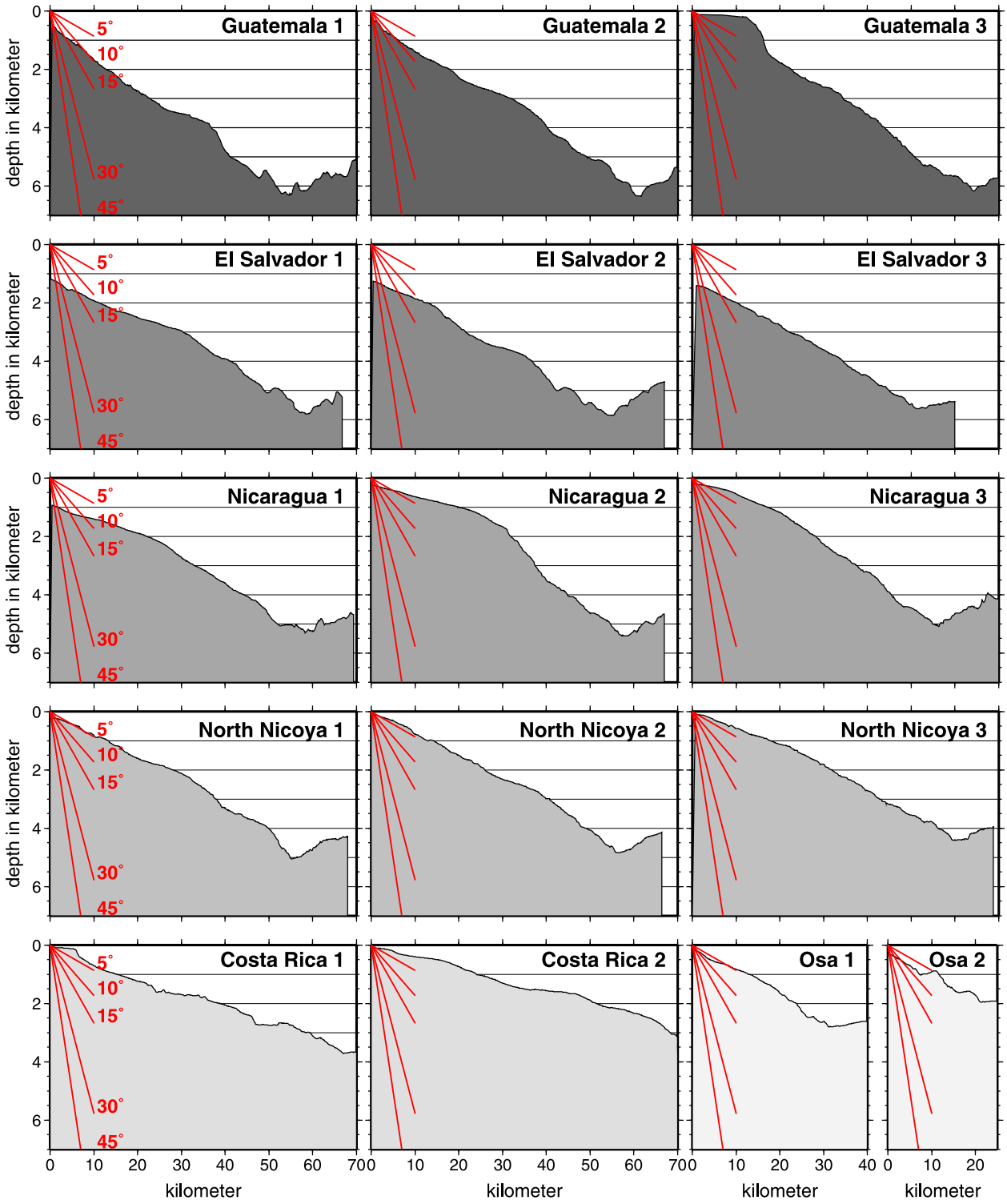

Figure 2. Selected bathymetric profiles across the different segments at representative locations to show regional slope morphology and slope dip angle (profile locations shown in Figure 1b).

but did not explicitly analyze the failure structures in the continental slope [*Ratzov et al.*, 2007].

1.2. Preconditioning and Trigger Mechanisms

[6] Preconditioning factors are those that may make areas prone to future failure, e.g., overall stress history, sediment type, grain size distribution, prior straining, degree of saturation and gas hydrate dissolution and dissociation [e.g., *Sultan et al.*, 2004]. The trigger of submarine mass movements is defined as the external stimulus that initiates slope instability [*Sultan et al.*, 2004], such as slope oversteepening, seismic loading, and storm wave loading. When occurring at exceptionally fast rates, some preconditioning factors might become triggers. Examples of these factors are very high sedimentation rates [e.g., *Sawyer et al.*, 2007], sediment underconsolidation caused by overpressures [e.g., *Flemings et al.*, 2008], overpressure generated by gas hydrate dissociation [e.g., *Mienert et al.*, 1998], groundwater sapping [*Johnson*, 1939], and factors related to glacial unloading (e.g., flexing of the crust), and rapid sedimentation of low-plasticity silts [*Locat and Lee*, 2002].

[7] Early studies along the MAT recognized signs of slope mass wasting offshore Guatemala and Costa Rica [*Aubouin et al.*, 1982; *Baltuck et al.*, 1985] but were based on geographically restricted data sets. The only investigations on mass wasting of regional significance have been carried out offshore central Costa Rica and a slope section offshore Nicaragua with limited bathymetric, seismic reflection data [*von Huene et al.*, 2004a], and in the same Costa Rica area with side-scan sonar data [*Hühnerbach et al.*, 2005]. *von Huene et al.* [2004a] showed how subduction of large seamounts in Costa Rica deforms the slope sediment and basement (the so-called margin wedge), causing large rotational slumps with deep-seated slide planes, the largest of which were possibly tsunamigenic [*von Huene et al.*, 2004a]. They also show that a sector of the Nicaragua slope contains translational slides, of uncertain origin, some of which might be related to a liquefaction phenomenon at intercalated ash layers [*Harders et al.*, 2010].

1.3. Tectonic Setting of the Active Erosive Margin of Middle America

[8] The convergent margin of the MAT is dominated by tectonic erosion processes. Evidence for tectonic erosion during much of Neogene time has been found at the Guatemala [*Vannucchi et al.*, 2004], Nicaragua [*Ranero et al.*, 2000] and Costa Rica [*Ranero and von Huene*, 2000; *Vannucchi et al.*, 2003] segments of the margin. Basal subduction erosion removes material from the underside of the overriding plate causing a progressive oversteepening of the continental slope. Frontal subduction erosion is a direct consequence of subducting ocean plate relief and slope failure. Both processes control the architecture of the margin created by long-term tectonics [*Ranero et al.*, 2008]. Related to subduction erosion the continental margin undergoes (1) fracturing and pronounced, spatially localized and temporally limited, uplift and oversteepening above subducting seamounts, ridges and large horsts of the underthrusting plate; (2) widespread extensional faulting subparallel to the trench axis; and (3) gradual slope oversteepening. All three processes favor occurrence of mass-wasting phenomena along these types of margins. About 85 km of oceanic plate are subducted per million years at current convergence rates [*DeMets et al.*, 1990], thus numerous seamounts, grabens and ridges underthrust the overriding plate in that time. This implies that most landslide scars and mass wasting deposits on the lower continental slope are rapidly modified by tectonics and the structures mapped in this study are possibly not older than several hundred thousand years. The preservation potential of slides at passive margins, or active margins with accretionary prisms is likely higher as these do not undergo continuous modification of surface and deep structures, except at those where a exceptionally high sediment input and related frequent failures overprint older features.

2. Methods

2.1. Seafloor Mapping

[9] Multibeam bathymetric data along the MAT were collected during German R/V *Sonne* cruises SO76, 81, 107, 144 legs 1 and 2, 150, 163 leg 1, and U.S. R/V *Maurice Ewing* cruises 0005 and 0104 using the Atlas Hydrosweep system and, *Sonne* 173 leg 2 cruise using the Kongsberg Simrad EM-120 system. Water velocity profiles were calculated from CTD measurements conducted during most of these cruises. The bathymetric data were cleaned and converted to depth soundings with the MB system [*Caress and Chayes*, 1996] and gridded with GMT [*Wessel and Smith*, 1998] at 0.001° node spacing [*Ranero et al.*, 2005]. Side-scan sonar data were collected along most of the Costa Rica slope and a segment off Nicaragua with the "towed ocean bottom instrument system" (TOBI system) during

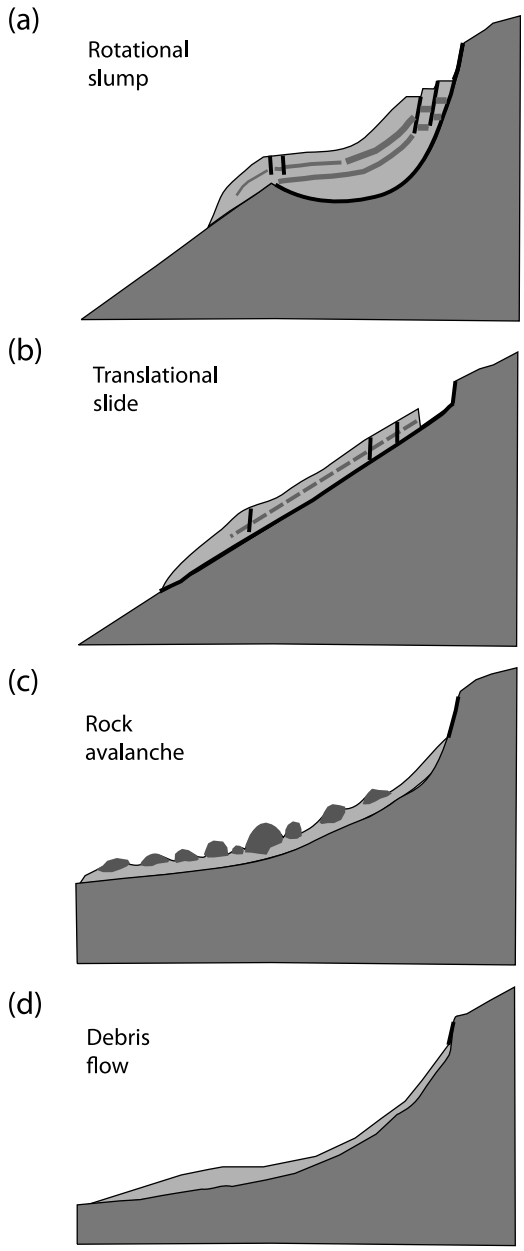

Figure 3. Conceptual cartoons of a cross section of submarine (a) rotational slump; (b) translational slide; (c) rock avalanche, a cohesionless slump with deposits containing large blocks; and (d) debris flow, cohesionless plastic flow containing boulders.

Sonne cruises 163, 144 and the "deep-towed side-scan sonar system" (DTS-1) during *Sonne* 173 [*Bialas et al.*, 1999; *Weinrebe and Flueh*, 2002; *Weinrebe and Ranero*, 2004; *Hühnerbach et al.*, 2005; *Sahling et al.*, 2008].

[10] Our inventory includes only failure structures with clear headwall scarps and flanking sidewalls. The horizontal resolution of the bathymetry allowed for the identification of landslides scars with dimensions of >0.5 km length, and >1 km width. The minimum height of vertical features, like headwalls, that could be indentified is >20–40 m high. Smaller features have been locally observed but they are not well defined along the margin segments and thus were not included in the inventory. In general, resolution of the bathymetric grids is higher in the shallower areas of the upper slope due to data redundancy and higher accuracy of water depth measurement, with net resolution also depending on coverage.

2.2. Classification and Terminology

[11] In this work we use the term landslide, mass wasting structure and slope failure as general terms, not implying specific mechanisms, whereas the terms "translational" slide and "rotational" slump imply a failure mechanism (Figure 3).

[12] We use the classification of *Hampton and Lee* [1996], as well as that of *Mulder and Cochonat* [1996] even though the "cohesion" of the failed material that is used to define the terms "translational slide" and "rotational slump" is often unclear in our study, as there was often no identifiable failure deposits. However, we think that we can use these classification schemes to characterize the mapped mass wasting structures on the fore arc: Rotational slumps are defined by a scoop-shaped slide plane, relatively short runout distances and relatively high headwalls. Translational slides with strata parallel slide planes display relatively long runout distances, in relation to their headwall heights. Rock avalanches display a cohesionless slump with deposits containing large blocks (Figure 3). Debris flows are cohesionless plastic flows containing boulders. Creep is defined as slow sediment deformation that does not result in a clear headwall, sidewalls or an exposed slide plane. Instead the seafloor shows wavy sediment features such as compressional ridges that are generated by slow, downslope movements of the sediment.

[13] We additionally use the Skempton ratio (max. headwall height to slide length ratio) to constrain the translational or rotational character of the slide or slump, if the failure plane does not show either a clear rotational or translational character. Ratios <0.15 define a translational slide and ratios >0.33 define a rotational slump [*Skempton and Hutchinson*, 1969]. Many failures in our study have a translational slide plane but are disintegrative and lack visible deposits outside the scar area. In those cases, only the scar with a headwall and sidewall could be

Table 1. Main Characteristics Defining the Segments of the Continental Slope[a]

Segment	Failure Mode			Continental Slope		Main Preconditioning Mechanism
	Upper Slope	Midslope	Lower Slope	Width (km), Minimum–Maximum, Average	Dip Angle (deg), Minimum–Maximum, Average	
Cocos Ridge–Osa Peninsula		RA, SP	RA, SP	6.5–20, 8	6–20, 8	Regional oversteepening by tectonic erosion. Fractures by ridge relief.
Seamounts–Central Costa Rica	SD	RA, SP	RA, SP	44–73, 56	2.5–4.5, 3.5	Local oversteepening and fractures by uplift by subducting seamounts.
North Nicoya		SD	SP	52–55, 53	4.5–4.7, 4.6	Ash layers.
Nicaragua		SD	SP	43–51, 48	4.6–5.6, 5.1	Oversteepening, regionally by tectonic erosion and locally by seamounts. Normal faults. Ash layer.
El Salvador	SD		SP	49–57, 52	3.6–4.7, 4.4	Oversteepening by canyon erosion.
Guatemala	SD	SP	SP	49–64, 55	4.8–6.1, 5.3	Oversteepening by tectonic erosion. Normal faults.

[a]RA, rock avalanche; SP, slump; SD, slide. Slope dip angle has been estimated from profiles of the entire width of the slope.

detected, and, therefore (under our scheme of classification) the runout distances are limited to the scar toe and represent only minimum distances. Lacking visible runout distances of the landslides makes comparisons with mass wasting structures of other margins more difficult, as the full information of dimension and the dynamic rheology (often inferred from the Skempton ratios) are not well constrained by that method here. Nevertheless, in our study morphologies of slide scars indicating translational character have Skempton ratios that fall into the translation type of slide, even when deposits could not be included in the measurement.

3. Results: Segmentation of Distribution of Slope Failures

[14] Using multibeam bathymetry from Guatemala to Panama and deep-towed side-scan sonar data from the continental slope of Nicaragua and Costa Rica we mapped 147 mass wasting structures that fall within 5 main failure types (rotational slump, translational slide, rock avalanche, debris flow, and creep) (Figure 1). Within these 5 main failure types we found that the prevailing styles of failure plane and deposits are different in several areas of the margin. We found that failure distribution displays a partitioning in six slope segments visible in their map distribution (Figure 1).

[15] The segmentation of the slope (Figure 1) is apparent when average slope dip and width (Figure 2), dominant failure mode, and failure abundance are compared (Table 1). Interestingly, a segmentation with similar dimensions occurs in the character of the ocean plate. The slope of the Cocos Ridge–Osa Peninsula segment contains mainly slumps and rock avalanches in the lower-middle slope. These failures are related to the subduction of sharp crests over the broad Cocos ridge (Figure 1 and Table 1). The Seamounts–Central Costa Rica segment shows rotational slumps and large scars caused by underthrusting of large seamounts. The North Nicoya segment is defined by a decrease in slope failure occurrence, and a few, comparatively small translational events characterize the segment. Here, the ocean plate is the smoothest along the trench (Figure 1 and Table 1). A transition leads to the Nicaragua segment, characterized by abundant, large translational slides, and an ocean plate containing abundant small seamounts and trench axis–parallel horst and graben relief. El Salvador segment is defined by a stable lower and middle slope, and abundant, small translational slides in the upper

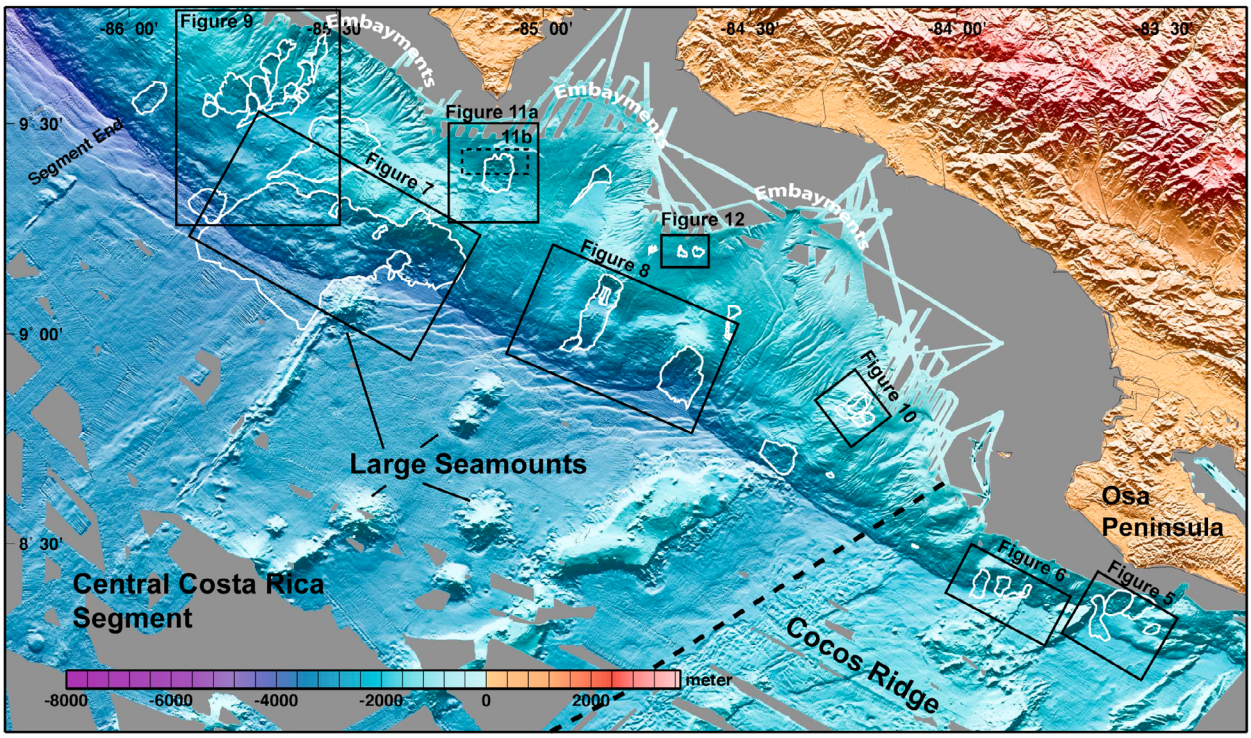

Figure 4. Seamounts–Central Costa Rica segment and Cocos Ridge–Osa Peninsula segment. The incoming plate of the segment is separated into a seamount-dominated and a ridge-dominated region. Failures in the slope also show a relation to the incoming plate relief domains. The margins display rotational slumps and scars from seamount subduction. Close-ups of representative structures and their interpretations are shown in Figures 5–12 as marked by the black boxes.

slope. Here the plate lacks seamounts and horst and grabens strike oblique to the trench. The Guatemala segment is dominated by abundant, comparatively small slumps across the lower-middle slope and a hummocky slope terrain. The ocean plate displays the most pronounced horst and graben relief.

3.1. Cocos Ridge–Osa Peninsula Segment

[16] The southernmost segment boundary is marked by data coverage. The north boundary is delineated by the outcrops of the Cocos Ridge crust. Here 1.0–1.5 km high crests ornamenting the broad, elevated topography of Cocos Ridge collide with the continent (Figure 4). The slope is narrow and steep with an average width of 8 km and angles of 6°–20° (Table 1 and Figure 2).

[17] Offshore Osa Peninsula (Figures 1 and 4) the >100 km wide Cocos Ridge is subducting. The ridge forms a 1.5 km high swell, with local seafloor relief 0.5–1 km high [*von Huene et al.*, 2000]. We mapped previously unidentified rotational slumps and associated rock avalanches caused by subduction of local ridges (Figures 4, 5, and 6). A subducting ridge crest with steep flanks caused the Sirena slump (Figure 5), with the failed material deposited along the southern steeper flank. The headwall height is 1000 m, with maximum slope angle of 51° in the uppermost part and 30° in the lower part. The length of transport of the deposits is visible, with the front of the failed mass forming a tongue shaped toe (Figure 5). The runout distance is 12 km, yielding a Skempton ratio of 0.006, indicating its translational character, although the steep failure plane has characteristics of a submarine slump or rockfall with rock avalanche deposits. Similar slumps linked to ridge subduction occur in the vicinity farther northwest (Figures 4 and 6), and indications of ongoing fracturing of the overriding plate are abundant (Figure 6).

3.2. Seamounts–Central Costa Rica Segment

[18] The northwestern limit is marked by a ridge in the oceanic plate that projects landward to a cohesive slump in the lower slope (Figures 1 and 4).

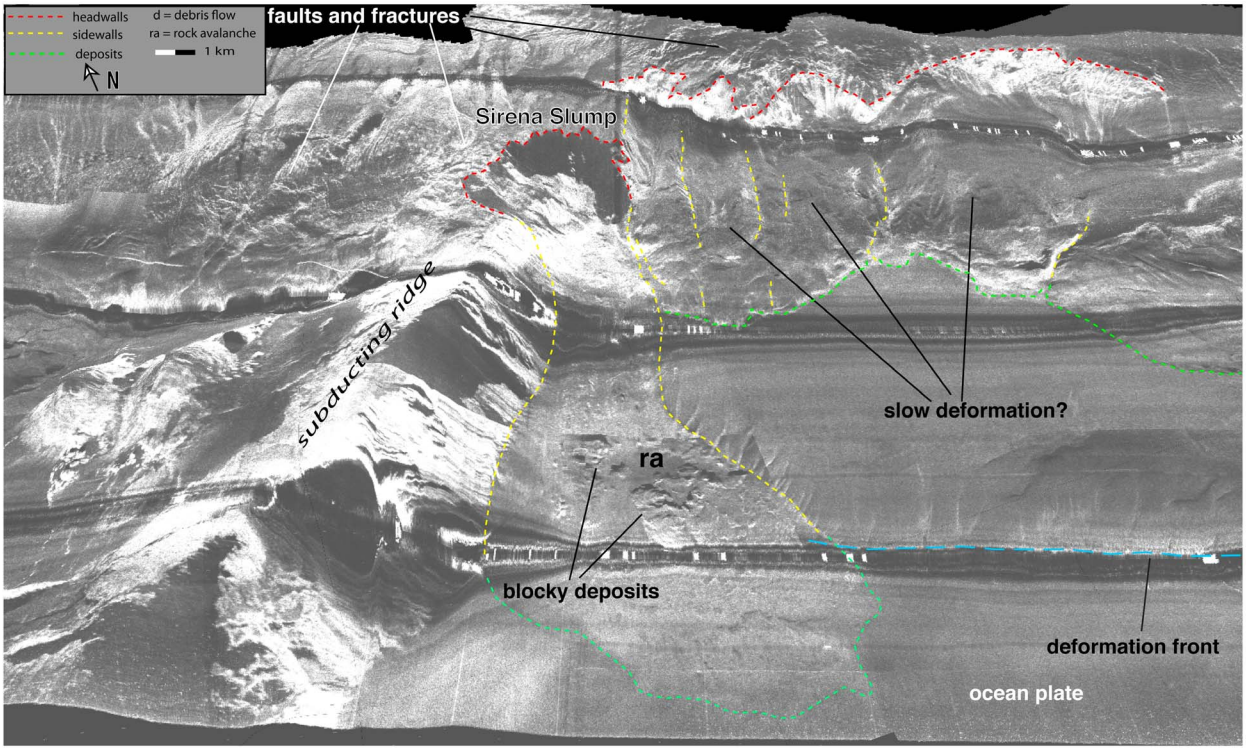

Figure 5. Perspective view of side-scan sonar imagery draped on multibeam bathymetry of the Sirena slump in the lower slope offshore Osa Peninsula and associated runout deposits, including large blocks, that reach the ocean plate (location in Figure 4). The slope scar is 12 km wide, with a 1 km high headwall that dips 30°–51°. The avalanche is related to subduction of a sharp ridge, cresting Cocos Ridge, clearly visible in the images. Southeast of the scar, high-backscatter slope-subparallel structures may be incipient headwalls (marked in red). Downslope of them, tongue-shaped bodies bounded by slope-normal structures (marked in yellow) might indicate developing gravity-related deformation.

Seamounts cover 40% of the oceanic plate and reach up to 4 km height and 40 km width [*von Huene et al.*, 2000]. The continental slope opposite displays geomorphic features generated by tectonic erosion [*von Huene et al.*, 2000], local reentries at the slope toe where seamounts have collided with the margin, slope grooves along seamount subduction paths, and rotational slumps (Figure 4). Large-scale (>20 km long or wide) rotational slumps and rock avalanches occurring in the lower and middle slope characterize this segment. Mean slope angles are 2°–5°, i.e., lower than at other segments (Table 1). However, the slope is locally uplifted to 20°, although headwall scarps are steeper (Figures 1b and 2). In contrast to other segments, the slope deformation of this segment has been relatively well studied before [*von Huene et al.*, 2000; *Ranero and von Huene*, 2000; *von Huene et al.*, 2004a, 2004b]. The seamounts, created by the Galapagos hot spot, have been subducted here for at least 300,000 years assuming a current convergence rates [*Werner et al.*, 1999; *von Huene et al.*, 2000], and most slope failures are probably related to that process.

3.2.1. Rotational Slumps

[19] Owing to their large dimensions most slumps and scars within this segment have been previously identified [*von Huene et al.*, 2000, 2004a]. Here we add and interpret new information based on the increased resolution bathymetry from about 200 to 100 m grid, and unpublished side-scan sonar data.

[20] The largest failure is the rotational Nicoya slump (Figures 4 and 7). The slump block is 35 km long and 60 km wide [*von Huene et al.*, 2004a]. Seismic profiles show its deep-rooted rotational slide plane, affecting the entire thickness of the overriding plate [*von Huene et al.*, 2004a]. Surface expressions of the slump include debris flows (d), debris avalanches (da) and rock avalanches (ra) (Figure 7). The headwall height increases from

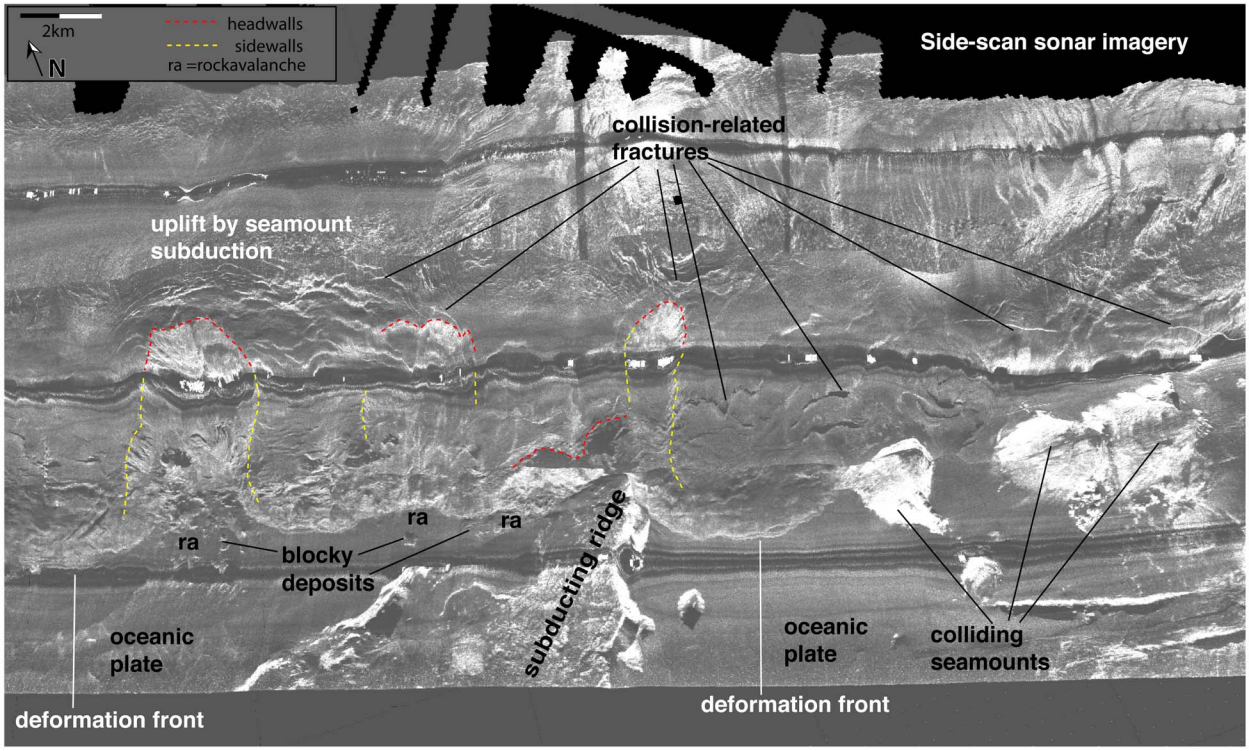

Figure 6. Perspective view of side-scan sonar imagery draped on multibeam bathymetry of the deformation and slope failures caused by ridges and associated seamount groups on the Cocos Ridge in the fore arc SW of Osa Peninsula (location in Figure 4). Numerous slope-parallel fractures in the slope occur upslope of the headwalls of slumps. Apparently, failures are disintegrative slumps that develop into rock avalanches.

350 m in the north up to 1000 m in the south. We infer that the dimensions of the Nicoya slump are caused by slumping of the fore arc over two subducting seamounts located both at about the same distance from the trench axis. We propose that in addition to a seamount described in previous papers located under the Rio Bongo uplift, there is a smaller subducting seamount to the northwest, and that sliding of the entire overriding plate over the flanks of the seamounts caused a structural modification of the rotational slump (Figure 7). This can be inferred from morphology, which consists of a relatively shallow and continuous headwall, and a slide plane along the plate boundary fault (i.e., <5°) imaged in seismic data [*von Huene et al.*, 2004a, Figure 2], and a 0.07 low Skempton ratio. The larger seamount in the southeast has caused a more disintegrative rotational part of the slump.

[21] Farther southeast is Jaco scar, a large slump caused by an underthrusting seamount that has left during the past ~300.000 years a 27 km long trace of slumped rock masses filling a furrow (Figure 8). The furrow sidewall scars can be traced to the deformation front. The most recent slump is at least 20 km long and 5 km wide, containing blocky deposits that traveled up to 17 km. The rotational failure plane has a ~1000 m high headwall, with an angle of up to 40°. Parrita scar located to the southeast (Figure 8) is a slump similar in size, shape, and a seamount-related furrow.

3.2.2. Translational Slides

[22] In this segment translational sliding style changes depending on slope morphology and failure location on the upper, middle or lower slope.

3.2.2.1. Slides With Planar Body Deposits

[23] Areas where high-topography features have repeatedly subducted display embayments (Figure 4) attributed to thinning by tectonic erosion [*Ranero and von Huene*, 2000]. Three embayments occur from Nicoya Peninsula to northwest of Osa Peninsula [*von Huene et al.*, 2000] (Figure 4). A series of overlapping scars on the steep flank of the northernmost embayment indicate successive, retrogressive translational slides (retrogressive means that other slides are induced above the original one,

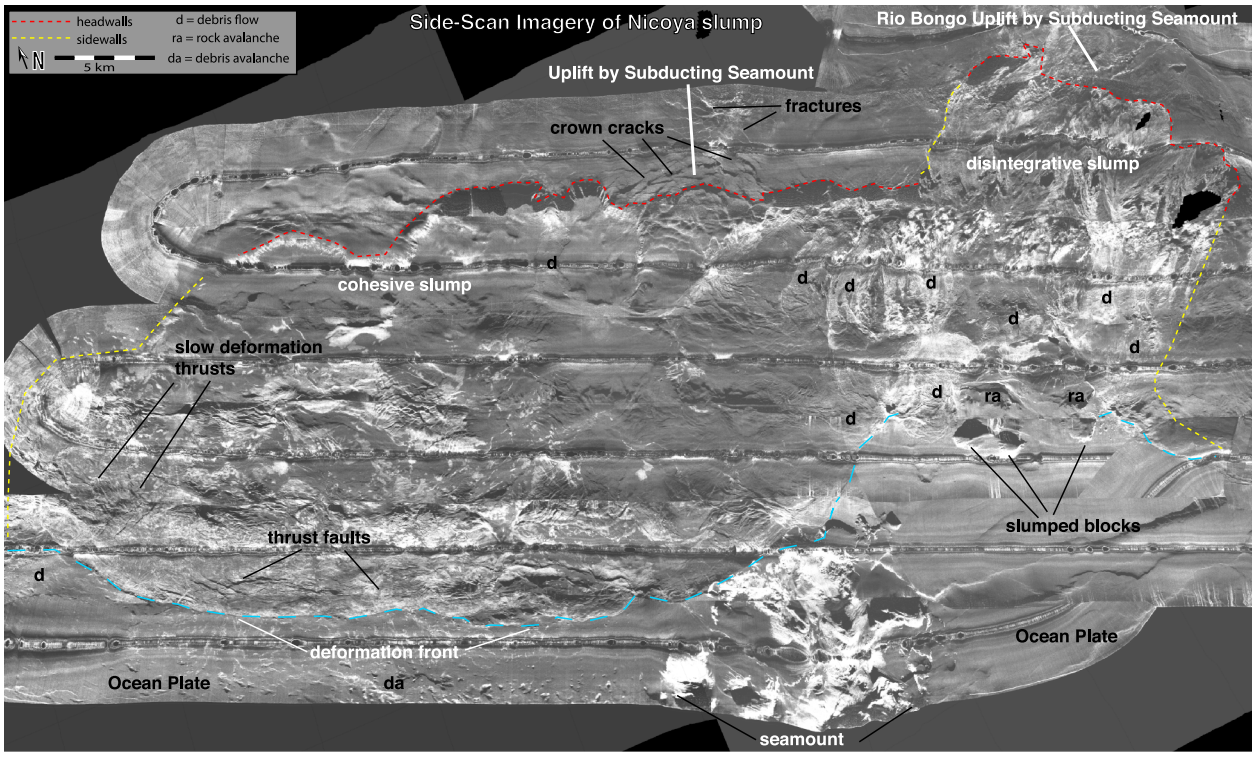

Figure 7. Side-scan sonar imagery of the region of Nicoya slump (location in Figure 4). The complex morphology of the >60 km wide slump probably developed when the slope failed over two subducting seamounts. A large seamount is located in the SE causing the Rio Bongo uplift, and a smaller seamount is located under the headwall near the middle region of the slump structure, indicated by crown-shaped cracks and associated fractures. The headwall and deposits of the northwestern part of the slump differ from the morphology of the slump in its southeastern area. Blocky deposits and high headwalls represent a slump with a disintegrative character that developed rock avalanches in the southeast, downslope of the Rio Bongo uplift. The northwestern two thirds of the slump shows a more cohesive translational character. Abbreviations are as follows: d, debris flow; da, debris avalanche; ra, rock avalanche.

building similar headwalls upslope [*Mulder and Cochonat*, 1996]) (Figures 9a and 9b). The mobilized material moved downslope into the embayment floor. Some planar sediment deposits there (Figure 9a), may represent "mixed slides," defined as slides with a planar body and a shallow headwall, akin to gliding snow slabs created during snow avalanches [*Mulder and Cochonat*, 1996]. The scars of the embayment walls are ~7 km long and ~4 km wide on average, with headwalls 30–60 m high and about 18° dip angles (Figure 9b).

3.2.2.2. Slides With Coherent Deposits

[24] As subducting seamounts and ridges underthrust deeper, they uplift the upper continental slope, and produce broader uplifts that cause moderate slope oversteepening (7°–10°). There, failure type changes to moderate to large (8–10 km long, 5–7 km wide) cohesive translational slides, rather than the slumps of the middle-lower slope. An example is Quepos slide formed at a slope angle of 7.5° near the shelf break (water depth 214 m) (Figures 4 and 10). The slide is ~8 km long and 9.5 km wide, with a headwall height of 160 m, and a headwall angle of 25°. The 0.02 Skempton ratio, indicates a translational character. The deposits front created a 100 m high ridge terminating in a tongue-shaped toe that shows compressional sediment structures (Figure 10). The slide consists of at least 4 events that possibly occurred sequentially in time, caused by the progressive southeastward migration of the obliquely oriented subducting ridge (Figure 4).

[25] A similar slide is Cabo Blanco slide, possibly initiated by upper slope uplift by a subducting seamount in the prolongation of the seamount that caused the Rio Bongo uplift and participated in Nicoya slump (Figure 4). The slide is 9.8 km long, 7.3 km wide and has a maximum headwall height of 160 m. Side-scan imagery and bathymetry show a complex morphology of a failed mass in the

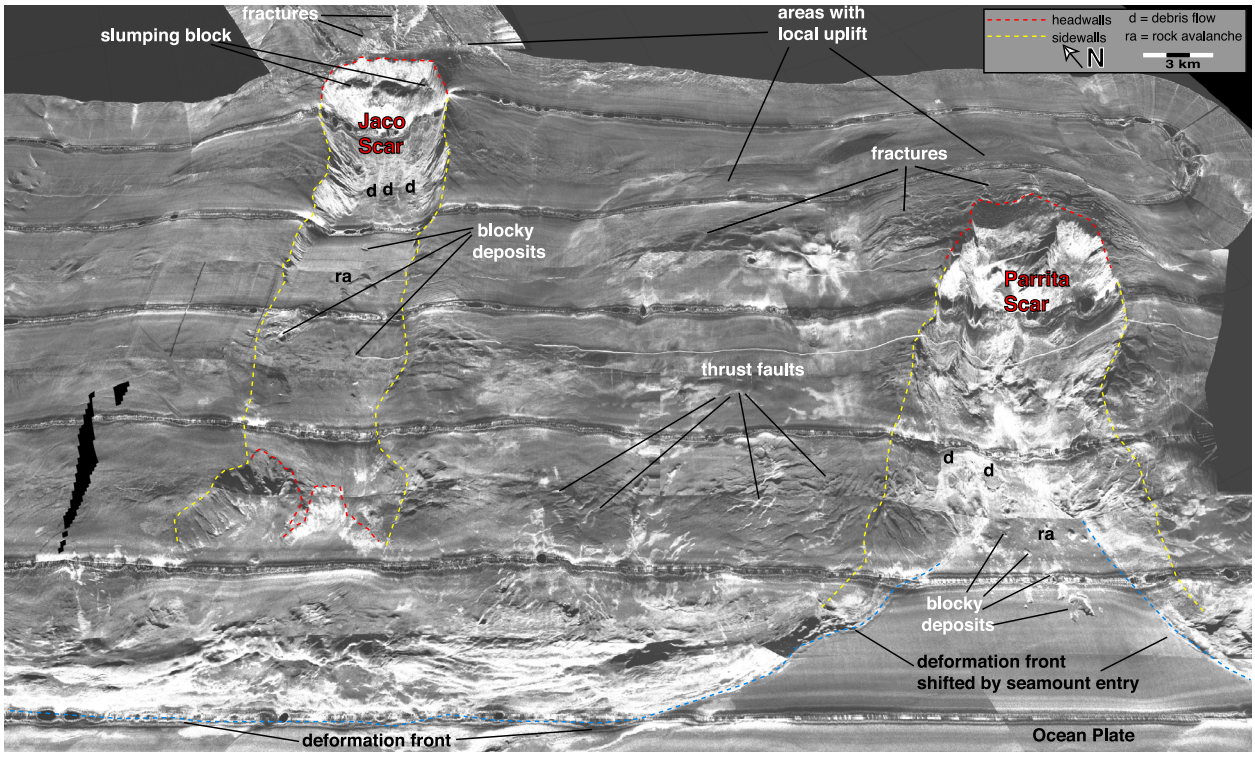

Figure 8. Perspective view of side-scan sonar imagery draped on multibeam bathymetry of the region of Costa Rica deformed by subducting seamounts. Two underthrusting seamounts are currently located under the so-called Jaco and Parrita scars (region location in Figure 4). The grooves in the slope bounded by sidewall faults mark the trajectory of the underthrusting seamounts and contain the deposits of a series of successive rotational failures produced as the seamounts subduct deeper under the overriding plate. The seamounts uplift and fracture an area considerably larger than the area that fails in their wake. Abbreviations are as follows: d, debris flow; ra, rock avalanche.

northwest that grades to slid blocks farther downslope. In the southeast, the upper region contains a partially detached block. Downslope occur a series of compressional ridges formed by a previous failure (Figures 11a and 11b).

3.2.2.3. Slides Without Visible Deposits

[26] In the uppermost slope, occur a series of comparatively small translational slides, which are not clearly related to subducting seamounts. Two of them, named the BGR and Geomar slides (Figure 12), have been studied in some detail but failure causes remain unclear [*Marquardt*, 2005]. These slides have ~40 m headwall heights and ~2 km total lengths.

3.3. North Nicoya Segment

[27] This segment occurs opposite the smoothest oceanic plate of the study area (Figures 1 and 4). The ocean plate was formed at the East Pacific Rise and it is separated from lithosphere to the south, formed at the Cocos-Nazca spreading center, by a ridge marking the paleoplate boundary (Figures 1 and 13a). The slope is smooth, with numerous normal fault scarps across the middle slope visible in bathymetry (Figures 13a and 13b) and side-scan sonar images (Figure 14). Mean slope angles of the middle slope are gentle (5–14°), increasing to 17° at the lower slope. The area contains many fewer failures than adjacent segments.

3.3.1. Translational Slides

[28] All slide scars in this segment are comparatively small and shallow, displaying translational character, typically with no visible deposits near the toe (Figures 13b and 14). The maximum slide length is 7 km, a maximum width of 3 km and maximum headwall height of ~40 m. Trench axis subparallel normal faults occur within the middle slope, where translational slides appear to start (Figure 14).

[29] A typical translational slide in this segment is Hermosa slide (Figures 13b and 14), which occurs

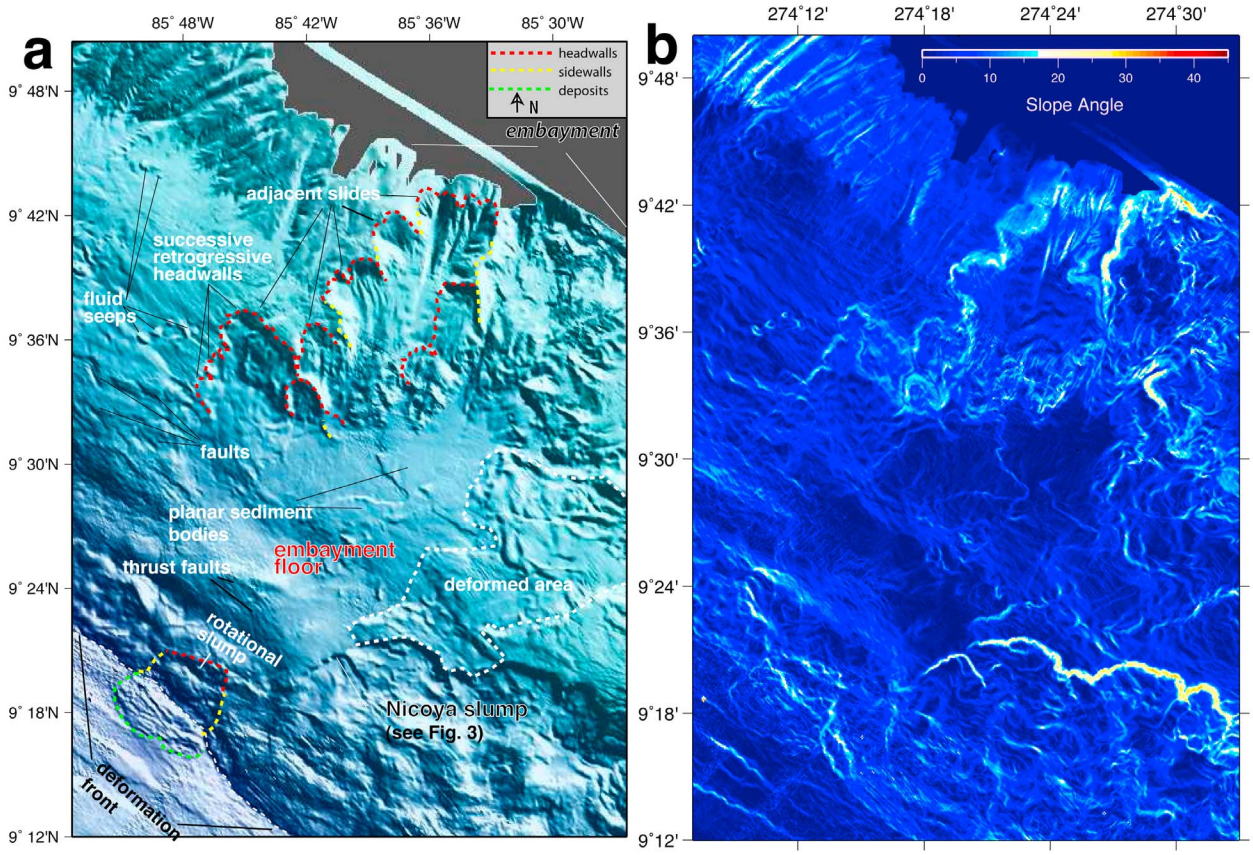

Figure 9. Northernmost embayment offshore Costa Rica. (a) Multibeam bathymetry map and (b) slope angle. The NW flank is sculptured by several headwalls and sidewalls of retrogressive translational slides. Slides developed on the inner wall of the embayment and the failed material followed canyon paths to build planar sediment bodies in the embayment floor.

together with 4 similar neighboring slides in the southeast [*Harders et al.*, 2010]. Hermosa slide occurs in 1900–2500 m water depth, with a 25 m headwall height and a 13° headwall angle. The sidewalls of the scar slightly converge toward the scar foot and can be followed about 7 km downslope, but the runout point is unclear. As for most translational slides along the MAT, the bathymetry data do not show an elevated deposition area near their toe. Side-scan sonar data of Hermosa slide show faults or fissures within failed sediment where parts form large block and sheet deposits overlying the slide plane (Figure 14).

3.3.2. Rotational Slump

[30] In the northwesternmost middle-lower slope section occurs a large (21 km wide and 22 km long) structure with hummocky morphology, containing mound structures and a slump scar in its uppermost part (Figures 15a and 15b). The structure consists of an uplifted area bounded trenchward by a well-developed 300 m high headwall, but no sidewalls occur downslope (Figures 15a and 15b). The sediments at the toe of the area show possible compressional faulting which may indicate short distance slow deformation or creep (Figure 15a). This structure is possibly related to a subducting seamount, imaged under the uplifted region in a seismic reflection profile [*McIntosh et al.*, 2007].

3.4. Nicaragua Segment

[31] This segment starts gradually where the offsets of normal faults cutting oceanic plate increase to form scarps >200–350 m high, and a series of seamounts (smaller than offshore Costa Rica) occur across the ocean plate (Figures 1 and 16). To the NW, the segment terminates where the trench axis changes strike to a NW-SE orientation, roughly coincident with a fracture zone that separates segments of the oceanic plate [*Wilson*, 1996]. Large

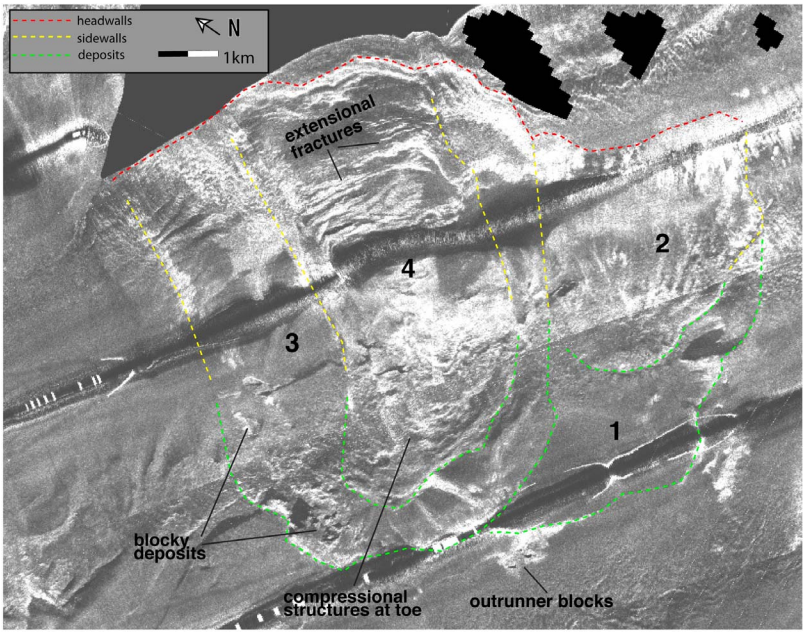

Figure 10. Perspective view of side-scan sonar imagery draped on multibeam bathymetry of the cohesive, translational Quepos slide related to uplift of the uppermost slope due to subduction of a ridge offshore central Costa Rica. Numbers 1–4 indicates four failure events that spatially overlap and possibly represent a time evolution (1 is the oldest and 4 is the youngest) in the development of the slide caused by the southeast oblique subducting of a ridge (location of region in Figure 4).

translational slides characterize this segment, and are concentrated along the middle slope with an average dip (7°–17°) steeper than in other segments (Figure 16).

3.4.1. Translational Slides

[32] Large retrogressive translational slides start along the steep upper to middle slope transition, coincident with NW trending normal faults with offsets of 50–200 m. The headwall height to length ratio of slides is typically low and reflects their translational character; even though only the slide plane length and not the full runout could be measured (Figure 16a). Slide plane dimensions range between 5 and 12 km in length and 3–7 km in width, with 50–450 m high headwalls. Scar sidewalls typically converge downslope, and the failure plane is bedding parallel, indicating that sliding probably occurred along a weak layer of stratified sediment. Many slides show slide blocks overlying the slide plane with a characteristic hummocky surface (Figures 16b and 16c). Near slide toes, where slide scars narrow, a channel occurs in some cases, which may have been incised by turbidity currents. Most slide scars disappear at the transition from middle to lower slope, where gradients decreases over 4–5 km, to give way to an increase up to 12° at the slope toe.

[33] A typical example of translational slide is the Masaya slide (Figure 16b). The slide starts in 1700 m water depth on the 8°–12° dip upper to middle slope. The headwall is up to 160 m high, with a 28° maximum dip. The main scar is 18 km long, up to 6.2 km wide and narrows to <2 km at its lower end. No deposits are visible downslope, but a channel at its toe may indicate disintegration of the slide into turbidites (Figure 16b).

3.4.2. Rotational Slumps

[34] Irregularly shaped rotational slumps are uncommon on the Nicaragua segment, but some occur at the low-angle transition from middle to lower slope (Figure 16d). In contrast to translational slides, these slumps show wide headwalls and short sidewalls. Dimensions are ~3 km in length, ~10 km in width and up to 200 m headwall heights.

3.5. El Salvador Segment

[35] Its SE border is marked by a change in strike of the MAT, and a fracture zone in the oceanic plate (Figures 1 and 17a). The northwestern bound-

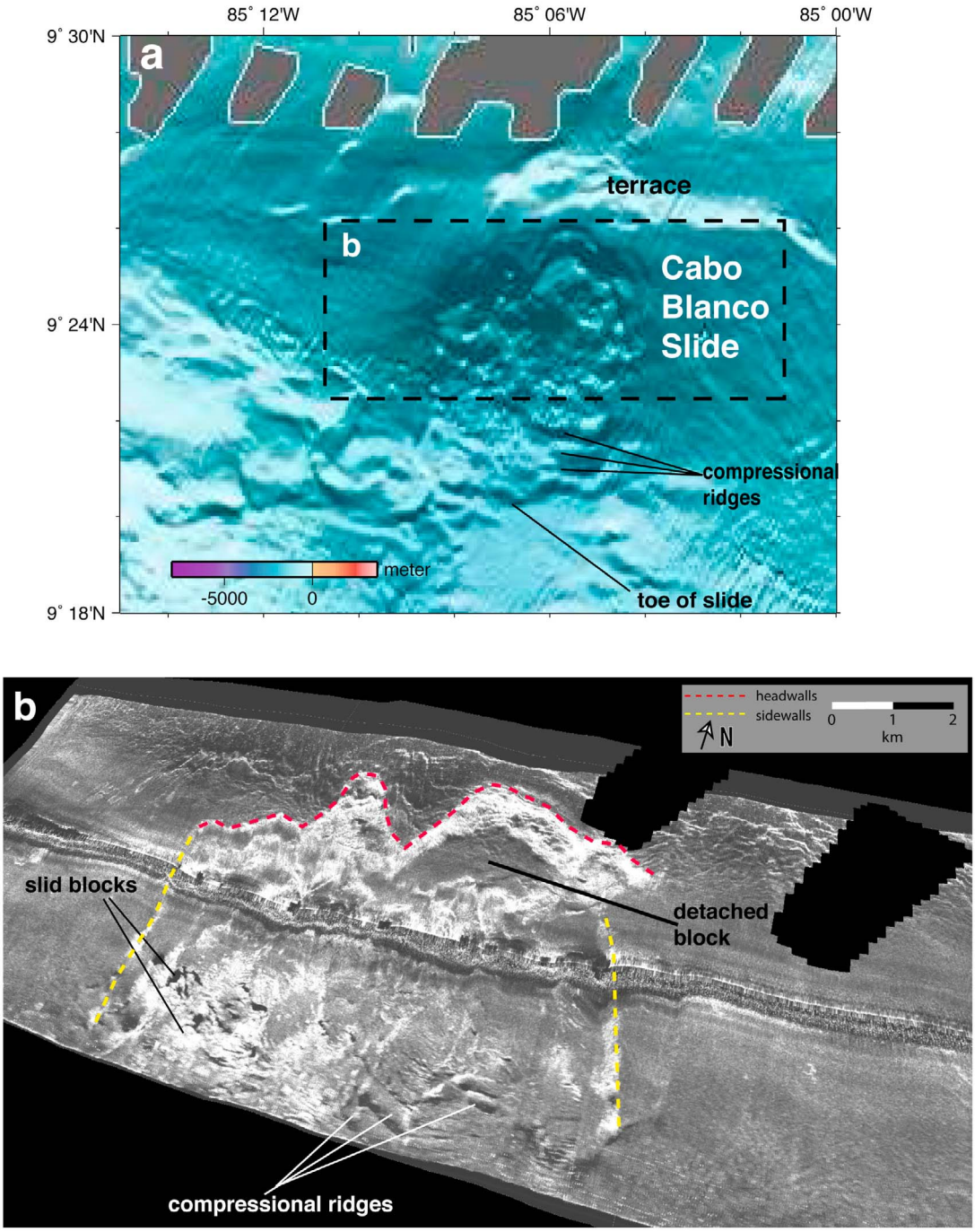

Figure 11. The Cabo Blanco slide, related to uplift of the uppermost slope due to subduction of a seamount, located southeast of Nicoya Peninsula. (a) Shaded relief bathymetric map (location of region in Figure 4). (b) Perspective view of side-scan sonar imagery draped on multibeam bathymetry of the upper portion of Cabo Blanco slide. Location of Figure 9b is marked in Figure 9a. The slide is a cohesive, translational type with detached, coherent blocks in the upper area, slid blocks in the middle portion, and compressional ridges in the lower segment.

ary is gradual, with no sharp change in the fabric of the ocean plate, but with an increase in failures in the middle slope (Figure 1).

[36] The El Salvador segment has few failure-related structures (Figure 17). Only small translational slides occur on the uppermost slope at the segment center. Similarly to the Nicaragua segment,

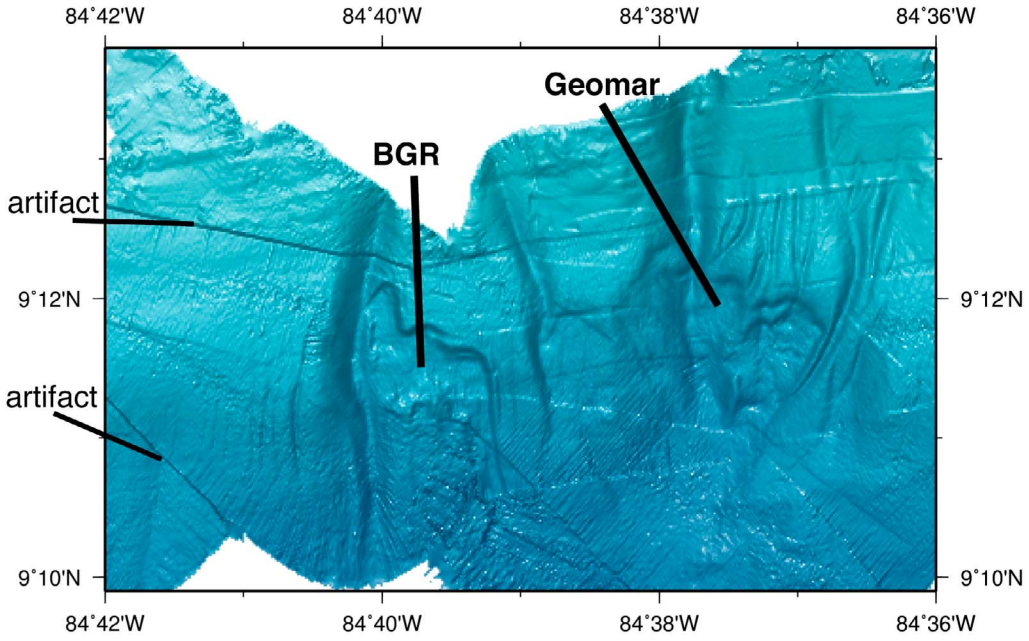

Figure 12. Shaded relief bathymetric map of the BGR and Geomar slides located in the uppermost slope offshore Costa Rica. The scars are small developed between 500 and 700 m water depth and do not appear to be related to deformation associated with currently subducting seamounts.

a steep middle slope contains normal faults, but with smaller seafloor scarps and are not associated with large failures.

3.5.1. Translational Slides

[37] Unique in the entire study area is a group of translational slides at canyon flanks of the upper slope. About 20 structures of comparable dimensions, <4 km long, <3 km wide, and ~150 m high headwalls occur mostly in a group at 1200–2000 m water depth on the 3°–7° dipping upper slope (Figure 17a). The slides occur in the area of deeply incised submarine canyons. The degree of margin incision by canyons is higher than in the Nicaragua segment (compare Figures 16 and 17). A typical failure is slide 370 (Figure 17b) at the southeast flank of a ridge flanked by two canyons. The slides have no deposits, and failed sediment probably traveled into the canyon and downslope, disintegrating into turbidity currents that may have been deposited in the flatter middle slope or into the trench axis.

3.5.2. Rotational Slumps

[38] A few small rotational slumps occur at the lower slope, near the trench axis. Average dimensions are 1 km length, 2 km width and 100 m high headwalls. Similar to the Nicaragua segment, the headwalls develop at normal faults and the slump scar shape seems influenced by fault geometry (Figure 17a).

3.6. Guatemala Segment

[39] In contrast to the El Salvador segment, the Guatemala slope contains abundant mass wasting structures and pervasive trench-subparallel normal faults (Figures 1 and 18a). In contrast to all other segments, here single, discrete slide scars are rare, slope failures of different morphologies and dimensions overprint each other. Apparently the sediment fails comparatively more frequently, particularly on the steep (up to 17°) middle and lower slope, where the largest failures occur.

[40] Along this segment, classification of some failures as rotational slumps or translational slides is unclear. The pattern of headwalls, and subparallel normal fault fabric are well displayed in the slope angle map (Figure 18d).

3.6.1. Rotational Slumps

3.6.1.1. Slumps Formed at Normal Faults

[41] The middle slope contains abundant slumps, with headwalls that predominantly appear to form

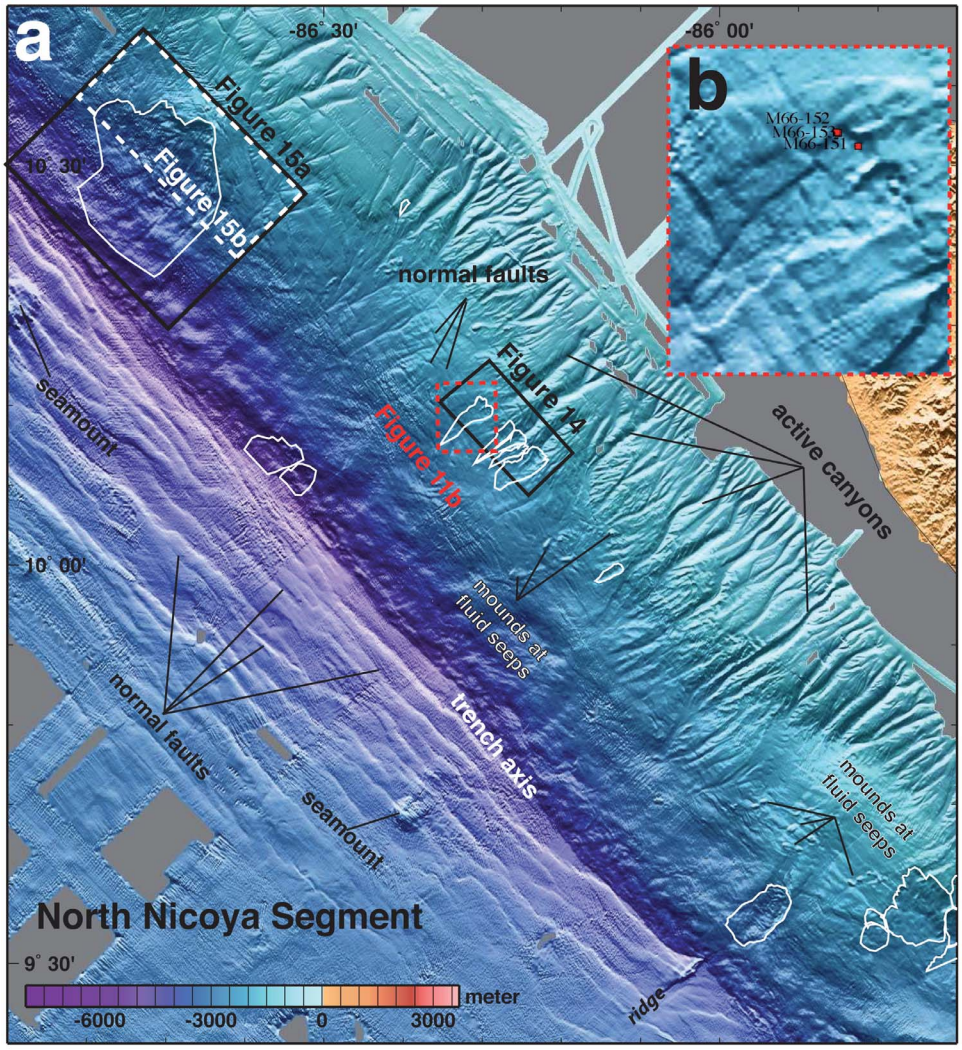

Figure 13. The North Nicoya segment (location in Figure 1a). (a) Shaded relief bathymetric map of the segment. The incoming plate displays the smoothest segment along the study area. The oceanic plate contains few seamounts compared to the SE segment of Costa Rica, and some small- to middle-sized normal faults compared to the segments toward the NW. The continental slope contains comparatively few failures (delineated in white). (b) Shaded relief bathymetric map of a type example of failure: The translational Hermosa slide. Red squares mark location of sediment cores M66-151, M66-152, and M66-153 described in detail by *Harders et al.* [2010]. Numerous scarps parallel to the slope strike indicate that abundant normal faults cut across the area.

at normal fault scarps (Figure 18c). The failure scars are in average 2–8 km long, 5–10 km wide and have 100–300 m high headwalls. Failure planes and sidewalls are short, commonly not well defined, and their downslope extent appears to be controlled by preexisting slope morphology (Figure 18c).

3.6.1.2. Slumps in the Upper Slope

[42] Slumps in the uppermost slope occur where dips are up to 32°. Scars are 1.5–7 km long, 3–8 km wide, and have 100–200 m high headwalls (Figure 18a). The shallow scars show erosional features of younger events obscuring the failure planes. No slump deposits are visible along the steep uppermost slope (Figure 18a).

3.6.1.3. Slumps Formed on the Lowermost Slope

[43] Where the subducting plate displays pronounced horst and graben relief, rotational slumps in the lowermost slope deliver debris into the trench. The thin frontal apex of the overriding plate deforms to mimic the underthrusting horst and

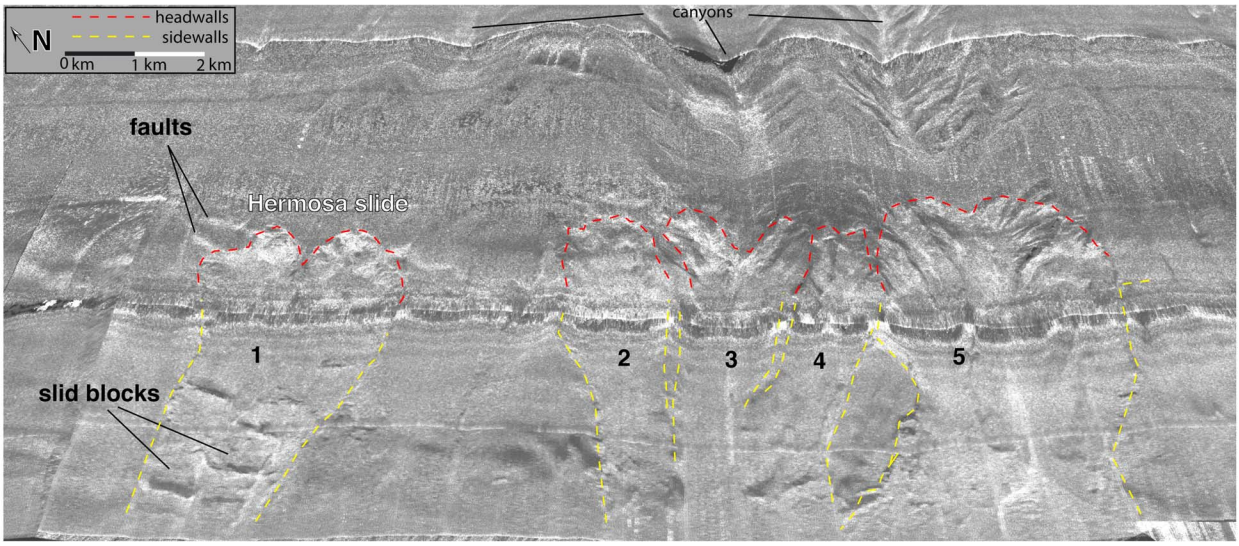

Figure 14. Perspective view of side-scan sonar imagery draped on multibeam bathymetry of a region of the middle slope of the North Nicoya segment (location in Figure 13). The image shows the Hermosa slide and four neighboring slide scars. The slides have formed near the mouth of canyons and where normal faults cut the slope, clearly visible in the northwest part of the headwall of Hermosa slide. Slid blocks are visible on top of the slide plane.

graben topography. This type of slump is most frequent in Guatemala (Figure 18) but with the exception of Costa Rica, it appears in all segments. Their dimensions and shape are similar from Guatemala to North Nicoya, ranging between 1.5 and 3 km long, 3 and 7 km wide, and 300 and 400 m high headwalls (Figures 1, 13a, 16a, 17a, and 18a).

3.6.2. Translational Slides

3.6.2.1. Large Slides Formed on the Lower Slope

[44] In the NW end of the segment, two large translational slides (7–12 km long, 3–5 km wide and 150–300 m high headwalls) are found at water depths >3500 m on the lower slope (Figure 18c). These slides appear to be local features, related to subduction relief of a fracture zone that locally oversteepens the slope (Figure 18b).

3.6.2.2. Slides Linked to Normal Faults Formed Across the Slope

[45] Normal faults slightly oblique to the trench create a rough slope topography. Here develop translational slides with irregular sidewalls and headwalls, and blocky debris deposits downslope (Figure 18a). The shape and lateral extent of failures seem associated with the location and along-strike length of normal faults. In cases, headwall and sidewalls appear to be limited to the extent of fault scarps.

4. Discussion

4.1. Preconditioning Factors

[46] One major question is whether the observed segmentation of the Central American margin, in terms of slide and slump frequency and size (Table 1), may be a function of material properties and/or tectonic setting. An often cited preconditioning are lateral or vertical changes in material properties in the stratigraphic column involved in failures. We have revised previous work on sediment properties along the margin. The slope sediment has been investigated with gravity cores sampling the upper tens of meters offshore Costa Rica and Nicaragua during cruises SO173, M54 and M66 [*Kutterolf et al.*, 2008; *Harders et al.*, 2010]. Also, drill cores from several hundred of meters of slope sediment were taken and analyzed during DSDP Leg 67 offshore Guatemala [*von Huene et al.*, 1980; *Aubouin and von Huene*, 1982], DSDP Leg 84 offshore Guatemala and Costa Rica [*Helm*, 1984], and ODP Leg 170 offshore Costa Rica [*Kimura et al.*, 1997]. It has been proposed that ash layers may act as discontinuity planes in the sediment column and favor formation of detachment planes [*Harders et al.*, 2010]. However, cores show that most of

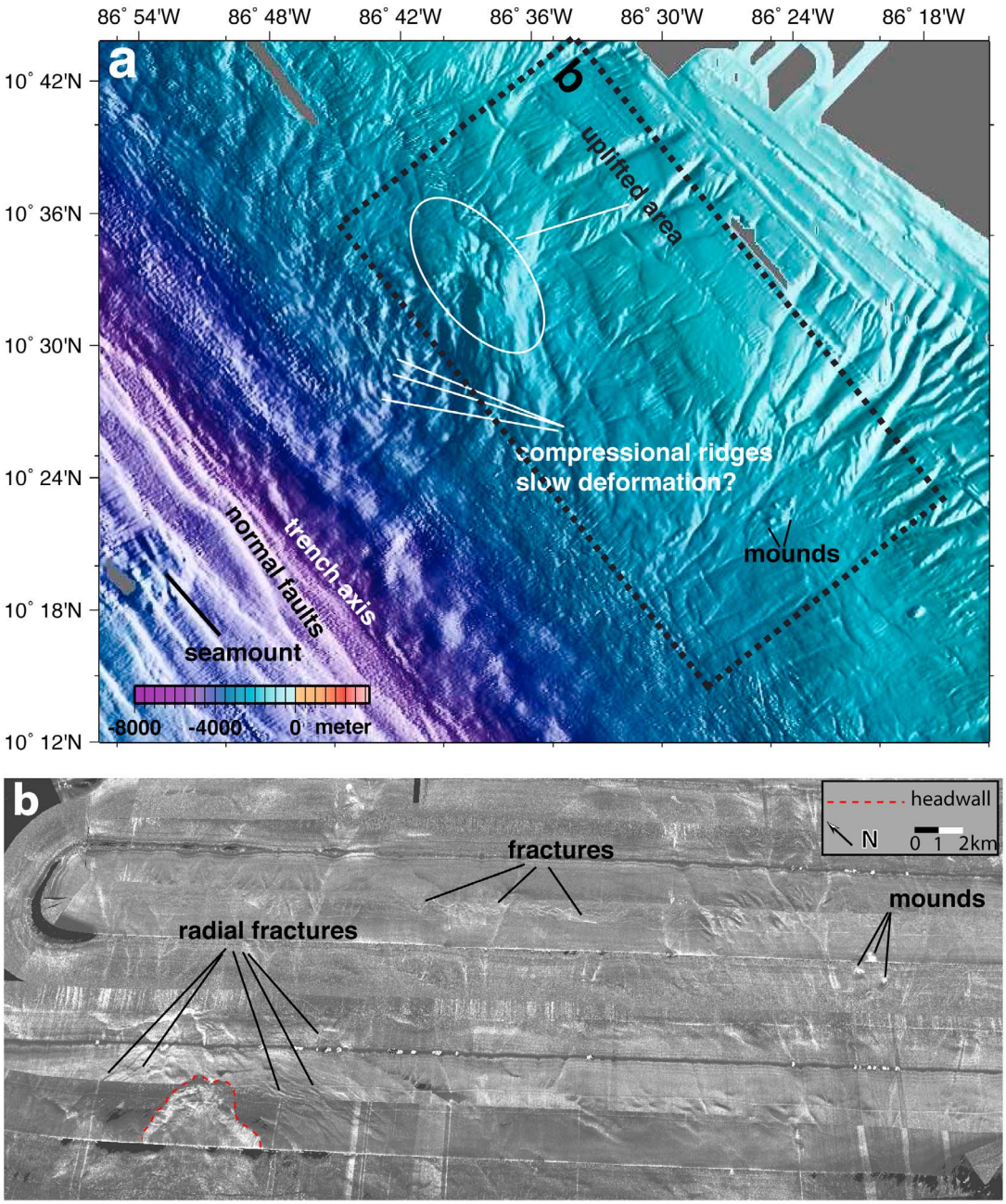

Figure 15. Seafloor maps of the NW region of the North Nicoya segment. (a) Shaded relief bathymetric map showing an uplifted area and, located downslope, a failure scar showing no clear slide sidewalls. Farther downslope occur possible compressional ridges that might indicate slow deformation. (b) Perspective view of side-scan sonar imagery draped on multibeam bathymetry of the middle to upper slope (location in Figure 15a). The image shows the group of radial fractures clustered on the uplifted area and associated headwall. Scarps of discrete normal faults cut the slope at numerous locations.

sediment involved in translational sliding and shallow slumps does not significantly change geographically in any particular property (lithology and stratigraphy, density, water content, and mineralogy). The Pliocene and Pleistocene sediments involved are uniform terrigenous olive green to gray clays, intercalated every few meters by 1–10 cm thick tephra ash layers of the Plinian and ignimbrite eruptions of the Central American Volcanic Arc (DSDP Leg 84 [*Helm*, 1984; *Kutterolf et al.*, 2008]). Typically, bulk densities of the clays increase within the first 200 m from 1.4 to 1.8 g/cm^3 and water

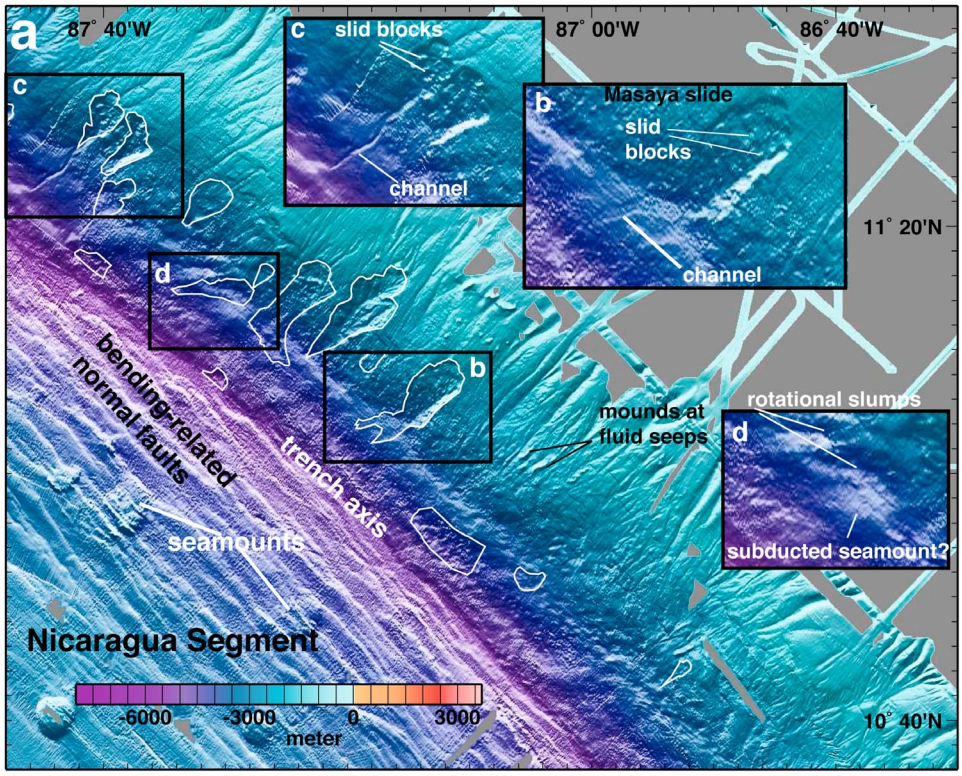

Figure 16. Shaded relief bathymetric map of the Nicaragua segment. (a) The segment displays large translational slides on the middle continental slope and seamounts on the ocean plate that are comparatively smaller than in the Seamounts–Central Costa Rica segment Cocos Ridge–Osa Peninsula segment. (b) Close-up of middle-slope translational Masaya slide showing the slide scar and overlying slid blocks. Failure deposits are missing at the base of the scar. The scar toe converges into a channel that may have been formed by the mass wasting transport processes. (c) Close-up of middle-slope translational slide scars with overlying slid blocks and channel initiating at the scar toe. (d) Close-up of middle- to lower-slope small rotation slumps possibly associated with failure induced by small-scale relief of the incoming oceanic plate.

content reduces between 60 and 30% in response to normal depth-dependent compaction [*von Huene et al.*, 1984]. Therefore, sediment behavior may change with depth from recent sediment to the upper Cretaceous turbidites overlying the igneous basement, but slope sediment stratigraphy does not significantly vary from Guatemala to Costa Rica, probably because the entire region has a similar geological evolution [*Ranero et al.*, 2000]. Further, a succession of dominant marine terrigenous with thin intercalated tephra layers is expected across the entire column since the volcanic arc initiated in the uppermost Cretaceous time [*Ranero et al.*, 2000].

[47] We interpret that long-term tectonic processes cause changes in slope morphology and in the structure of the stratigraphic column [*Ranero et al.*, 2008] that create the most relevant preconditioning factors for slope instability. These factors are combinations of changes in slope dip and upper plate fracturing, both factors caused either locally by subducting topographic features of the ocean plate, or more regionally by tectonic erosion causing normal faulting and oversteepening. Subduction of high-relief features causes slope uplift and oversteepening in the wake of the underthrusting feature, with the locus of oversteepening migrating as the feature moves farther under the margin [*von Huene et al.*, 2000, 2004a, 2004b]. Uplift is also associated with local intense fracturing, that probably cuts across the entire overriding plate [*Ranero and von Huene*, 2000]. These deep penetrating fractures are reactivated during slumping [*von Huene et al.*, 2004a]. Subduction erosion along the underside of the overriding plate removes material that is transferred to the subduction channel and transported away. This process causes gradual thinning of the overriding plate that subsides and extends along normal faults [*Ranero and von Huene*, 2000; *von Huene and Ranero*, 2003]. The intensity

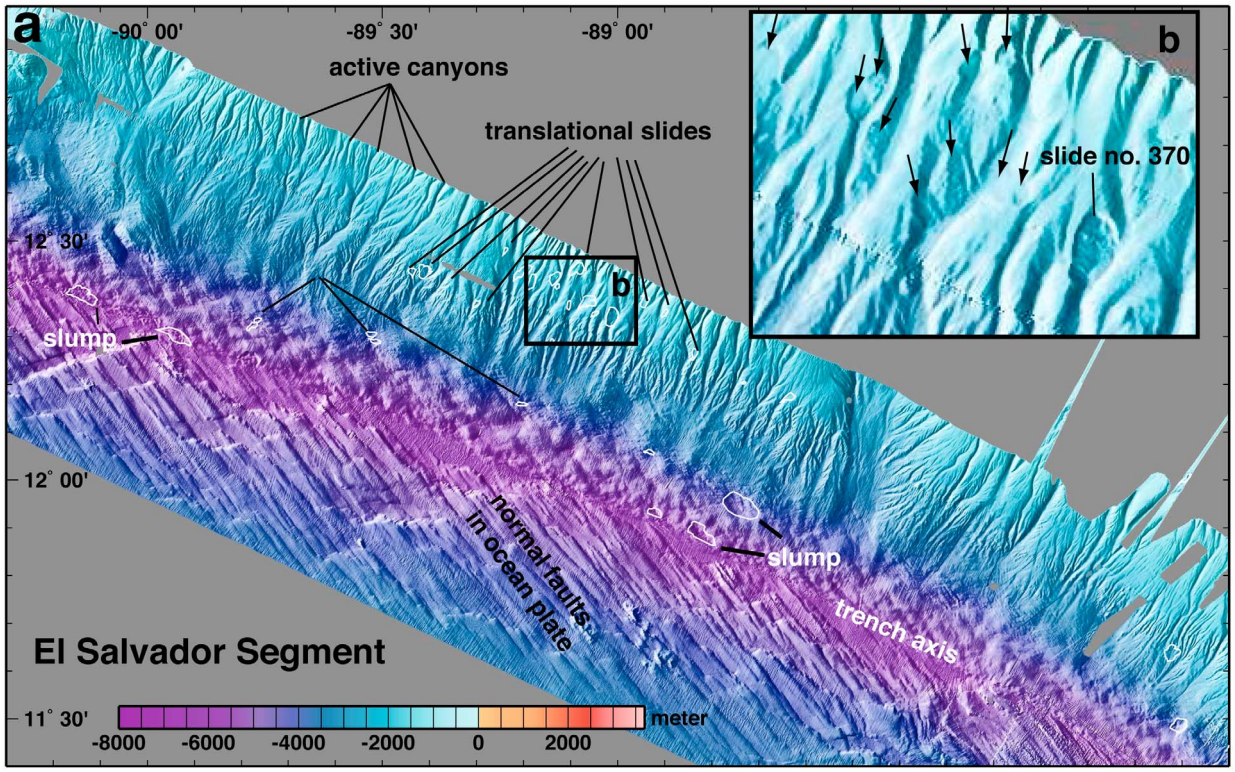

Figure 17. Shaded relief bathymetric map of the El Salvador segment. (a) The segment is characterized by the best developed upper-middle slope canyon system of the study area that possibly implies a comparatively more stable slope. In accord, the segment contains the fewest slope failures of all segments. Typically, these are small translational slides in the upper slope. A few rotational failures seem to initiate at normal fault scarps in the middle to lower slope. A well-developed bending-related normal fault system with large offsets characterize the incoming ocean plate, but no seamounts are present. (b) Close-up of upper slope small translational slides that represent the most abundant type and typically occur at canyon walls.

of erosion appears to change along and across segments, causing differential amount of subsidence and leading to oversteepening typically at the middle slope of some segments and also to variable intensity of faulting that cuts the sediment and in cases the entire overriding plate [*Hensen et al.*, 2004].

[48] El Salvador segment, displays the least active tectonics along the margin, and incision of sediment by canyons in the uppermost slope causes local oversteepening. Oversteepening of canyon walls and intervening ridge flanks may be a preconditioning factor, however of secondary importance in terms of failure abundance and dimensions at a margin dominated by tectonic processes.

[49] The presence of gas hydrates is often cited as a potential preconditioning factor. Gas hydrates, inferred from seismically images bottom simulating reflectors, occur along the margin [*Pecher et al.*, 2001], and might have play a role in small-scale failures in the uppermost slope, but do not explain segmentation.

4.2. Triggering Mechanisms

[50] Trigger mechanisms, understood as the external stimulus that initiates the slope instability process [*Sultan et al.*, 2004], may change for the different segments and failure types. An obvious trigger is gravitational collapse of fractured material in the wake of underthrusting ocean plate relief. This mechanism form slumps in the lowermost slope where hundreds of meters high horst-and-graben relief subducts. This accounts for rotational slumps near the slope toe typically found in Guatemala and El Salvador segments. A similar mechanism has formed the largest rotational slumps in the lower-middle slope of the Seamounts–Central Costa Rica segment. However, seamount subduction under the upper slope of central Costa Rica causes translational sliding. Subduction of comparatively smaller seamounts in Nicaragua produces only translational landslides.

[51] Large subducting seamounts, fracture the entire overriding plate under the middle slope (~5–8 km

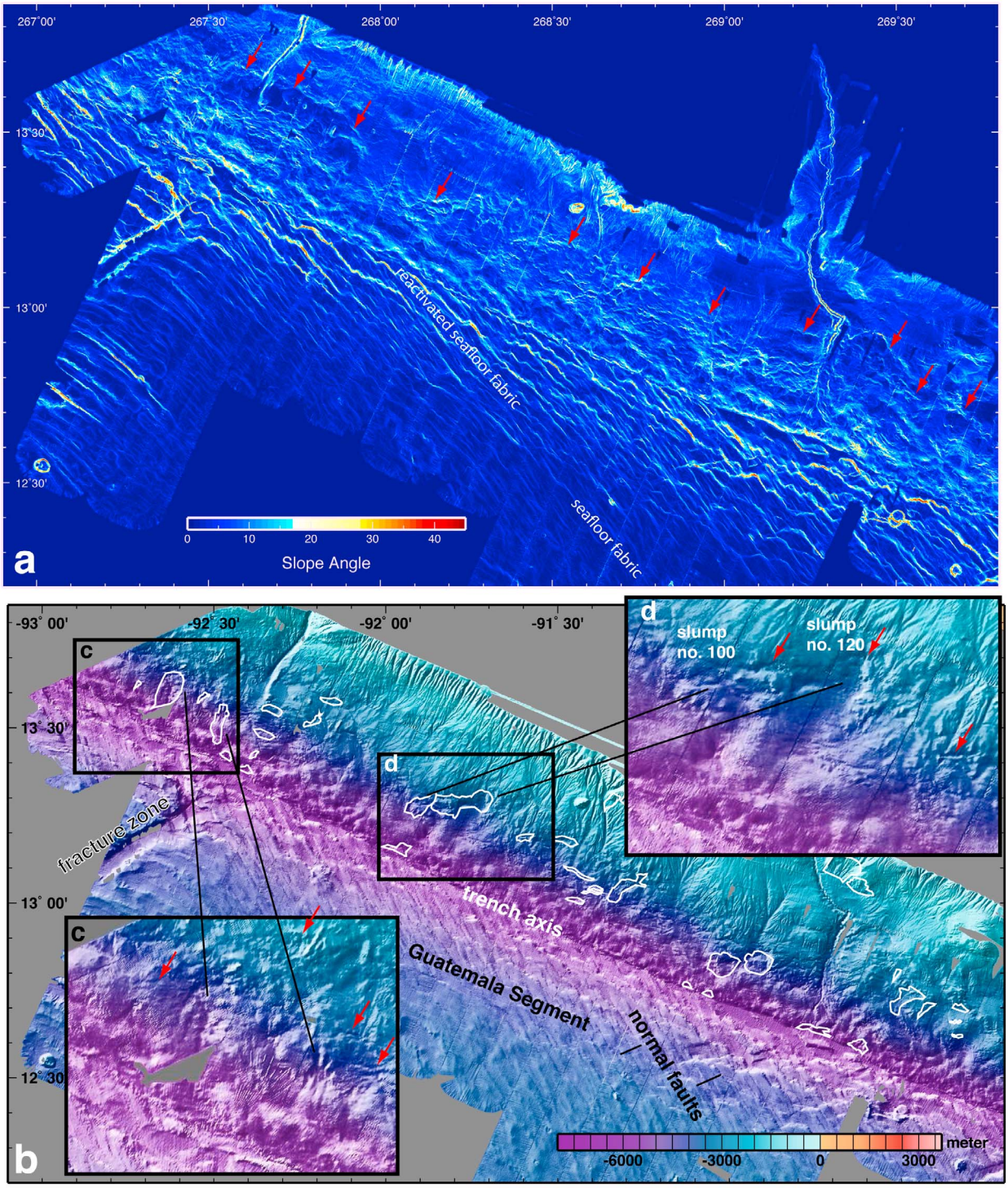

Figure 18. Seafloor maps of the Guatemala segment. (a) Shaded relief bathymetric map of the segment. It displays the greatest variability of types of mass wasting structures of all segments. (b) Local slope angle. The image displays numerous normal fault scarps. Normal faulting initiates in the upper part of the middle slope, indicated by red arrows, and develops across the middle-lower slope, affecting the development and shape of slope failures. The rough topography of the slope possibly indicates a comparatively high frequency of slope failure. (c) Close-up of the lower slope translational slides, which are oriented along fault scarps indicated by arrows. (d) Close-up of the middle slope. Rotational failures with irregular shapes start at or near normal fault scarps indicated by arrows and are difficult to distinguish from faulting scarps.

thick). These fractures will then be the location where deep-rooted detachments of slumps develop [*von Huene et al.*, 2004a]. The slump moves downslope as the seamount underthrusts further, and the previously uplifted area collapses. Examples are Jaco, Parrita and Nicoya slumps. When large seamounts underthrust the upper slope, like offshore Costa Rica, the plate flexes upward, but it is sufficiently thick (~8–12 km thick) not to be broken. Here failure is not along steep scarps, and shallower (few hundred meters thick) translational slides (e.g., Quepos and Cabo Blanco slides) form. In Nicaragua, seismically imaged underthrusted seamounts [*McIntosh et al.*, 2007] have not made a furrow in the slope along their trail, indicating that they do not break the entire overriding plate. Here, sediment fails along strata-parallel detachment planes (e.g., Masaya slide). Rapid oversteepening above subducting topography may trigger translational slides in the upper slope of central Costa Rica and middle slope of the Nicaragua segment.

[52] How failure ultimately evolves during collapse is unclear, and the downslope progress of a landslide may be influenced by a combination of processes including seismicity and fluid flow that may work in conjunction or in a cumulative manner. The largest historical earthquakes in the region are interplate thrusts with magnitude >6, Mw < 8, occurring at depths of 20–30 km, and 50–100 years recurrence time [*Ambraseys and Adams*, 1996]. Several studies indicate that interplate earthquakes of >Mw ~6 occur every 30–50 years along several sectors of each segment. The identified 147 failures include some that contain multiple failures and thus the total failure abundance is somewhat larger. Taking that into account and assuming a linear correspondence between large earthquakes and slides, would suggest that all slides could be created in a few hundreds of years, which appears to be unlikely. We know that the furrow reaching Jaco scar (Figures 4 and 8) has formed in ~230000 years, which is the time required for the seamount to underthrust to its present position assuming current convergence rates. The furrow contains a few slides that suggest a comparatively larger time span for sliding that for large earthquakes. We interpret that if large magnitude earthquakes and slumping occurred at similar rates, there should be more failures. Integrating large intracrustal and bending-related intraplate events would only increase the probability that the two processes occur at different rates. Thus, even though ground acceleration during earthquake rupture may ultimately influence slumping, the rates of both phenomena are dissimilar.

[53] Fluid flow along detachment planes and fracture networks might also play a role. Outflow of deep source fluid originating at the plate boundary and traversing the upper plate has been discovered at many seafloor seepages and fault scarps along the slope of the MAT [*Hensen et al.*, 2004; *Sahling et al.*, 2008; *Ranero et al.*, 2008]. Fluids probably also ascent along seamount subduction induced fractures, and abundant chemosynthetic fauna found on Jaco scarp [*Sahling et al.*, 2008] support that deep-sourced, nutrient-rich fluids ascent along steep detachments.

[54] Translational sliding may be controlled by discrete sediment layers and deformation by faults. Typically the successions contain several meters thick terrigenous turbidites, intercalated by several cm thick ash layers. The ash layers may form weak layers in the sediment column. *Harders et al.* [2010] report that a core taken near the upper headwall area of the translational Hermosa slide recovered the slide plane, identified as a regionally mapped ash layer (Figure 13b). The upper part of the ash layer was removed, leaving only the coarse-grained basal section overlain by marine clays. *Harders et al.* [2010] interpret that the layer experienced liquefaction during earthquake shaking. Liquefaction created a water film sandwiched between clay-rich sediment, promoting translational sliding along the lubricated zone. Cores taken on cruises SO 173, M54, and M66 on the slope from Guatemala to Nicaragua found 5–10 cm thick ash layers intercalated about every 1 m, creating the distinct coarse tephra and clay layering. This makes the mechanism of weak fluid-rich, coarse ash layers (preconditioning) and earthquakes (trigger) viable for translational sliding in the entire area.

[55] Fluids and/or gas from gas hydrate dissociation are often proposed trigger mechanisms. Hydrate dissociation might trigger comparatively small slides in the uppermost slope offshore Costa Rica (Figure 12). These slides occur at ~550 m water depth, near to the upper limit of gas hydrate stability, seismically imaged in this area [*Marquardt*, 2005]. Numerical modeling of degradation of organic matter, using data from cruises M54, SO173 and ODP Leg 140 Site 1041, estimated that in situ formation of methane is insufficient to reach methane saturation in pore water to precipitate gas hydrate, and thus gas hydrate dissociation appears to be unlikely as failure trigger [*Marquardt*, 2005]. However, the spatial correspondence of bottom simulating

reflectors and several slides in the uppermost slope supports a causal relationship, and a role of deeper methane (biogenic or thermogenic) migrating and accumulating upslope cannot be discarded.

[56] Subduction of seamounts and ridges appear to play a major role in slope preconditioning offshore Costa Rica and Nicaragua, and horst and graben relief for slumping in the lower slope of the region. However, other processes probably precondition the middle and upper slope of El Salvador and Guatemala. Offshore El Salvador, normal faulting is relatively subdued and canyons incise the upper slope where they are particularly well developed in comparison to any other segment of the margin, indicating a comparatively tectonically stable segment. Abundant translational slides cut the flanks of carved ridges and canyon flanks. We interpret that these structures result from oversteepening. Progressive incision along long-lived canyons create steep canyon walls that fail in relatively small slides. The unlikely influence of the subducting plate topography on the upper slope appears to indicate that seismic shaking and perhaps fluid outflow at the canyon flanks might be potential triggers. Offshore Guatemala a steep middle-upper slope is cut by numerous slightly trench-oblique normal faults. The result is a hummocky terrain possibly formed by comparatively frequent failures, however failures are considerably smaller that in Nicaragua and Costa Rica. The failures are randomly distributed, have short runout distances and overprint earlier events. The failures seem to predominantly form at normal fault scarps, with broad and short scars extending parallel to the faults. The short runout distances may be due to the hummocky slope morphology that stops failed sediment. We interpret that preconditioning in the Guatemala is dominantly caused by basal tectonic erosion. This process leads to gradual thinning of the overriding plate, associated normal faulting, and progressive steepening of slope sectors. A particular triggering mechanism here is not obvious, and could be any one of the mechanisms discussed above.

5. Conclusions

[57] This work presents the first comprehensive study of mass wasting processes at a continental slope of an extensive section of a convergent margin dominated by subduction erosion. We have detected and analyzed an inventory of 147 failure structures along ~1300 km of the continental slope of the MAT.

[58] We mapped various types of translational slides, more abundant in central Costa Rica, Nicaragua and El Salvador segments. Two types of rotational slumps are related to seamount subduction offshore central Costa Rica and to normal faults in the slope in the Guatemala segment. We identified large rockfalls only along the narrow and steep slope offshore Osa Peninsula, where Cocos Ridge subducts. Other segments like North Nicoya and El Salvador display a comparatively low abundance of failures, and the few failures are relatively small.

[59] The combination of distribution and abundance of failures, and slope width and angle indicates a segmentation of the slope into six regions containing different assemblies of mass-wasting features (Figure 1 and Table 1). Different types of failure usually characterize the lower, middle and upper slope sectors of each segment. We conclude that the variability of structures that define the along-margin segmentation, and across-slope changes primarily reflects variations in tectonic processes, controlled by variations the style and intensity of tectonic erosion, and in deformation related to relief of the oceanic plate. Variations in deformation patterns along and across the slope are possibly related to a first degree to changes in both topography of subducting volcanic constructions (conical seamounts, guyots, ridges), and relief formed by bending-related deformation of the oceanic plate (horst and graben). In support, along-trench changes in character of the oceanic plate exhibit a distribution that corresponds to the interpreted segmentation of the continental slope opposite.

[60] Other preconditioning factors like sedimentation rate, changes in sediment type, and presence of gas hydrate commonly invoked in other settings, do not noticeably change along the strike of the margin, and although may locally be involved in failure, cannot explain the distribution and style of failure.

[61] Gravitational collapse above moving underthrusting relief is a likely failure trigger for slumps. Fast oversteepening above subducting topography may trigger translational slides in the middle slope of Nicaragua or upper slope of Costa Rica. Other possible trigger is earthquake shaking. However, we suggest that the rate of sliding is considerably lower that than recurrence time of large earthquakes (>Mw6). Earthquake magnitude and recurrence time do not appear to be variable enough along the MAT [*Ambraseys and Adams*, 1996] to explain the segmentation of mass-wasting structures.

Acknowledgments

[62] This study is contribution 202 of the Sonderforschungsbereich (SFB) 574 funded by Deutsche Forschungsgemeinschaft (DFG). The data were collected during cruises of German R/V *Sonne* funded by the Ministry of Science and Education (BMBF) and R/V *Meteor* funded by the Deutsche Forschungsgemeinschaft (DFG) and U.S. R/V *M. Ewing* funded by NSF. We acknowledge the journal reviewer comments by J. Chaitor and D. Scholl that helped improve the clarity of the paper.

References

Ambraseys, N. N., and R. D. Adams (1996), Large-magnitude Central American earthquakes, 1898–1994, *Geophys. J. Int.*, *127*, 665–692, doi:10.1111/j.1365-246X.1996.tb04046.x.

Aubouin, J., and R. von Huene (1982), *Initial Reports of the Deep Sea Drilling Project*, vol. 67, Deep Sea Drill. Program, U.S. Gov. Print. Off., Washington, D. C., doi:10.2973/dsdp.proc.67.1982.

Aubouin, J., J. F. Stephan, J. Roump, and V. Renard (1982), The Middle America Trench as an example of a subduction zone, *Tectonophysics*, *86*, 113–132.

Baltuck, M., E. Taylor, and K. McDougall (1985), Mass movement along the inner wall of the Middle America Trench, Costa Rica, *Initial Rep. Deep Sea Drill. Proj.*, *84*, 551–570.

Bialas, J., E. Flueh, and G. Bohrmann (1999), FS SONNE, cruise report SO144/1 and 2PAGANINI; San Diego–Caldera (September 7–November 7, 1999), *Rep. 94*, pp. 1–437, Leibniz Inst. of Mar. Sci. at Univ. of Kiel (IFM-GEOMAR), Kiel, Germany.

Caress, D. W., and D. N. Chayes (1996), Improved processing of Hydrosweep DS multibeam data on the R/V *Maurice Ewing*, *Mar. Geophys. Res.*, *18*, 631–650, doi:10.1007/BF00313878.

DeMets, C., R. G. Gordon, D. F. Argus, and S. Stein (1990), Current plate motions, *Geophys. J. Int.*, *101*, 425–478, doi:10.1111/j.1365-246X.1990.tb06579.x.

Fine, I. V., A. B. Rabinovich, B. D. Bornhold, R. Thomson, and E. A. Kulikov (2005), The Grand Banks landslide-generated tsunami of November 18, 1929: Preliminary analysis and numerical modeling, *Mar. Geol.*, *215*, 45–57, doi:10.1016/j.margeo.2004.11.007.

Flemings, P. B., H. Long, B. Dugan, J. Germaine, C. M. John, J. H. Behrmann, D. Sawyer, and IODP Expedition 308 Scientists (2008), Pore pressure penetrometers document high overpressure near the seafloor where multiple submarine landslides have occurred on the continental slope, offshore Louisiana, Gulf of Mexico, *Earth Planet. Sci. Lett.*, *269*, 309–325, doi:10.1016/j.epsl.2007.12.005.

Hampton, M. A., and H. J. Lee (1996), Submarine landslides, *Rev. Geophys.*, *34*, 33–59, doi:10.1029/95RG03287.

Harders, R., S. Kutterolf, C. Hensen, T. Moerz, and W. Brueckmann (2010), Tephra layers: A controlling factor on submarine translational sliding?, *Geochem. Geophys. Geosyst.*, *11*, Q05S23, doi:10.1029/2009GC002844.

Helm, R. (1984), Mineralogy and diagenesis of slope sediments offshore Guatemala and Costa Rica, Leg 84, *Proc. Deep Sea Drill. Program Initial Rep.*, *15*, 571–594.

Hensen, C., K. Wallmann, M. Schmidt, C. R. Ranero, and E. Suess (2004), Fluid expulsion related to mud extrusion off Costa Rica—A window to the subducting slab, *Geology*, *32*, 201–204, doi:10.1130/G20119.1.

Hühnerbach, V., D. G. Masson, G. Bohrmann, J. M. Bull, and W. Weinrebe (2005), Deformation and submarine landsliding caused by seamount subduction beneath the Costa Rica continental margin—New insights from high-resolution sidescan sonar data, in *Submarine Slope Systems: Processes and Products*, edited by D. M. Hodgons and S. S. Flint, *Geol. Soc. Spec. Publ.*, *244*, 195–205.

Johnson, D. W. (1939), Origin of submarine canyons, *J. Geol.*, *2*, 42–60, 133–158, 213–236.

Kimura, G., E. Silver, P. Blum, and the Leg 170 Scientific Party (1997), *Proceedings of the Ocean Drilling Program, Initial Reports*, vol. 170, Ocean Drill. Program, College Station, Tex.

Kukowski, N., J. Greinert, and S. Henrys (2010), Morphometric and critical taper analysis of the Rock Garden region, Hikurangi Margin, New Zealand: Implications for slope stability and potential tsunami generation, *Mar. Geol.*, *272*, 141–153, doi:10.1016/j.margeo.2009.06.004.

Kutterolf, S., A. Freundt, W. Peréz, T. Mörz, U. Schacht, H. Wehrmann, and H.-U. Schmincke (2008), Pacific offshore record of plinian arc volcanism in Central America: 1. Along-arc correlations, *Geochem. Geophys. Geosyst.*, *9*, Q02S01, doi:10.1029/2007GC001631.

Locat, J., and H. J. Lee (2002), Submarine landslides: Advances and challenges, *Can. Geotech. J.*, *39*, 193–212, doi:10.1139/t01-089.

Marquardt, M. (2005), Investigation of a submarine landslide off Costa Rica: Reconstruction of the date and the sedimentary and geochemical development of the BGR-landslide, diploma thesis, Inst. of Geosci., Fac. of Math. and Nat. Sci., Christian-Albrechts-Univ. of Kiel, Kiel, Germany.

McAdoo, B. G., L. F. Pratson, and D. L. Orange (2000), Submarine landslide geomorphology, US continental slope, *Mar. Geol.*, *169*, 103–136, doi:10.1016/S0025-3227(00)00050-5.

McIntosh, K. D., E. A. Silver, I. Ahmed, A. Berhorst, C. R. Ranero, R. K. Kelly, and E. R. Flueh (2007), The Nicaragua Convergent Margin: Seismic reflection imaging of the source of a tsunami earthquake, in *The Seismogenic Zone of Subduction Thrust Faults*, edited by T. Dixon and J. C. Moore, pp. 257–287, Columbia Univ. Press, New York.

Mienert, J., J. Posewang, and M. Baumann (1998), Gas hydrates along the northeastern Atlantic margin: Possible hydrate-bound margin instabilties and possible release of methane, in *Gas Hydrates: Relevance to World Margin Stability and Climatic Change*, edited by J.-P. Henriet and J. Mienert, *Geol. Soc. Spec. Publ.*, 137, 275–291.

Mulder, T., and P. Cochonat (1996), Classification of offshore mass movements, *J. Sediment. Res.*, *66*, 43–57.

Orange, D., and N. Breen (1992), The effects of fluid escape on accretionary wedges: 2. Seepage force, slope failure, headless submarine canyons, and vents, *J. Geophys. Res.*, *97*(B6), 9277–9295, doi:10.1029/92JB00460.

Pecher, I., N. Kukowski, C. R. Ranero, and R. von Huene (2001), Gas hydrates along the Peru and Middle America Trench systems, in *Natural Gas Hydrates: Occurrence, Distribution, and Detection*, *Geophys. Monogr. Ser.*, vol. 124, pp. 257–271, AGU, Washington, D. C.

Ranero, C. R., and R. von Huene (2000), Subduction erosion along the Middle America convergent margin, *Nature*, *404*, 748–752, doi:10.1038/35008046.

Ranero, C. R., R. von Huene, E. Flueh, M. Duarte, D. Baca, and K. McIntosh (2000), A cross section of the convergent Pacific margin of Nicaragua, *Tectonics*, *19*(2), 335–357, doi:10.1029/1999TC900045.

Ranero, C. R., A. Villaseñor, J. Phipps Morgan, and W. Weinrebe (2005), Relationship between bend-faulting at trenches and intermediate-depth seismicity, *Geochem. Geophys. Geosyst.*, *6*, Q12002, doi:10.1029/2005GC000997.

Ranero, C. R., I. Grevemeyer, H. Sahling, U. Barckhausen, C. Hensen, K. Wallmann, W. Weinrebe, P. Vannucchi, R. von Huene, and K. McIntosh (2008), The hydrogeological system of erosional convergent margins and its influence on tectonics and interplate seismogenesis, *Geochem. Geophys. Geosyst.*, *9*, Q03S04, doi:10.1029/2007GC001679.

Ratzov, G., M. Sosson, J.-Y. Collot, S. Migeon, F. Michaud, E. Lopez, and Y. Le Gonidec (2007), Submarine landslides along the North Ecuador–South Colombia convergent margin: Possisible tectonic control, in *Submarine Mass Movements and Their Consequences*, edited by V. Lykousis, D. Sakellariou, and J. Locat, pp. 47–55, Springer, Dordrecht, Netherlands, doi:10.1007/978-1-4020-6512-5_6.

Sahling, H., D. G. Masson, C. Ranero, V. Hühnerbach, W. Weinrebe, I. Klaucke, D. Bürk, W. Brückmann, and E. Suess (2008), Fluid seepage at the continental margin offshore Costa Rica and southern Nicaragua, *Geochem. Geophys. Geosyst.*, *9*, Q05S05, doi:10.1029/2008GC001978.

Sawyer, D. E., P. B. Flemings, R. C. Shipp, and C. D. Winker (2007), Seismic geomorphology, lithology, and evolution of the late Pleistocene Mars-Ursa turbidite region, Mississippi Canyon area, northern Gulf of Mexico, *AAPG Bull.*, *91*, 215–234, doi:10.1306/08290605190.

Skempton, A. W., and J. N. Hutchinson (1969), Stability of natural slopes and embankment foundations: State-of-the-art report, paper presented at 7th International Conference on Soil Mechanics and Foundation Engineering, Soc. Mex. de Mec. de Suelos Mex., Mexico City.

Sultan, N., et al. (2004), Triggering mechanisms of slope instability processes and sediment failures on continental margins: A geotechnical approach, *Mar. Geol.*, *213*, 291–321, doi:10.1016/j.margeo.2004.10.011.

Tappin, D. R., P. Watts, G. M. McMurtry, Y. Lafoy, and T. Matsumoto (2001), The Sissano, Papua New Guinea tsunami of July 1998—Offshore evidence on the source mechanism, *Mar. Geol.*, *175*, 1–23, doi:10.1016/S0025-3227(01)00131-1.

Vannucchi, P., C. R. Ranero, S. Galeotti, S. M. Straub, D. W. Scholl, and D. McDougall-Ried (2003), Fast rates of subduction erosion along the Costa Rica Pacific margin: Implications for nonsteady rates of crustal recycling at subduction zones, *J. Geophys. Res.*, *108*(B11), 2511, doi:10.1029/2002JB002207.

Vannucchi, P., S. Galeotti, P. Clift, C. R. Ranero, and R. von Huene (2004), Long term subduction erosion along the Middle America Trench offshore Guatemala, *Geology*, *32*, 617–620, doi:10.1130/G20422.1.

von Huene, R., and C. R. Ranero (2003), Subduction erosion and basal friction along the sediment-starved convergent margin off Antofagasta, Chile, *J. Geophys. Res.*, *108*(B2), 2079, doi:10.1029/2001JB001569.

von Huene, R., et al. (1980), Leg 67: The Deep Sea Drilling Project Mid-America Trench transect off Guatemala, *Geol. Soc. Am. Bull.*, *91*(7), 421–432, doi:10.1130/0016-7606(1980)91<421:LTDSDP>2.0.CO;2.

von Huene, R., et al. (1984), *Proceedings of the Deep Sea Drilling Program, Initial Reports*, vol. 84, U.S. Gov. Print. Off., Washington, D. C.

von Huene, R., J. Bourgois, J. Miller, and G. Pautot (1989), A large tsunamogenic landslide and debris flow along the Peru Trench, *J. Geophys. Res.*, *94*(2), 1703–1714, doi:10.1029/JB094iB02p01703.

von Huene, R., C. R. Ranero, W. Weinrebe, and K. Hinz (2000), Quaternary convergent margin tectonics of Costa Rica, segmentation of the Cocos Plate, and Central American volcanism, *Tectonics*, *19*, 314–334, doi:10.1029/1999TC001143.

von Huene, R., C. R. Ranero, and P. Watts (2004a), Tsunamigenic slope failure along the Middle America Trench in two tectonic settings, *Mar. Geol.*, *203*, 303–317, doi:10.1016/S0025-3227(03)00312-8.

von Huene, R., C. R. Ranero, and P. Vanucchi (2004b), Generic model of subduction erosion, *Geology*, *32*, 913–916, doi:10.1130/G20563.1.

Weinrebe, R. W., and E. R. Flueh (2002), Cruise report SO163—Subduction I internal report, *Contrib. 14*, SFB 574, Leibniz Inst. of Mar. Sci. at Univ. of Kiel (IFM-GEOMAR), Kiel, Germany.

Weinrebe, R. W., and C. R. Ranero (2004), Cruise report SO173/2 "Seduction"—Seismogenesis and tectonic erosion during subduction: Middle America Margin internal report, *Contrib. 48*, SFB 574, Leibniz Inst. of Mar. Sci. at Univ. of Kiel (IFM-GEOMAR), Kiel, Germany.

Werner, R., K. Hoernle, P. van den Bogaard, C. Ranero, R. von Huene, and D. Korich (1999), Drowned 14-m.y.-old Galápagos archipelago off the coast of Costa Rica: Implications for tectonic and evolutionary models, *Geology*, *27*, 499–502, doi:10.1130/0091-7613(1999)027<0499:DMYOGP>2.3.CO;2.

Wessel, P., and W. H. F. Smith (1998), New improved version of generic mapping tools released, *Eos Trans. AGU*, *79*, 579, doi:10.1029/98EO00426.

Wilson, D. S. (1996), Fastest known spreading on the Miocene Cocos-Pacific plate boundary, *Geophys. Res. Lett.*, *23*, 3003–3006, doi:10.1029/96GL02893.

4

An overview of the role of long-term tectonics and incoming plate structure on segmentation of submarine mass wasting phenomena along the Middle America Trench

Rieka Harders, César R. Ranero and Wilhelm Weinrebe

In press as chapter 35 in:Y. Yamada et al. (eds.), Submarine Mass Movements and Their Consequences, Advances in Natural and Technological Hazards Research 31, doi: 10.1007/978-94-007-2162-3_35,

An overview of the role of long-term tectonics and incoming plate structure on segmentation of submarine mass wasting phenomena along the Middle America Trench

Rieka Harders[1], César R. Ranero[2], Wilhelm Weinrebe[1]

1. SFB 574 and IFM-GEOMAR. Wischhofstrasse 1-3, 24148, Kiel, Germany.

2. ICREA at CSIC, Barcelona Center for Subsurface Imaging, Instituto de Ciencias del Mar, Pg. Marítim de la Barceloneta 37-49, 08003, Barcelona, Spain.

Abstract

We study mass wasting along the Middle America Trench (MAT), a subduction zone dominated by tectonic erosion, using a comprehensive data set of seafloor relief. We integrate previous studies of long-term tectonic processes to analyze how they influence the evolution of the slope structure and precondition the continental slope for mass wasting. We have used the distribution of an inventory of 147 slope failure structures along the MAT to discuss their relation to subduction erosion. We interpret that preconditioning of the slope by long-term tectonics, interacts in a shorter-term scale with features on the under-thrusting oceanic plate to modulate the abundance and types of mass wasting phenomena. The complex origin of the incoming oceanic plate has produced abrupt lateral changes in plate age, crustal thickness, relief, and response to bending deformation at the trench, leading to its partitioning into 6 segments. We found that the continental-slope failure style and abundance are partitioned into 6 segments that spatially match the ocean plate segments.

Keywords: Submarine landslide, convergent margin, subduction erosion

1. Introduction

At convergent margins with accretionary prisms most landslides and slumps seem related to contractional tectonics and fluid seepage, and have shorter lengths than failures at Atlantic continental slopes (McAdoo et al. 2000). Studies of submarine mass wasting at convergent margins dominated by tectonic erosion are comparatively limited; however, this type of system is active in about 50% of the world subduction zones. Failures have been studied at slopes in Peru (von Huene et al. 1989), Costa Rica and Nicaragua (von Huene et al. 2004a; Hünerbach et al. 2005) and New Zealand (Kukowski et al. 2010) but extensive studies have not been attempted. Harders et al. (in press) have constructed an inventory of 147 slope failure structures along ~1300 km of the continental slope of the MAT. The data have been collected along the MAT from the Mexico-Guatemala border to southernmost Costa Rica. This region has been investigated by international programs during the last four decades and particularly

during the last decade as focus area of the US-Margins and German SFB 574 programs. The goal of this contribution is to analyze how preconditioning of the continental slope by long-term tectonics and interacts with changes in the character of the currently subducting oceanic plate to modulate mass wasting phenomena.

1.1 Oceanic plate segmentation

The oceanic Cocos Plate subducts under the Caribbean Plate along the MAT at a rate of ~85 mm/yr in the study region (DeMets 2001). The Cocos Plate is composed of lithosphere formed at the Cocos-Nazca and East Pacific Rise spreading centers, one of them affected by a hot spot (Fig. 1). The complex origin of the plate has produced abrupt lateral changes in plate character, including variation in plate age, crustal thickness, plate relief, and response to bending deformation at the trench (Barckhausen et al. 2001; Ranero et al. 2005). The section of the plate subducting under most of Costa Rica was formed at the Cocos-Nazca spreading center influenced by Galapagos hotspot. Changes in hotspot-ridge interaction formed distinct plate segments (Figure 1).

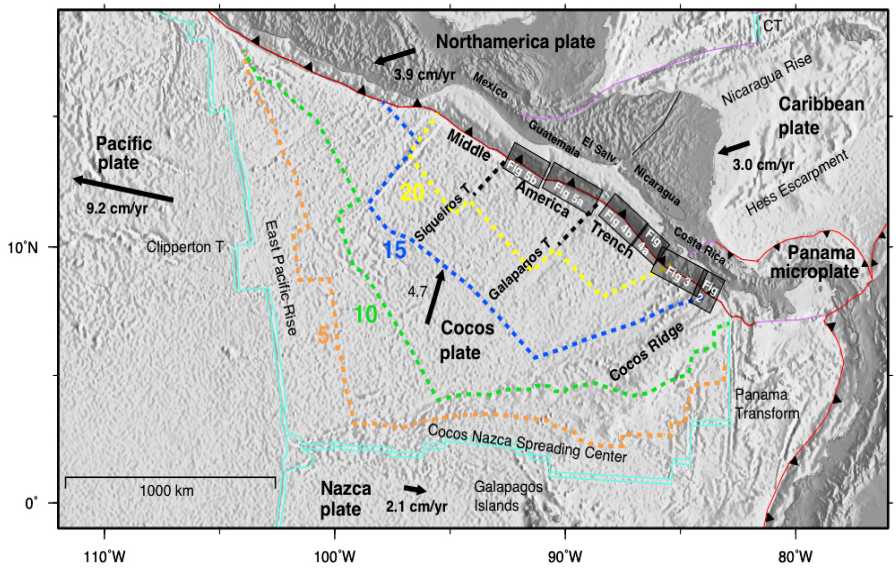

Figure 1. Tectonic plates of the subduction system of Central America. The plate subducting along the Middle America Trench was formed at the Cocos-Nazca Spreading Center in the southeastern and at the East Pacific Rise in the north. Isochrones are marked by dashed-lines, with age in million years. The semi-transparent box marks study region with segments discussed in the text..

The Cocos Ridge segment has 10-18-km-thick crust that creates a comparatively shallow swell with a relief festooned by elongated km-high ridges and few-hundred-meter high seamounts. To the NW is a seamount segment characterized by 7-8 km-thick crust with 2-3 km-high, 10-30 km wide seamounts, guyots and ridges. Offshore of the North Nicoya Peninsula the smoothest ocean seafloor of the entire region is subducted. The plate under-thrusting from offshore North Nicoya Peninsula to Guatemala was formed at the East Pacific rise (Fig. 1). The segment offshore Nicaragua has ~5.5 km-thick-crust, numerous ~0.5-1.0-km-high seamounts and is heavily faulted by bending of the plate before under-thrusting. Normal faults form a rugged terrain, with 200-500-m-high horst and graben relief striking parallel to the trench axis. Two other segments subducts under El Salvador and Guatemala. The Guatemala segment has the highest

topography of up to 800-m-high ridges formed by bending-related faults that strike oblique to the trench axis (Ranero et al., 2005).

1.2 Tectonic erosion processes

The study region of the MAT is dominated by long-term tectonic erosion processes that have operated in the entire area for the last ~15-25 m.y. (Ranero et al. 2000,). Tectonic erosion processes remove material from the base of the overriding plate and transfer it to the subduction channel to be transported to deeper levels. Thus, tectonic erosion implies the progressive migration of the plate boundary into shallower levels of the overriding plate. The upward movement of the plate boundary fault is probably assisted by over-pressured fluids at the fault zone, that hydrofracture the base of the overriding plate and migrate up, leading to the establishment of a new shallower decollement (von Huene et al. 2004b). Tectonic erosion causes large-scale fracturing and faulting, slope over-steepening, and subsidence that fundamentally influence the structural evolution of the geological units under, and the morphology of, the continental slope (Ranero et al. 2008). The intensity and location of tectonic erosion processes appear to be spatially constrained by the relative abundance of fluids at the plate boundary (*Ranero et al., 2008)*. The intensity and location of tectonic erosion has been interpreted as the dominant process that determines the structural evolution of the continental slope (von Huene et al., 2004b, Ranero et al., 2008).

2. Relationships between ocean plate character, tectonic erosion and mass wasting.

The six segments of the oceanic plate described in section 1 are found to correspond to six segments of the continental slope. Each of the slope segments displays distinct tectonic styles, slope morphology, and differences in type, abundance and spatial occurrence of mass wasting structures.

2.1 Osa Peninsula - Cocos Ridge segment.

The thick crust of Cocos ridge forms a ~100 km broad swell of seafloor about 1.0-2.0 km shallower that the rest of the incoming plate segments. The buoyancy of the young plate (14 Ma) with thick crust has dramatic effects in subduction processes. The plate does not appreciably bend approaching the trench axis and collides with the overriding plate causing slope-wide deformation (Fig. 2). The young plate age is associated to high heat flow and sediment dehydration in the subduction channel occurs across a comparatively narrow, shallow area about 20 km wide (Ranero et al. 2008). This area is positioned under, and spatially matches the width of, the narrowest (15-20 km) and steepest (average of 10º-15º) continental slope in the region, situated offshore Osa Peninsula (Fig. 2). We interpret that the slope width is governed by the width of the underlying area of mineral dewatering, so that it is controlled by basal tectonic erosion of material of the overriding plate with concomitant subsidence.

The slope terrain is characterized by mass-failure morphology including concave scarps and rotational failures, and associated rock avalanches which deposit debris over the incoming plate seafloor (Fig. 2). Deformation of the slope appears so intense that canyon systems are poorly developed. In the SE, the slope is impinged by 0.5-1.0-km-high sharp crests of the Cocos Ridge that have created through time a rugged morphology across upper to lower slope. Landslides are ≤ 12 km long and ≤ 5 km wide. Their headwall are steep scarps up to 1 km high with angles ranging from 50º in the

upper part to 30º in the lower part. Block deposits consist of large boulders up to 50 m high and 600 m long that extend 3-6 km into the smooth ocean plate seafloor. Deposits from some scarps are probably tectonically kneaded into the slope frontal units at the convergence rate of ~9 km per 100,000 year.

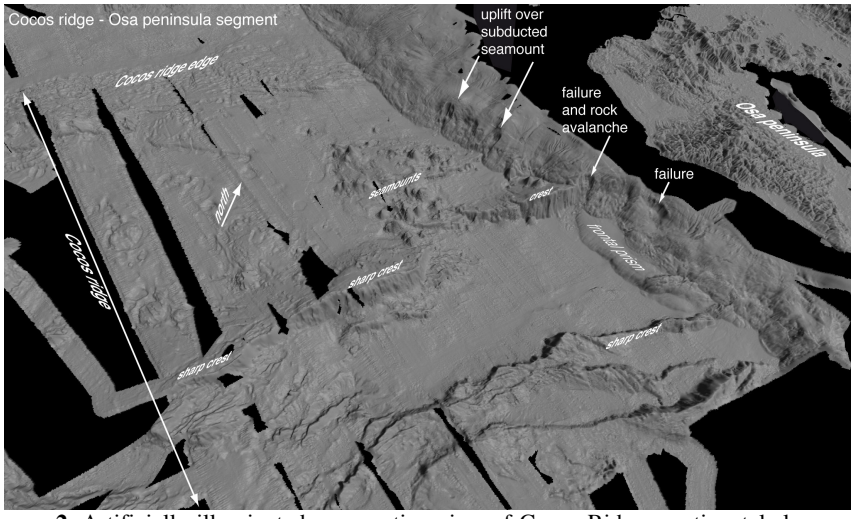

Figure 2. Artificially illuminated, perspective view of Cocos Ridge, continental slope, and Osa Peninsula (3x vertical exaggeration [v.e.]). The image is 130 km wide along the trench axis. Ridge topography is elevated 1-2 km compared to the plate to the north. Trench axis depth is 1950 m at SE edge of figure and 2920 m at NW edge. The plate is ornamented with ridges up to ~1 km above surrounding seafloor and groups of small seamounts.

2.2 Central Costa Rica - Seamounts segment

The central Costa Rica segment immediately north of the Cocos Ridge segment, is marked by an abrupt broadening of the slope from ~15-20 km to ~50-60 km width and a change in the average slope dip to less than 5º (Figs. 2 and 3). Here, the incoming oceanic plate is spotted with large conical seamounts, low ridges, and guyots created by the Galapagos Hotspot (Figs. 1 and 3). The prominent slope deformation caused by subduction of the features on the incoming plate for at least the last 300,000 years in this segment has attracted considerable scientific investigation, and major failures have been extensively studied (von Huene et al. 2004a, Harders et al. in press).

Colliding seamounts remove sectors of the slope toe, causing a 10-20 km landward retreat of the deformation front. A frontal sediment prism is subsequently re-built by sediment kneading possibly coming from slope mass wasting. As collision progresses, seamounts under-thrust and uplift the slope as indicated by domes located above the seamounts (Ranero and von Huene 2000). Uplift causes widespread fracturing of the overriding plate extending further that the dome. Further movement of the seamounts causes rotational slumping in their wake. Slumps are > 20 km long and wide and with rotational slide planes with steep headwalls up to 40º dip and 1 km high (Harders et al., in press.). This segment ends northwards where a fossil triple junction on the oceanic plate and associated low ridge under-thrust the continental plate (Barckhausen et al., 2001). The ridge causes a cohesive rotational slope failure (Harders et al., in press.).

Some slumps appear complex, and involve blocks with deep detachment planes that possibly cut the entire overriding plate of up to a 4-5 km thick in the lower or middle slope (Ranero and von Huene 2000). Evidence for deep-cutting headwalls comes from fluids rising from the plate boundary during subduction that have been measured at

faults and headwalls at various places along the slope (Ranero et al., 2008). Collocated shallower detachment planes involve strata collapsing as rock avalanches along 20-30-km wide slope furrows marking seamounts progression (Figure 3). Further seamount under-thrusting beneath the upper slope changes the style of failure. In the upper slope, the plate is 10-12 km thick and it seems to be too strong to be entirely fractured (von Huene et al., 2000). Local uplift is accompanied by moderate over-steepening to < 10º dip causing translational sliding of sediment (Harders et al., in press.).

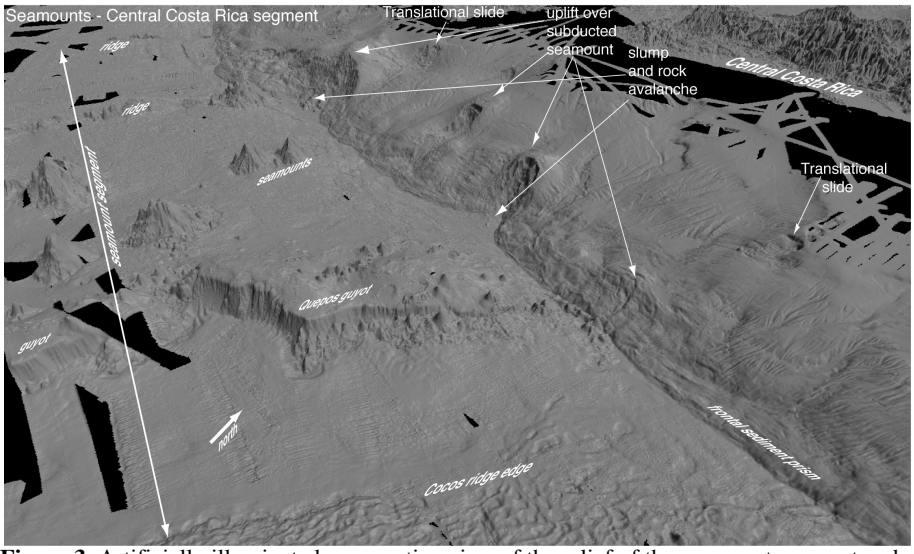

Figure 3. Artificially illuminated, perspective view of the relief of the seamount segment and slope off Central Costa Rica (3x v.e.). The image is 270 km wide along the trench axis. Trench axis depth is 2000 m at SE edge of figure and 4200 m at NW edge. The ocean plate is festooned with 2-3 km tall seamounts and guyots and 0.5-1.0 km high ridges.

In spite of the intense deformation caused by subduction of numerous high-relief features in this segment, which are almost as extensive as structures ornamenting Cocos Ridge, canyon systems are better developed here. Canyons are largely absent or confined to the upper slope offshore along most of Osa Peninsula where the shallowest section of Cocos Ridge subducts (Fig. 2). However, canyon systems are more abundant, reaching the middle or lower slope across the wider slope of Central Costa Rica segment (Figure 3) This observation indicates a different slope evolution and somewhat longer slope stability for sectors of this segment. The greater stability, shallower average slope dip angle, and broader slope may be related to changes in tectonic erosion processes along the plate boundary. This proposition is supported by a comparatively lower heat flux in this segment, leading to a wider region of early mineral dehydration along the plate boundary (Ranero et al., 2008), and thus a comparatively broader area where over-pressured fluids and associated hydrofracturing promote removal of overriding plate material and concurrent subsidence.

2.3. North Nicoya - Smooth ocean floor segment

This segment displays a remarkable different morphology compared to the other segments. The incoming plate is similar in age to the Central Costa Rica-seamount segment (Barckhausen 2001), and although the thermal structure is locally cooler, at segment scale the temperature at the plate boundary does not differ much to the seamount segment. The width of the slope is also similar, and average slope dips of 5º-10º somewhat higher (Fig. 4). These observation indicate a comparable width of the area of tectonic erosion, and gradual subsidence. In spite of evidence of extensional

normal faulting associated to tectonic erosion and slightly higher average slope dip angle, the segment lacks noticeable failures. Here, slope failures are limited to a few small translational slides (~3 km wide headwalls) within the middle slope (Harders et al. 2010). The different slope stability of this segment when compared the other segments is probably related to the absence of large topographic features on the subducting plate, as inferred from the featureless incoming plate of this segment.

2.4. Nicaragua - Oceanic Bend-faulting segment

Although the transition from the North Nicoya to the Nicaragua segment is not abrupt but gradual in both the continental slope and ocean plate morphology (Fig. 4), the change leads to a slope displaying the most fractured terrain and denser distribution of landslide scars in the study region. Similarly, the oceanic plate is cut by bending-related extensional faulting that gradually increases in offset and intensity paralleling the increase in overriding plate deformation.

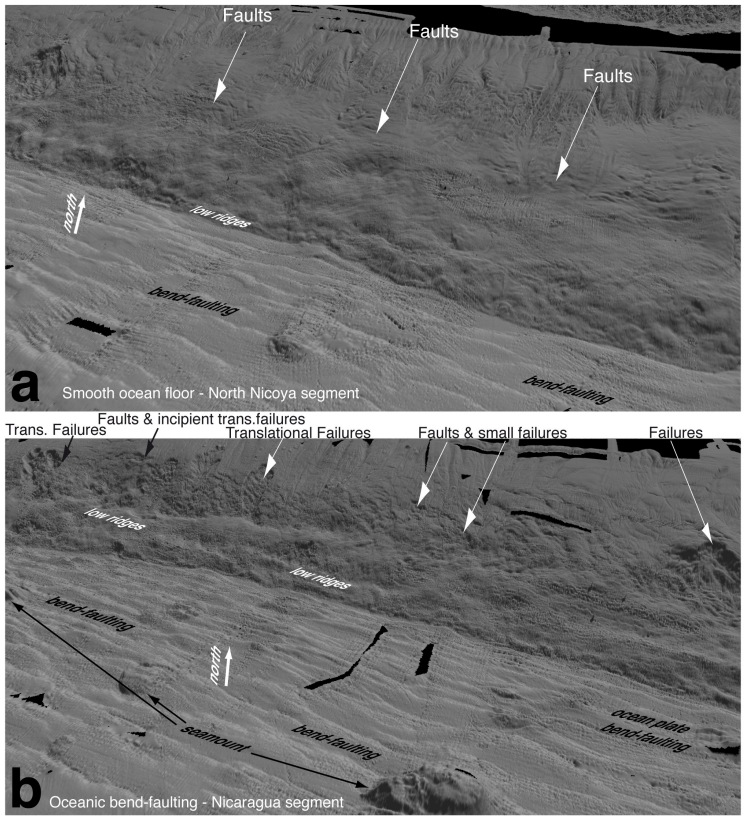

Figure 4. Artificially illuminated, perspective view of the relief of the ocean plate and continental slope offshore North Nicoya Peninsula and Nicaragua (3x v.e.). (**a**) The comparatively smooth ocean plate and tectonically little-disturbed offshore North Nicoya Peninsula. The image is 120 km wide along the trench axis, depth along trench axis is 4200 m at SE edge and 5100 m at NW edge). (**b**) The heavily faulted ocean plate with numerous seamounts. The image is 130 km wide along the trench axis. Trench axis depth is 5000 m at SE edge and 5400 m at NW edge. The middle continental slope is strongly fractured, cut by extensional faults and has many translational landslide scars.

The distribution of the continental slope morphology of this segment contrasts to that of other segments. The slope is divided in a gently sloping upper, steep middle and

comparatively featureless lower slope. The relatively steep continental middle slope, with 10º-15º average gradient, is cut by pervasive trench-axis parallel extensional faults and concentrates most slope failures that often seem to initiate at coalescent fault plates (Figure 4). Landslide scars are generally smaller that in Central Costa Rica and Osa Peninsula segments, ranging in size from a few km to a maximum of 6 km width and 12 km length and with headwalls ≤ 260 m. In marked contrast to the central Costa Rica and Osa Peninsula segments, all landslides in the North Nicoya segment are translational (Harders et al., in press.). The distinct character of the continental slope morphology indicates a new change in the tectonic processes that govern its evolution.

The three sectors morphology of the continental slope is probably related to the effect that the ocean plate relief has on tectonic erosion processes along the plate boundary. The ocean-plate faults form half-grabens that create a terrain of long ridges with relief up to 0.5 km high at the trench axis. Subduction of those trench-axis-parallel ridges deforms the lower continental slope creating low ridges that strike parallel to, and morphologically mimic, the ocean plate ridges (Figure 4). The continental plate is deformed and faulted as it rides over the subducted oceanic half grabens. The subducted grabens are possibly also an efficient mean for transportation of fractured upper plate material deeper into the subduction zone. Tectonic erosion by the subducting ridges is probably most efficient under the lower slope, where increased material removal possibly causes over-steepening and extension of the middle slope, promoting faulting and landsliding that increase in intensity in parallel to the lateral increase in bending-related fault intensity in the oceanic plate from North Nicoya to Nicaragua (Figure 4).

In addition, the oceanic plate contains abundant seamounts of dimensions smaller than in the Central Costa Rica segment, but which may have some localized effect in mass wasting processes along this segment. In particular, it is possibly that local uplift above seamounts imaged with seismic data (McIntosh et al., 2007) may have helped in the failure process of the largest slides. However, upper plate fracturing by seamounts is very limited –in comparison to Central Costa Rica- and all slides are translational.

2.5. El Salvador - Oblique bend-faulting segment

The along strike transition from the Nicaragua to the El Salvador segment is abrupt and appears to be the consequence of two superimposed changes. A major modification is a change in the strike of the deep slab which is displayed at the surface as a change in trench axis strike of the (Fig. 1) (Ranero et al., 2005). This change causes bending-related faults in the oceanic plate to under-thrust at an oblique angle of ~40º to the trench strike (Fig. 5). The second change is that the ocean plate is separated from the Nicaragua segment by the fossil Galapagos Transform trace, which implies that the plate was created in a different segment of the spreading center (Fig. 1). A fundamental difference across the transform trace is that the ocean plate in the El Salvador segment contains few seamounts of much smaller dimensions (compare Figs. 4b and 5a).

In spite of the intense ocean plate faulting, the effect on the overriding plate on the El Salvador segment appears less pronounced than in the Nicaragua segment. The lower continental slope displays subdued ridges that parallel the ridges in the incoming plate, but basal erosion of the overriding plate appears to be less intense. The result is that the middle slope seems comparatively less faulted and slide scars are noticeably absent. The upper slope also displays some indication of longer tectonic stability because canyon systems, sculpted by small translational failures (≤ 5 by 3 km), seem better established. These failures do not appear directly related to tectonic processes.

2.6. Guatemala - Ocean propagator topography segment

The transition from El Salvador to Guatemala segment is gradual and involves changes in the continental slope and ocean plate morphology that take place over a few tens of km. The style of deformation has produced a slope that at first sight may resemble similar to Nicaragua segment, but in Guatemala abundant failures are typically small and rotational, and large translational slides as those in Nicaragua are absent (Figure 5b). Failure appears related to normal faulting across the slope that is of comparatively larger dimensions than at Nicaragua or El Salvador segments. In general, the slope is more tectonically deformed than in the neighbor El Salvador segment and displays a considerable more rugged morphology and shallower canyon systems in the upper slope. An exception are two large canyon near the tow edges of the segments that reach near the trench axis and are unique features along the study sector of the MAT.

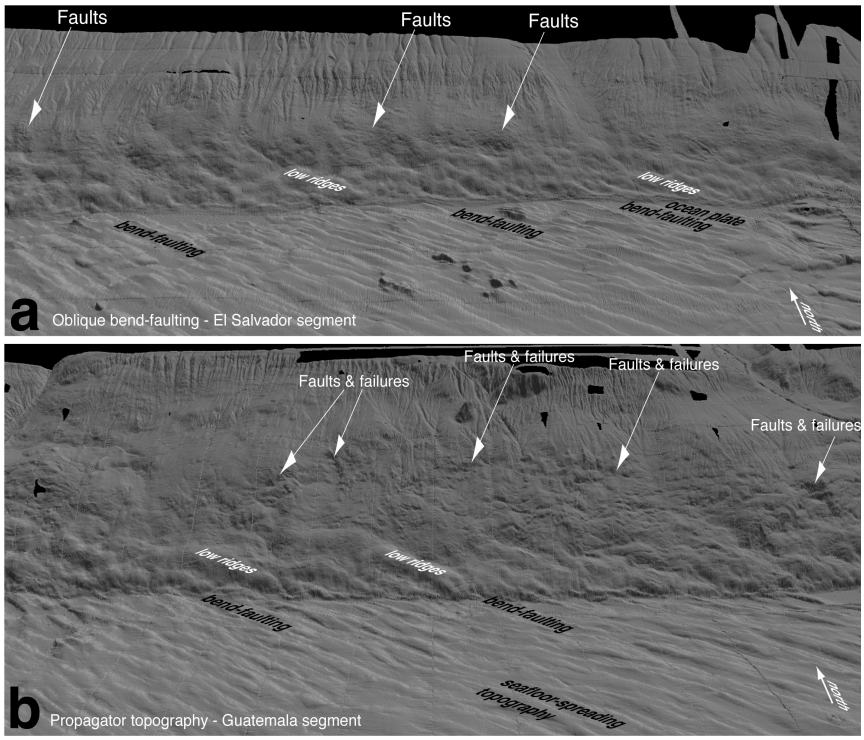

Figure 5. Artificially illuminated, perspective view of the ocean plate and continental slope offshore El Salvador and Guatemala (3x v.e.). (**a**) Relief of the strongly faulted ocean plate and tectonically disturbed slope offshore El Salvador. The image is 200 km wide along the trench axis. Trench axis depth is 5300 m at SE edge and 5800 m at NW edge. (**b**) Relief of the ocean plate and rugged slope offshore Guatemala. The image is 164 km wide along the trench axis. Trench axis depth is 6100 m at SE edge and 6500 m at NW edge.

The ocean plate of this segment displays the highest seafloor-spreading inherited topography, visible away from the trench axis in spite of ~300 meters of hemipelagic sediment cover (Fig. 5b). This several-hundred-meter high topography formed by interaction of a palo-spreading center propagator and the Siqueiros transform (Fig. 1) mapped at the northern segment edge. This topography is exacerbated approaching the trench axis by bending-related faulting, creating the most prominent ocean-plate terrain in the study region. The upper-plate deformation caused by under-trusting this topography may relate to the comparatively increased faulting and associated slope

failures of this segment.

3. Conclusions

Our analysis indicates that long-term subduction tectonics processes precondition the structure of the continental slope. Those processes are possibly controlled by factors like long term sediment supply to the trench, thickness and nature of subducting sediment, convergence rate, and plate age. Superimposed over that millions-of-year-long evolution, shorter term processes determined by the character on the currently subducting incoming oceanic plate appear to determine the type, dimensions and abundance of mass wasting events in an area. The main plate characteristics that seem to modulate landsliding phenomena include crust thickness, plate age and topographic features on the plate. Lateral changes in long-term tectonic interacting with variation of the character of the incoming oceanic plate along the MAT have led to a segmentation of mass wasting processes at the continental slope.

References

Barckhausen G.A, Ranero C R, von Huene R, Cande S, Roeser H (2001) Revised Tectonic Boundaries in the Cocos Plate off Costa Rica: Implications for the Segmentation of the Convergent Margin and for Plate Tectonic Models. J Geophys. Res 106: 19207-19220.

DeMets C (2001) A new estimate for present-day Cocos-Caribbean plate motion: implications for slip along the central american volcanic arc. Geophys Res Lett 28: 4043–4046.

Harders R, Kutterolf S, Hensen C, Moerz T, Brueckmann W (2010) , Tephra layers: A controlling factor on submarine translational sliding? Geochem. Geophys. Geosyst 11, Q05S23, doi:10.1029/2009GC002844. 2010.

Harders R, Ranero CR, Weinrebe W, Behrmann JH (in press) Submarine slope failures along the convergent margin of the Middle America Trench dominated by subduction erosion: A new setting of mass wasting processes Geochem. Geophys. Geosyst.

Hühnerbach V, Masson DG, Bohrmann G, Bull JM, Weinrebe W (2005) Deformation and submarine landsliding caused by seamount subduction beneath the Costa Rica continental margin—New insights from high-resolution sidescan sonar data, in Submarine Slope Systems: Processes and Products, edited by D. M. Hodgons and S. S. Flint, Geol. Soc. Spec. Publ., 244, 195–205.

Kukowski N, Greinert J, Henrys S (2010) Morphometric and critical taper analysis of the Rock Garden region, Hikurangi Margin, New Zealand: Implications for slope stability and potential tsunami generation, Mar Geol272: 141-153, ISSN 0025-3227, DOI: 10.1016/j.margeo.2009.06.004.

McAdoo BG, Pratson LF, Orange DL (2000) Submarine landslide geomorphology, US continental slope. Mar Geol 169: 103-136.

McIntosh, Kirk D., E. A. Silver, I. Ahmed, A. Berhorst, C. R. Ranero, R. K. Kelly, and E. R. Flueh, The Nicaragua Convergent Margin: Seismic Reflection Imaging of the Source of a Tsunami Earthquake, Rica, in: *The seismogenic zone of subduction thrust faults*, T. Dixon and J.C. Moore eds., Columbia University Press, NewYork, pp 257-287. 2007.

Ranero CR, von Huene R (2000) Subduction erosion along the Middle America convergent margin. Nature 404: 748.

Ranero CR, Villaseñor A, Phipps Morgan J, Weinrebe W (2005) Relationship between bend-faulting at trenches and intraslab seismicity. Geosystems, Geophys, Geochem Q12002 doi:10.1029/2005GC000997.

Ranero CR, Grevemeyer I, Sahling H, Barckhausen U, Hensen C, Wallmann K, Weinrebe W, Vannucchi P, von Huene R, McIntosh K (2008) The hydrogeological system of erosional convergent margins and its influence on tectonics and interplate seismogenesis. Geochemistry, Geophysics, Geosystems 9: Q03S04, doi:10.1029/2007GC001679.

von Huene, R., Bourgois, J., Miller J., Pautot G. (1989). A large tsunamogenic landslide and debris flow along the Peru Trench. J. Geophys. Res. 94(2):1703-1714.

von Huene R, Ranero CR, Watts P (2004a) Tsunamigenic slope failure along the Middle America Trench in two tectonic settings. *Mar Geol*203: 303-317.

von Huene R, Ranero CR, Vannucchi P (2004b) A model for subduction erosion. Geology 32:913; doi: 10.1130/G20563.1..

Acknowledgements:

This publication is contribution no. 210 of the Sonderforschungsbereich 574 "Volatiles and Fluids in Subduction Zones" at Kiel University funded by Deutsche Forschungsgemeinschaft (DFG). The data were collected during cruises of German R/V Sonne funded by the Ministry of Science and Education (BMBF) and R/V Meteor the Deutsche Forschungsgemeinschaft (DFG), and US R/V Ewing funded by NSF. We acknowledge the reviews of J. Chaytor and R. von Huene that helped improve the clarity of the paper.

5

Tephra layers: A controlling factor on submarine translational sliding?

R. Harders, S. Kutterolf, C. Hensen, T. Moerz, W. Brueckmann

Published in G^3, Volume 11, No 5, May 2010, Q05S23, doi:10.1029/2009GC002844
ISSN: 1525-2027

Geochemistry Geophysics Geosystems G3

Published by AGU and the Geochemical Society

Article
Volume 11, Number 5
11 May 2010
Q05S23, doi:10.1029/2009GC002844
ISSN: 1525-2027

Click Here for Full Article

Tephra layers: A controlling factor on submarine translational sliding?

Rieka Harders, Steffen Kutterolf, and Christian Hensen
SFB 574, Leibniz-Institut für Meereswissenschaften an der Universität Kiel (IFM-GEOMAR), Wischhofstrasse 1-3, D-24148 Kiel, Germany (rharders@ifm-geomar.de; skutterolf@ifm-geomar.de; chensen@ifm-geomar.de)

Tobias Moerz
MARUM, Leobener Strasse, D-28359 Bremen, Germany (tmoerz@uni-bremen.de)

Warner Brueckmann
Leibniz-Institut für Meereswissenschaften an der Universität Kiel (IFM-GEOMAR), Wischhofstrasse 1-3, D-24148 Kiel, Germany (wbrueckmann@ifm-geomar.de)

[1] Submarine slope failures occur at all continental margins, but the processes generating different mass wasting phenomena remain poorly understood. Multibeam bathymetry mapping of the Middle America Trench reveals numerous continental slope failures of different dimensions and origin. For example, large rotational slumps have been interpreted to be caused by slope collapse in the wake of subducting seamounts. In contrast, the mechanisms generating translational slides have not yet been described. Lithology, shear strength measurements, density, and pore water alkalinity from a sediment core across a slide plane indicate that a few centimeters thick intercalated volcanic tephra layer marks the detachment surface. The ash layer can be correlated to the San Antonio tephra, emplaced by the 6000 year old caldera-forming eruption from Masaya-Caldera, Nicaragua. The distal deposits of this eruption are widespread along the continental slope and ocean plate offshore Nicaragua. Grain size measurements permit us to estimate the reconstruction of the original ash layer thickness at the investigated slide. Direct shear test experiments on Middle American ashes show a high volume reduction during shearing. This indicates that marine tephra layers have the highest hydraulic conductivity of the different types of slope sediment, enabling significant volume reduction to take place under undrained conditions. This makes ash layers mechanically distinct within slope sediment sequences. Here we propose a mechanism by which ash layers may become weak planes that promote translational sliding. The mechanism implies that ground shaking by large earthquakes induces rearrangement of ash shards causing their compaction (volume reduction) and produces a rapid accumulation of water in the upper part of the layer that is capped by impermeable clay. The water-rich veneer abruptly reduces shear strength, creating a detachment plane for translational sliding. Tephra layers might act as slide detachment planes at convergent margins of subducting zones, at submarine slopes of volcanic islands, and at submerged volcano slopes in lakes.

Components: 9600 words, 14 figures, 1 table.

Keywords: submarine landslides; mass wasting; ash layers; liquefaction; translational sliding; permeability.

Index Terms: 3070 Marine Geology and Geophysics: Submarine landslides (1031); 3060 Marine Geology and Geophysics: Subduction zone processes (1031).

Received 11 September 2009; **Revised** 23 February 2010; **Accepted** 23 March 2010; **Published** 11 May 2010.

Harders, R., S. Kutterolf, C. Hensen, T. Moerz, and W. Bruekmann (2010), Tephra layers: A controlling factor on submarine translational sliding?, *Geochem. Geophys. Geosyst.*, *11*, Q05S23, doi:10.1029/2009GC002844.

Theme: Central American Subduction System
Guest Editors: G. Alvarado, K. Hoernle, and E. Silver

1. Introduction

[2] Along the Middle America Trench, slope failure has been related to (1) subduction of large seamounts [e.g., *von Huene et al.*, 2000, 2004] and (2) widespread tectonic erosion removing material from the lower part of the overriding plate [*Ranero and von Huene,* 2000; *Ranero et al.*, 2008]. Multibeam bathymetry along ~600 km of the continental slope of Costa Rica and Nicaragua displays abundant large slope failures (a failure every ~20 km) occurring as rotational slumps or translational slides of different dimensions (Figure 1). The age of the slides calculated by estimating the time required filling the deepest scars by sediment accumulation rates of 30–40 cm kyr^{-1} after *Kutterolf et al.* [2008c], ranges between at least 500 ka and present.

[3] The mechanisms involved in bedding-parallel translational slides imply the presence of bedding planes containing discrete weak layers because the movement of the failing sediment takes place along the stratification [*Hampton and Lee,* 1996]. By contrast, rotational slumps can occur in homogenous sediments, where a listric rupture surface forces them to rotate along this surface [*Mulder and Cochonat,* 1996]. Slides and slumps can be morphologically classified using the value of the Skempton ratio t/l, where t is the slide thickness and l the slide length. Translational slides usually have Skempton ratios <0.15 and rotational slumps >0.33 with a transition range between 0.15 and 0.33 [*Skempton and Hutchinson,* 1969].

1.1. Seamount Subduction

[4] Offshore Costa Rica large seamounts 2–4 km tall and ~20 km wide underthrust the continental margin. As the seamounts underthrust and subduct under the continental margin, large rotational slumps, 50–60 km lateral width and 50 ≤ 600 m headwalls, collapse in their wakes. Seamount-related mass wasting creates grooves in the slope, caused by the landward retrogression of the headwalls [*von Huene et al.*, 2004]. Bedding planes apparently do not control the movement of large seamount-induced rotational slumping because in many cases the slump involves the basement rock. In contrast, offshore Nicaragua, where smaller seamounts (0.5–2 km high) and lower relief horsts and grabens enter the subduction zone, the presence of large translational slides with 10–12 km long slide planes, 5–6 km lateral width and up to 250 m headwalls, indicates the existence of controlling weak bedding planes (Figure 1). Although deep penetration seismic reflection data have shown that subducting seamounts may also be involved in the generation of the large sediment failures offshore Nicaragua [*McIntosh et al.*, 2007], the slide scars in the slope exhibit an unexplained translational rather than rotational character.

[5] Seismic activity between Costa Rica and Nicaragua causes frequent large earthquakes. *Ambraseys and Adams* [1996] have shown that there have been at least five earthquakes with $M_s > 7$ since 1898, two of which caused tsunamis. The latest $M_s > 7$ earthquake in 1992 caused the tsunami that produced the highest damage along the coast of Nicaragua. Multibeam bathymetry data collected subsequently revealed the presence of large submarine scars in the slope offshore Nicaragua [*von Huene et al.*, 2000], which led to a discussion concerning a potential generation of the tsunami by the submarine slides. *von Huene et al.* [2004] tested the tsunamigenic potential of the largest translational slides offshore Nicaragua located near the epicenter of the 1992 earthquake. They calculated that the slide may have caused a water layer deformation with a maximum amplitude of 6.6 m, causing a tsunami that could potentially affect about 40 km of the Nicaraguan coast, but they could not find any evidence that the slope failures occurred during the 1992 earthquake.

1.2. Slope Stability and Trigger Mechanisms for Translational Sliding

[6] *Spangenberg* [2002] estimated slope stability nearby the largest translational slides offshore Nicaragua by calculating a Safety Factor (SF). He calculated a SF for static and dynamic conditions from piston and box core samples of the clayey deposits collected during R/V *Sonne* cruise 107.

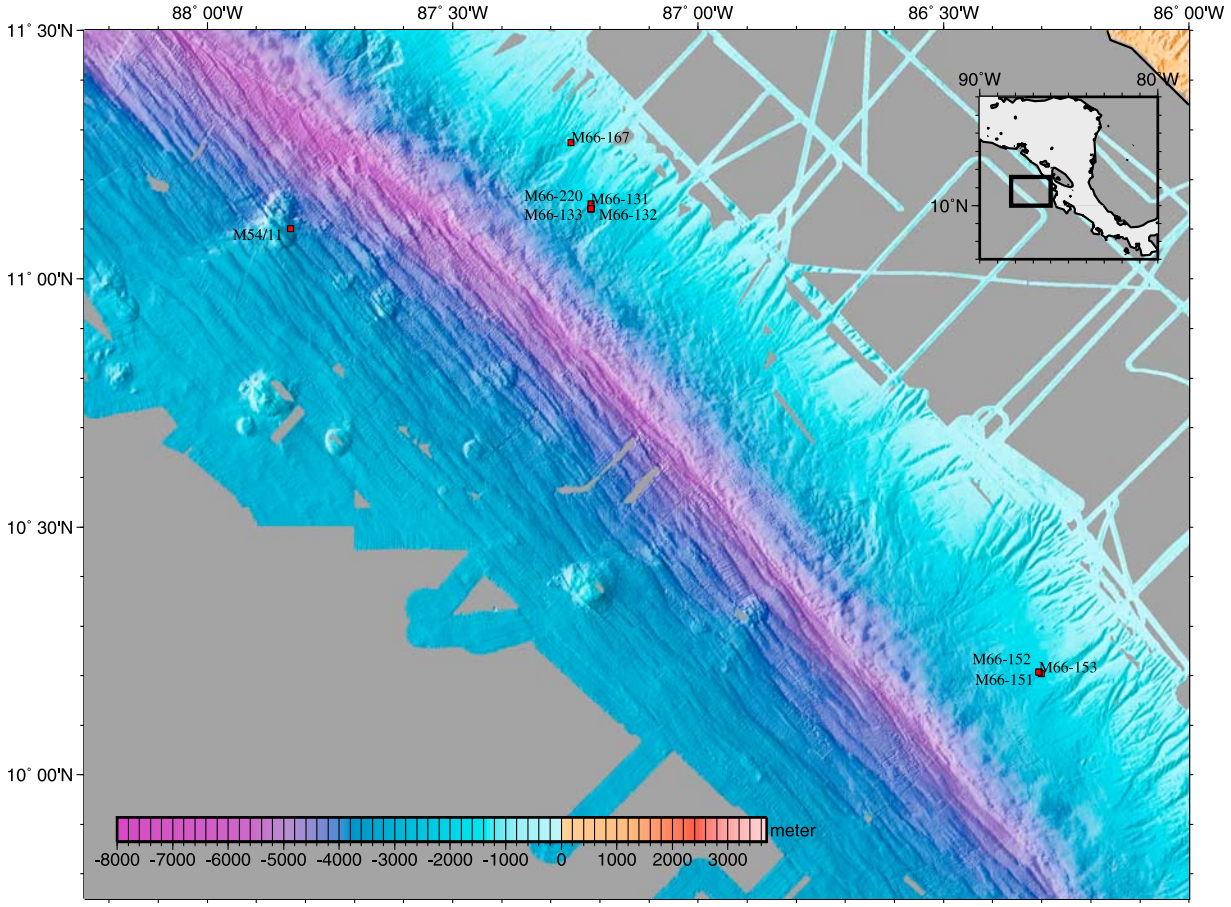

Figure 1. Shaded relief map offshore Central America. Bathymetry data are color coded from pale blue to dark blue. Numbers refer to cores taken with German research vessel *Meteor* cruises M54 and M66 and German research vessel *Sonne* cruise SO 107. Cores 131–133 were taken at Masaya slide, a big slide scar of 12 km × 6 km. Numbers 151–153 refer to cores taken at the medium-sized Hermosa slide (scar of 3 km × 7 km), with core 151 discussed in section 3.2.

For undrained, static conditions, he used the SF formula and method after *Graham* [1984] where

$$SF = \mathrm{cu}/j' h(\sin i \cos i) \quad (1)$$

(with cu = undrained shear strength, j′ = relative bulk density (expressed as the difference between bulk density and the water density), h = sediment thickness between seafloor and slide plane, i = slope angle) and calculated values between 5 to 30, indicating a stable slope. For undrained, dynamic conditions, he used the procedure after *Karlsrud and Edgers* [1982] with the formula

$$SF = \mathrm{cu}/\left(\mathrm{j}'\mathrm{h}\left((1/2)\sin 2i + a\left(\mathrm{j}/\mathrm{j}'\cos^2 i\right)\right)\right) \quad (2)$$

(with j = wet bulk density and a = horizontal ground acceleration earthquakes) assuming earthquake shaking with magnitudes >4.5, (linked to a peak ground acceleration of 0.3 m s^{-2}), and slope angles >12°. Under these conditions SF is close to 1, implying that the slope is prone to failure. However, like in many other studies, these estimations did not account for stratification of the slope sediment and the potentially different mechanical behaviors of the layers, which may enhance the potential for translational sliding. In particular both, the nature of the detachment plane and the failure mechanism causing translational sliding have not yet been investigated.

[7] Here we examine the importance of ash layers as heterogeneities in the otherwise typically terrigenous and pelagic slope sediment sequences and their potential role in slope stability. Tephra layers are formed by pyroclastic matter from explosive volcanic eruptions that disperse material at stratospheric heights and are common horizons in the sediment record offshore Pacific Central America [*Kutterolf et al.*, 2007a, 2007b]. Stratified soil containing layers of different grain size, and therefore different permeability, has been the focus of research dealing with liquefaction and slope

stability since the late 1960s [*Castro,* 1969]. Intensive laboratory work has been performed to study the behavior of stratified soil and the buildup of water films sandwiched between less permeable soil, and liquefied sand, potentially triggering slides.

[8] *Kokusho* [2003] has tested lateral flow failure initiated by earthquake shaking with laboratory shake table tests and demonstrated that void redistribution in sand deposits creates water films if low-permeability layers are present that trap the water films beneath them. *Field et al.* [1982] investigated the submarine failure that occurred during the 1980 earthquake offshore California on the Klamath River and could clearly relate it to a submarine liquefaction phenomenon. However, most liquefaction studies were conducted in subaerial conditions.

[9] In our study we present a new model of liquefaction of ash layers in the submarine environment offshore Nicaragua. Here, we have found 1 to 15 cm thick tephra layers interlayered roughly every 1 m, between marine clays, to be potential weak layers. We propose that ash layers may partially liquefy during earthquake shaking, building up water films sandwiched between the less permeable clay, and finally leading to translational sliding.

2. Methods

2.1. Seafloor Mapping

[10] Multibeam bathymetry data were collected during German R/V *Sonne* cruises SO76, 81, 107, 144, 150, 163-1 and U.S. R/V *M. Ewing* cruises 0005 and 01404 using the Atlas Hydrosweep system and *Sonne* 173 cruise using the SIMRAD EM-120 system from Krongsberg. Water velocity profiles we calculated from CTD measurements. The bathymetric data were cleaned and converted to depth soundings with the MBsystem [*Caress and Chayes,* 1996] and gridded with GMT [*Wessel and Smith,* 1998] at 0.001 degrees node spacing.

2.2. Core Location, Positioning, and Gravity Core Recovery

[11] Gravity cores were 6–9 m long steel tubes filled with a 10 cm wide inner PVC liner. Core locations were planned using Multibeam bathymetry maps and Parasound profiles, shot perpendicular to the headwall of the slides. Cores were positioned in the slide scar close to the headwall and also in undisturbed sediments upslope of the headwall. Positioning during coring was controlled by on board GPS and simultaneous Parasound images. Due to weak rope tension of the core device at water depths >1000 m derivations from the planned position may be up to ~250 m (E. Stehn, technical assistant, R/V *Meteor* cruise M66/3a, personal communication, 2006). Recovered cores were cut into 1 m segments, locked at both sides and stored at 4°C. Measurements were taken within less of 1 h.

2.3. Sediment Analysis

[12] Core segments were analyzed with the GEOTEK Ltd. multisensor whole core logger (MSCL) [*Blum,* 1997], for the data used in this study. Core segments were described, photographed, sampled for pore water chemistry, moisture content, mineral density, and additionally undrained shear strength was measured. Pore water was retrieved by pressure filtration. For further information see http://www.ifm-geomar.de/index.php?id=mg_analytik. Moisture content and mineral density were determined through mass and volume determinations [*Blum,* 1997], measuring the specimen's mass before and after removal of interstitial pore fluid through oven drying for 24 h at temperatures from 90° to 110°C. Moisture content, porosity, and void ratio are defined by the mass or volume of extracted water, corrected for the mass and volume of salt evaporated during the drying, following ODP procedures [*Blum,* 1997]. Undrained shear strength was determined with a fall cone penetrometer, and calculated after *Hansbo* [1957] with the coefficients from *Houlsby* [1982].

2.4. Shear Tests

[13] To measure total displacement, shear strength and compaction of ash layers under a load and during a shear event, dry mono grain size ashes and combinations of different grain sizes were loosely put into a shear box of a direct shear test device following the indications given by *Deutsches Institut für Normung* [2002]. For the tests, grain sizes of cored ash layers were determined by wet sieving or by a laser particle analyzer. A volume of ~100 cm^3 in the shear box was loaded with 16 kg, producing an effective vertical stress of 40 kPa, similar to vertical stress existing at 7 m depths bsf. Shearing in one direction started after 10 min of preconsolidation with a velocity of 0.5 mm min^{-1} until residual shear strength was reached and put to reverse with the same velocity back to the starting point. Sharing went on until no significant changes in peak shear strengths were detected (at least 4 rounds).

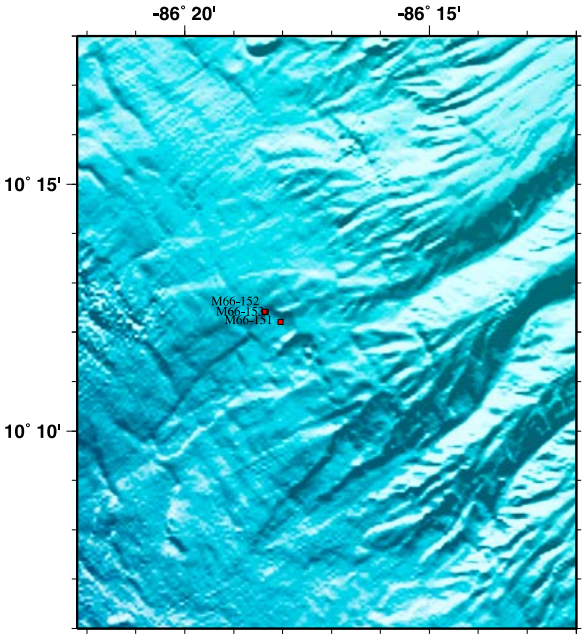

Figure 2. Shaded relief map offshore Costa Rica showing Hermosa slide (scar of 3 km × 7 km), with core locations (red squares) M66/151 to M66/153 in the northwest of the upper slide scarp.

2.5. Ash Layer Chemistry and Correlation

[14] Marine ash beds and matrix glass of onshore samples were analyzed by electron microprobe (EMP) for major and minor elements at IFM-GEOMAR, Kiel as well as Laser ablation inductively coupled mass spectrometry (La-ICP-MS) at University of Frankfurt am Main (Institute of Mineralogy). Standard deviation is less than 2% for major elements and <10% for tracer elements. All analyses have been normalized to 100% to eliminate the effects of variable postdepositional hydration from the comparison between marine and/or on-land tephras [*Kutterolf et al.*, 2008a]. For age determination volcanic offshore ashes were chemically correlated with on land deposits [*Kutterolf et al.*, 2008a].

3. Observations

3.1. Translational Slides and Material at the Slide Plane

[15] Morphologically, scarps caused by translational slides offshore Nicaragua and the northwestern part of Costa Rica have a short headwall area that grows retrogressively upslope, and relatively long converging side flanks (Figures 1–4). The retrogressive character indicates that the original slide causes secondary slides. The secondary events are typically smaller than the main event.

[16] Interpretation of side scan sonar and bathymetry data indicates that most headwalls possibly developed at trench parallel fault scarps (Figure 5). Seafloor offsets by faulting are up to 200 m within the steep (12–17°) middle slope, and the maximum thicknesses of the slides and their headwall, range from 25 to 200 m. The minimum runouts are 1.5 to 12 km, implying Skempton ratios <0.15 that typically characterize translational slides. But many slides have no identifiable deposits because they seem to have run into the trench axis.

[17] Most of the material involved in the slides is hemipelagic to turbididic terrigenous slope sediment that mainly consists of clay with abundant foraminifers [*Spangenberg,* 2002; *Kutterolf et al.*, 2008a]. In general the grain size of these sediments is smaller than 32 μm, which implies that they have low specific hydraulic conductivities (k_f values) of around $<1 \times 10^{-9}$ m s^{-1} [*Hoelting and Coldewey,* 2009] and cohesive properties. The k_f value is given within Darcy's law as

$$k_f = Q/(A*i) \quad (3)$$

with Q (units of volume per time in m^3 s^{-1}), A (cross-sectional area to flow in m^2), and i (dimensionless hydraulic gradient defined as h/l, describing the pressure drop (h) and over a certain length (l)).

[18] These none conductive slope sediments are interlayered every ~1 m with 1–15 cm thick ash layers. The grain size of those discrete ash layers ranges between 63 and 500 μm (silt to sand size), which implies that they have higher hydraulic conductivities and noncohesive properties, compared to the terrigenous slope sediment.

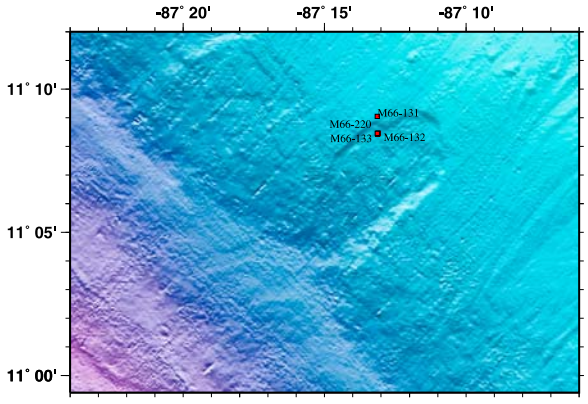

Figure 3. Shaded relief map offshore Nicaragua, showing core locations M66/131 to M66/133, taken at Masaya slide (slide scar 12 km × 6 km).

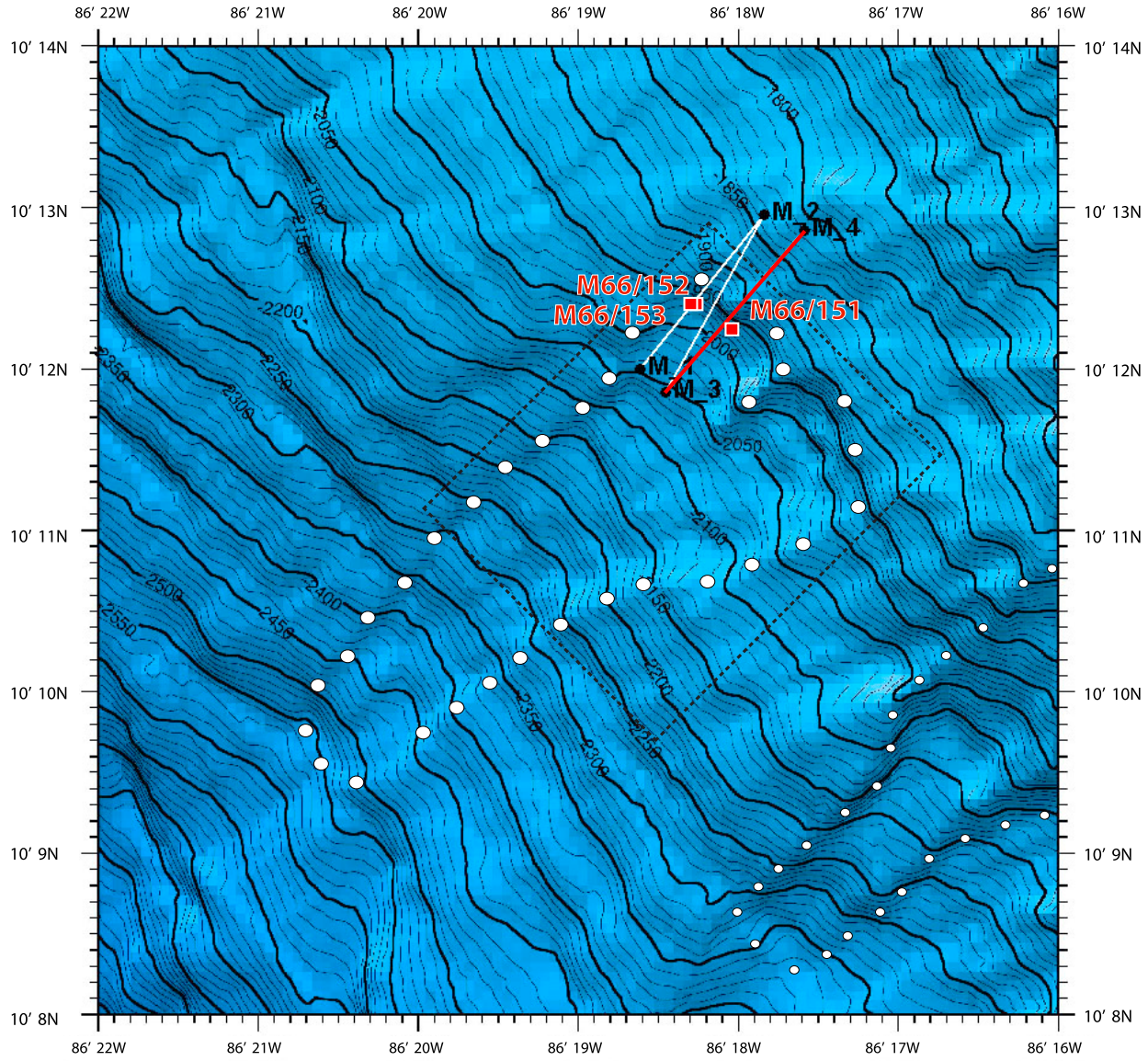

Figure 4. Multibeam bathymetry map of Hermosa slide with contour lines every 10 m. The slide and a near by similar feature are delineated by white filled black circles. Locations of gravity cores M66/151, M66/152, and M66/153 are marked with red squares. Subbottom seismic profiler parasound track is indicated by lines across the headwall (M1–M4 are navigation waypoints). The seismic image from the red track is shown in Figure 6. Black dashed box shows the location of side scan sonar data shown in Figure 5.

3.2. Translational Hermosa Slide

[19] To study translational sliding, R/V *Meteor* cruise 66 targeted several slope failures offshore Costa Rica and Nicaragua. Prior to coring, subbottom profile images were collected with the Parasound system across the headwall area of each of the chosen slides to determine the coring locations. Here we focus on the medium-sized Hermosa scarp (Figure 2), where coring succeeded to penetrate the slide plane.

[20] The scarp extends from 1900 to 2500 m water depth, with a headwall height of about 25 m, and a headwall dip of 12.7°. The undisturbed slope next to the slide has an average dip of 5.7°, lower than the slope dip angles next to most other large translational slides (12–17°) offshore Nicaragua, e.g., Masaya slide (Figure 3).

[21] Parasound images across the headwall and upper first kilometer of the slide plane show the upper tens of meters of the sediment sequence

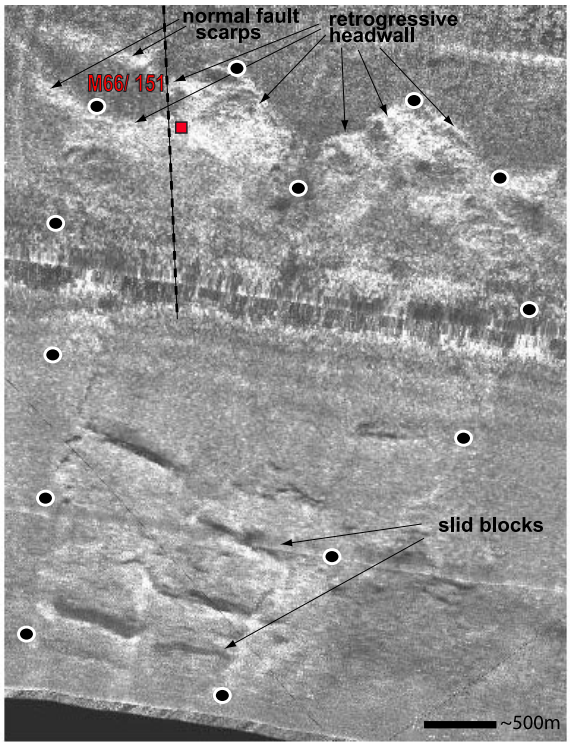

Figure 5. TOBI side scan data of the upper region of the Hermosa slide. Dots (black, encircled in white) mark the outline of the slide. Arrows point to the retrogressive character of the headwall and slid blocks on the slide plane as well as to normal fault scarps in the slopes sediment. Core position M66/151 (marked as red square) is located where slide plane and headwall merge. The location of the Parasound profile (Figure 6) is marked as a black dashed line. Location is shown in Figure 4 as black dashed box.

(Figure 6). Disturbed layers (water depth >2000 m) are visible below the headwall, and in the slide plane. Stratified layers above the headwall appear as parallel reflections and are interpreted as the undisturbed slope sediment. The bathymetry and side scan sonar data show that the headwall area of Hermosa slide consists of two concave shaped headwalls, separated by a central ridge (Figure 2, 4, and 5). The sidewalls of the scar slightly converge and terminate in a tongue-shaped foot of the scar about 7 km downslope from the headwall (Figure 2, 4, and 5). However, most of the displaced mass lies as large block or sheet deposits on the scar plane, which is visible in the Parasound image (Figure 6) and side scan sonar data (Figure 5). The Slide sediments also contain cracks and fissures. Like for most translational slides offshore Nicaragua and Costa Rica, a lobe of sediment accumulation is not observed at the toe of the scar (Figures 2 and 3). *Spangenberg* [2002] and *von Huene et al.* [2004] interpreted this to be related to translational sediment blocks disintegration into density flows. However, at Hermosa slide, side scan sonar data indicate that much of the deposits remain within the slide area, mostly in the upper part of the slide. In order to penetrate through the deposits into the slide plane, the uppermost region of the slide scarp was selected for coring, where the slide sediments are generally thinner.

[22] Attempts to penetrate the slide plane at the large Masaya slide with cores M66/131, M66/132, M66/133 and M66/220 were unsuccessful (Figures 1 and 3). These cores recovered reworked brown to grayish silty clays with few intercalations of mafic or felsic ash layers, which were analyzed geochemically and subsequently used for tephra stratigraphy [*Kutterolf et al.*, 2008a]. Core M66/151 succeeded to sample across the uppermost area of the scar at the smaller Hermosa slide (Figures 1, 2, and 4–6), at a location immediately beneath the headwall, in the upper northwestern part of the scar (Figures 4–6).

[23] Since there was only a thin sediment cover on top of the slide plane it was possible to recover a distinct transition through undisturbed young sediments, slide deposits, a slide plane and the shallowest portion of undisturbed older material within a 3 m long gravity core.

[24] Evidence that a slide plane was reached during coring is supported by all data obtained from the analysis of the core. The MSCL density data, porosity and undrained shear strength laboratory data, as well as pore water alkalinity of the core, show an abrupt change between 1.40 and 1.70 m below seafloor (bsf) (Figure 7), across a coarse-grained 0.5 cm thick mafic ash layer that separates two sediment units. A 10 cm thick layer of reworked material containing finer grained ash clasts as well as rounded mud clasts overlying the 0.5 cm thick coarse ash layer also supports this interpretation (Figure 7).

[25] Above and below ~170 cm bsf the pore water alkalinity profile taken from the core shows two different linear trends, forming a so-called "kink-type" curve, which can be interpreted as the result of a slide event [*Zabel and Schulz,* 2001; *Hensen et al.*, 2003]. Within undisturbed marine sediment alkalinity is typically continuously increasing with increasing sediment depth due to ongoing biodegradation processes. A kink or discontinuity in a pore water profile, as observed in this case, usually

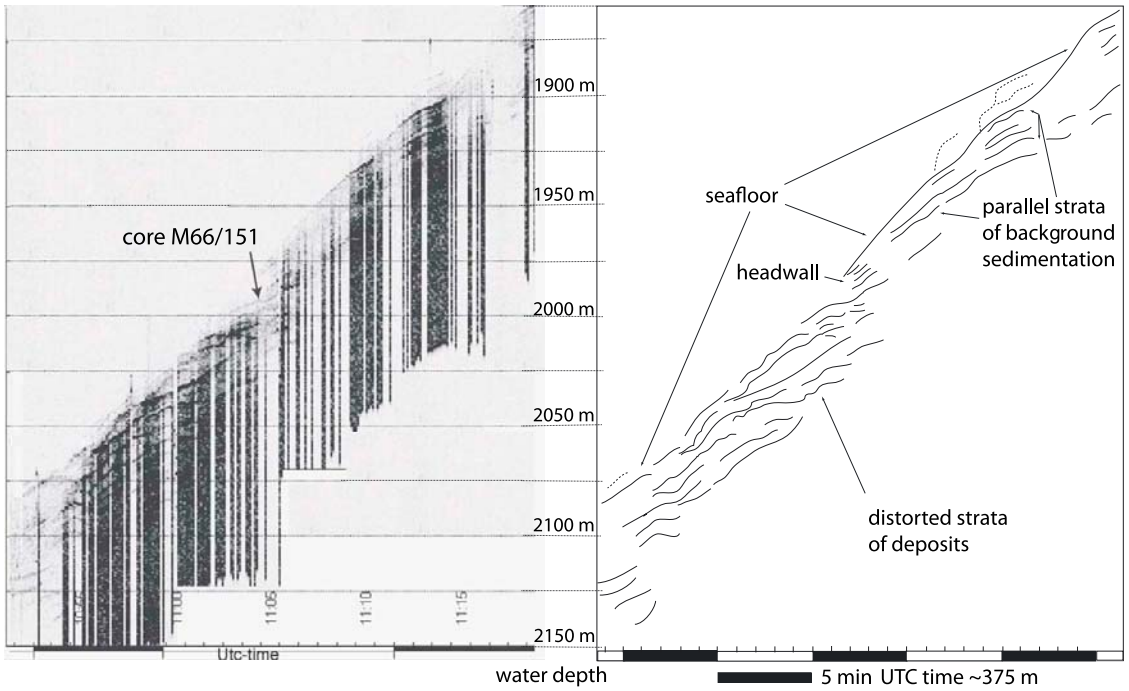

Figure 6. Parasound subbottom seismic profiler image and line interpretation across the headwall of Hermosa slide (see profile location in Figure 4 marked as red line). In spite of interferences with the signal of other instruments shown as black stripes in the image the strata and headwall scarp are clearly visible. Five minutes of UTC time ~375 m on *x* axis.

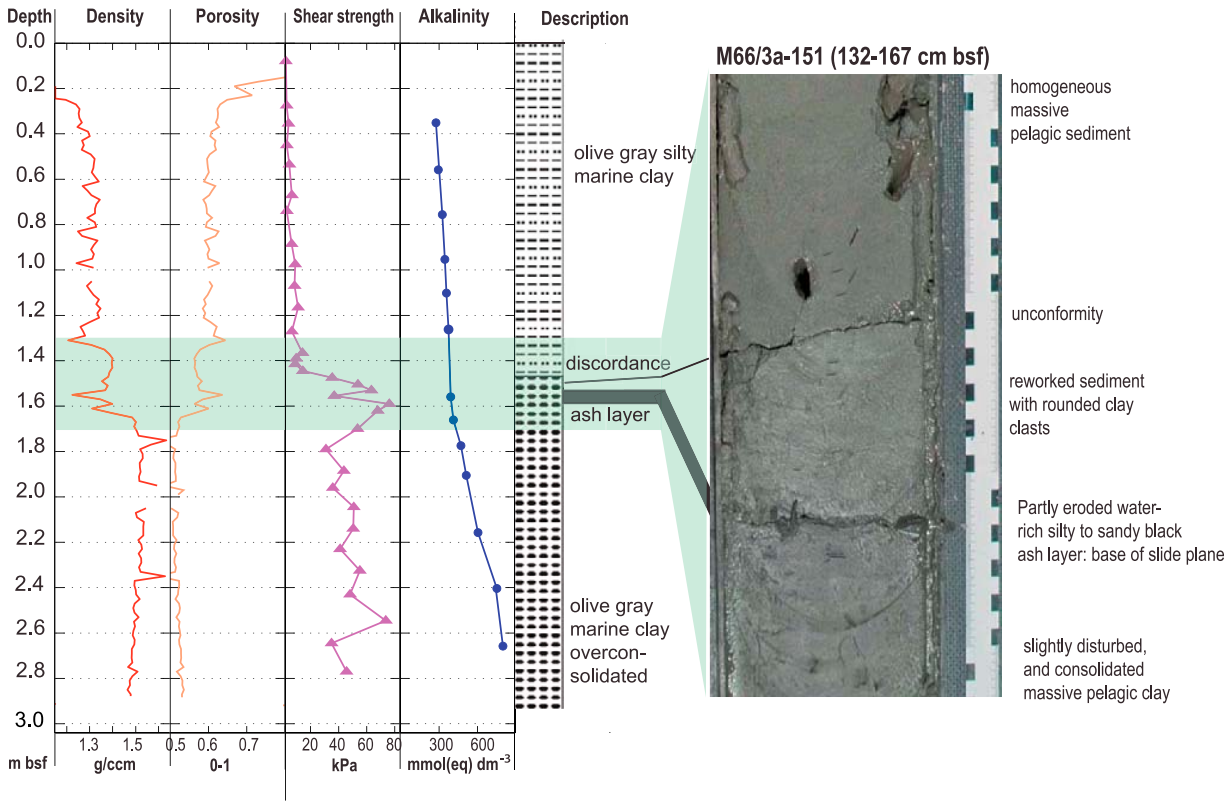

Figure 7. Multisensor core logger data and analog measurements of density, porosity, shear strength, and pore water alkalinity as well as lithology from core M66/151 of Hermosa slide.

Table 1 (Sample). Selected Correlative Major and Trace Elements of Marine and On-Land San Antonio Tephra in Comparison to Other Possible On-Land Masaya Tephras From *Kutterolf et al.* [2008a][a] [The full Table 1 is available in the HTML version of this article]

Tephra Layer	Number	Na_2O	SiO_2	MgO	FeO_t	Al_2O_3	TiO_2	K_2O	CaO	Y	Nb	Cs
Ticuantepe Lapilli/Masaya Tuff	26/5	2.70 (0.61)	53.82 (1.24)	3.87 (1.00)	12.73 (1.97)	15.04 (1.66)	1.39 (0.25)	1.43 (0.24)	8.49 (0.83)	28.26 (0.93)	4.28 (0.07)	0.87 (0.07)
Masaya Triple Layer	96/4	2.82 (0.30)	52.52 (0.55)	4.34 (0.29)	13.46 (0.55)	14.44 (0.40)	1.51 (0.09)	1.47 (0.10)	9.06 (0.32)	32.47 (0.82)	4.79 (0.22)	0.96 (0.02)
La Concepcion Tephra	80/5	2.83 (0.34)	51.58 (0.77)	4.68 (0.68)	13.57 (0.93)	14.69 (0.71)	1.54 (0.20)	1.43 (1.31)	9.28 (0.78)	28.21 (2.21)	4.08 (0.17)	1.02 (0.07)
Fontana Tephra	98/13	3.07 (0.42)	54.51 (4.06)	3.81 (1.08)	12.11 (2.00)	14.91 (0.63)	1.24 (0.25)	1.56 (0.63)	8.36 (1.58)	29.26 (2.00)	3.72 (0.13)	1.10 (0.06)
San Antonio Tephra	98/5	2.90 (0.38)	52.41 (1.61)	4.59 (0.89)	12.96 (1.27)	14.97 (0.82)	1.23 (0.16)	1.37 (0.30)	9.04 (1.01)	24.78 (0.50)	2.89 (0.07)	0.88 (0.02)
M54-11/20-20	32/1	3.00 (0.15)	52.71 (1.04)	4.27 (0.50)	12.64 (0.41)	15.16 (0.22)	1.35 (0.11)	1.43 (0.21)	8.89 (0.67)	25.10 (-)	3.15 (-)	0.88 (-)
M66-167/95-105	35/6	2.94 (0.53)	52.40 (0.88)	4.24 (0.53)	13.15 (1.20)	15.29 (0.80)	1.21 (0.19)	1.35 (0.23)	9.02 (0.61)	23.60 (3.86)	2.24 (0.32)	0.88 (0.13)
M66-151/156-157	21/6	3.18 (0.38)	52.29 (0.84)	4.15 (0.62)	12.22 (1.66)	16.25 (1.64)	1.10 (0.21)	1.05 (0.23)	9.31 (0.93)	21.54 (1.05)	2.44 (0.42)	0.89 (0.15)

[a]Other source areas are excluded due to different trace element compositions and relative stratigraphic order [*Kutterolf et al.*, 2008a]. Number in parentheses shows deviation of single measurements. Number, single measurements per tephra at EMP and LA-ICP-MS.

means that the system is not in balance or in "steady state." Pronounced changes in sedimentary conditions are well known to substantially affect diagenetic processes in marine sediments [e.g., *Thomson et al.*, 1984; *Wilson et al.*, 1986; *Riedinger et al.*, 2005]. Hence, the sharp increase of the alkalinity profile below the mafic ash layer may be indicative for the emplacement of a young sediment unit on top of older strata separated by a discordance, which relates to the slide event.

[26] In line with this interpretation, density, porosity and shear strength profiles also show different trends below and above the mafic ash layer (Figure 7). Above the ash layer density and shear strength values abruptly decrease, while porosity increase.

[27] The 10 cm thick section above the mafic ash layer is made of reworked material containing mafic ash lenses, rounded clay clasts, and carbonatic clay clasts (Figure 7). Within this reworked section, density and shear strength values decrease upward, but are considerably higher than the values in the overlying material. The reworked section is separated from the overlying section by an abrupt change in sediment properties across a discontinuity marked in the core by a crack (possibly secondary in origin and caused by separation at the lithological contact during core recovery). The uppermost section extends up to the seafloor and consists mainly of undisturbed, unconsolidated, water-rich clay. The low alkalinity, shear strength, and density values of this uppermost section clearly suggest that it represents the most recent, post-failure hemipelagic sediment accumulation. Visual inspection support that, in spite of minor disturbance by bioturbation, these clays are mechanically undisturbed and not reworked. On the basis of the physical and geochemical properties (Figure 7) and visual core analysis we conclude that the mafic ash occurs at the top of a section that is over-consolidated considering its burial depth.

3.3. San Antonio Tephra Layer

[28] Cored tephra layers generally have a sharp basal contact to the underlying pelagic clay and many are normally graded in grain size [*Kutterolf et al.*, 2008a]. Marine ash layers from the Central American Volcanic Arc (CAVA) were chemically correlated with tephras of individual eruptions on land using an established database of bulk rock, mineral and glass compositions and eruptions ages, resulting from extensive field expeditions [*Kutterolf et al.*, 2008a]. Evaluation of the chemical composition of the marine mafic ash layer of core

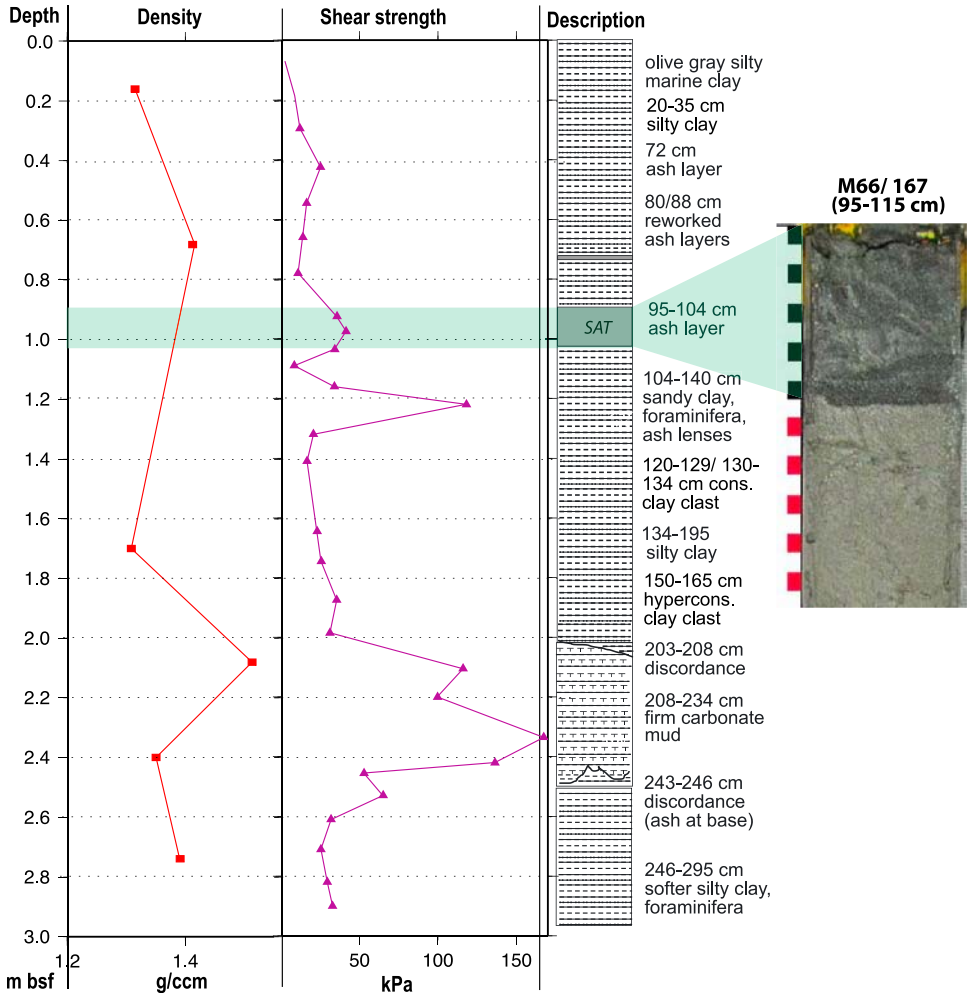

Figure 8. Description and analog data of density and shear strength of core M66/167. The SAT ash layer is marked at 95–104 cm bsf, showing a higher initial shear strength compared to the clay. Note that the overall "normal" trend of the data (increase of shear strength and density with increasing core depth) and peaks in density and shear strength are due to overconsolidated clay clasts or overconsolidated material extruded by the mud mound (Mound Culebra [see also *Kutterolf et al.*, 2008d]).

M66/151 (Table 1 and Figure 7) through EMP and La-ICP-MS analysis revealed that it matches the ~6 ka San Antonio Tephra (SAT) [see also *Kutterolf et al.*, 2008a, 2008c] from the Masaya Caldera [*Peréz and Freundt,* 2006; *Kutterolf et al.*, 2007b]. The SAT was erupted during a plinian eruption that injected volcanic material up to 27 km into the stratosphere where it was transported with the prevailing strong winds toward the Southwest. Therefore deposits of this eruption can be found up to 300 km from its source in the Pacific Ocean and contribute strongly to a calculated erupted tephra volume of ~13.5 km^3 [*Kutterolf et al.*, 2007b, 2008a, 2008b]. The isopaches map of the SAT [*Kutterolf et al.*, 2008b] indicated that it should be 3–6 cm thick within the vicinity of core M66/151, but it is 0.5 cm thick.

[29] We compared chemical analysis of the potential SAT, its grain size distribution, and layer thickness found in the two other offshore cores closest to core M66/151. The most comparable cores, bearing the SAT are M66/167 and M54/11-2 (Figures 1, 8, and 9 and Table 1), taken at roughly similar distances from the Masaya Caldera and from core M66/151 [see also *Kutterolf et al.*, 2008a]. Core M66/167 (Figure 8) was taken at the continental slope, on the flank of a large fluid escape structure named Mound Culebra [*Sahling et al.*, 2008], 160 km northwest of core M66/151 (Figure 1) and 50 km closer to the Masaya volcano. In this core, the SAT was normally graded, 10 cm thick and found at 95–105 cm bsf. Core M54/11-2 (Figures 1 and 9) was taken from the oceanic plate at 200 km distance to the Masaya volcano, 200 km

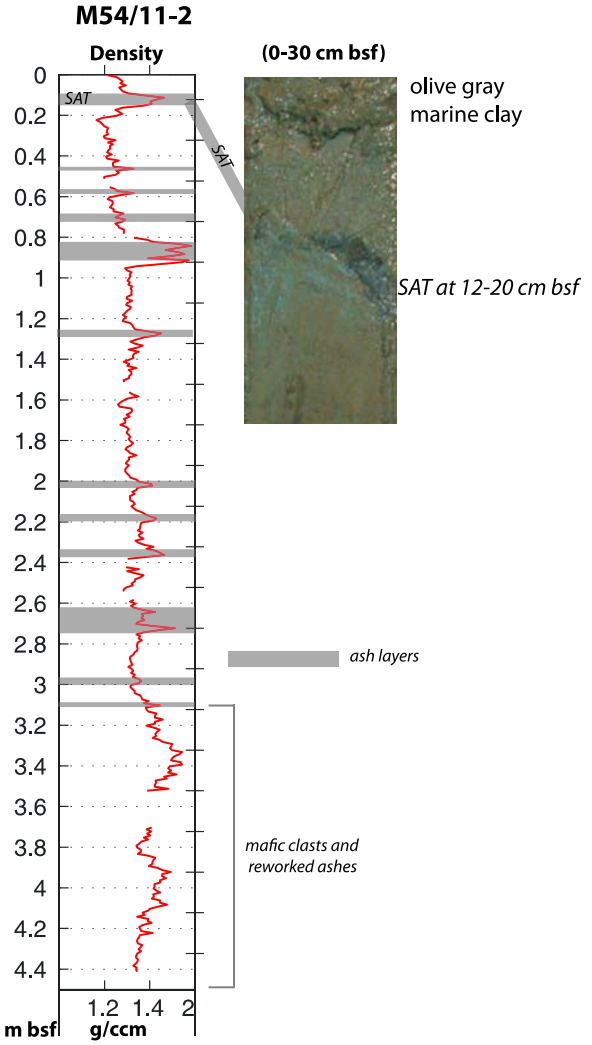

Figure 9. Multisensor core logger data of density and location of ash layers (highlighted in gray) of core M54/11-2 taken from the ocean plate (see also Figure 1 for core location). The SAT ash layer is marked at 12–29 cm bsf (locations of ash layers taken from *Kutterolf et al.* [2007a, Figure 4]).

northwesterly of core M66/151 at Hermosa slide and consisted of a normally graded, 8 cm thick SAT at 12–20 cm bsf. We applied grain size analyses for both cores with a laser particle analyzer, with three repetition measurements per sample and plotted the results as cumulative grain size distribution curves (Figure 10). The distance to the volcano of core M54/11-2 and core M66/151 at Hermosa slide are similar, so that both sites should have the same thickness and grain size distribution. A grain size analysis through wet sieving of the SAT in core M66/151 (Figure 10) demonstrates that the finer top fraction is completely missing and the coarser grained base is only 0.5 thick, which may well be explained by erosion due sliding.

[30] Since the grain size decay is proportional to the thickness decay two arguments support that at Hermosa slide 3–9 cm (80–95%) of the SAT is missing due to the sliding event: Cores close to core M66/151, but outside the failure area, contain a 8–10 cm thick ash layer and finally the regional isopach map indicates at a 3–6 cm thick SAT layer at the location.

3.4. A Model of Sliding at Hermosa Slide Scarp

[31] According to the age of the SAT, the cored slide event must be younger than 6 ka [*Kutterolf et al.*, 2008a, 2008c]. Considering the thickness of 130 cm of undisturbed sediment above the reworked material, and applying sediment accumulation rates of 30–40 cm kyr^{-1} [*Kutterolf et al.*, 2008c], the slide should have occurred about 3700 ± 540 years ago. And it removed about 60–70 cm of sediment, deposited during the previous 2300 ± 540 years. Considering the thin sediment section, and comparing this to the 25 m headwall, which represents the total thickness of the Hermosa slide, the core must have recovered deposits of a smaller retrogressive event within the upper region of the main Hermosa Slide. Therefore we interpret that the cored event occurred above of an older Hermosa slide main event, located over the main slide plane.

3.5. Shear Test Experiments

[32] To study the role of tephra layers potentially affecting the shear strength profile of continental slope sediments we tested the mechanical behavior of ashes and compared it with other terrigenous silt and sand material representative of the embedding sediment layers. In particular, we tested whether the particle fabric of ash layers has an effect on the mechanical response to simple shear compared with normal terrigenous sand. In a study of susceptibility for liquefaction of the Fraser River sand, *Wijewickreme et al.* [2005] pointed out that differences in the particle structure may be a controlling factor of the mechanical response of sand under cyclic loading. The hypothesis to test is whether dry ashes may consolidate more, and/or more rapidly than other dry silt and sand material during a standard shear test. Such behavior would indicate that liquefaction is possible in submerged continental slopes. A specific onshore liquefaction

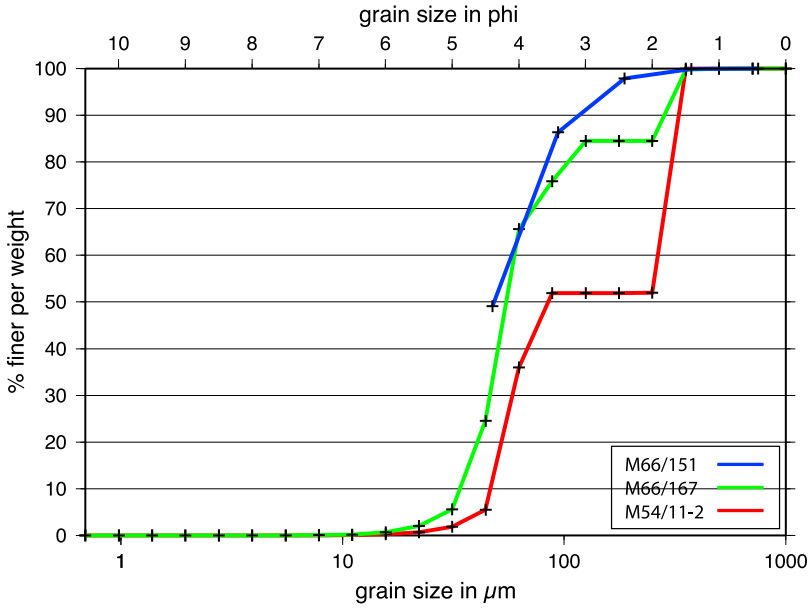

Figure 10. Cumulative grain size distribution curve showing the entire SAT layer of samples M66/151 (grain size <32 not analyzed), M66/167, and M54/11-2. All samples are coarse silt to middle sand (20–600 μm). The k_f values were calculated after *Hazen* [1892], using these curves to determine d_{10} and d_{60} if U < 5 with the formula $k_f = 0.0116 * (d_{10})^2$ and with $U = d_{60}/d_{10}$ and d_y with the value (%) at the grain size (μm) defined along the curve.

mechanism was identified by *National Research Council* (*NRC*) [1985] as "NRC Mechanism B" and is defined as a liquefaction-induced flow failure occurring in loose (not cemented) sand layers overlain by considerably less permeable material, which does not permit drainage during earthquake shaking. For this purpose we measured contractancy (volume reduction) during shearing.

[33] To obtain measurements that span a range of material present in the slope, we used samples not only from the cored SAT layer, but also from other marine mafic and felsic ashes, as well as tephras sampled on onshore deposits. We used samples with a grain shape and grain size distribution similar to the SAT. The samples were collected during *Meteor* cruise M66 and *Sonne* cruise SO173 on the continental slope off Nicaragua, and onshore from the Tierra Blanca Joven deposit in El Salvador.

[34] Examination under optical microscope showed that most tephras, including the SAT, consist of disc-shaped mafic glass shards. To evaluate the influence of grain shape on contractancy, tests were conducted using two different materials: One set of samples composed of disc-shaped felsic or mafic ash grains from Central America and a second set of samples of rounded quartz grains, with a grain size distribution similar to the ashes. Clay was not tested because its cohesive properties and low hydraulic conductivity do not allow fast settlement in water-saturated conditions and will not present a similar layer structure.

[35] We set up a simple dry shear test with a 163 cm^3 shear box with a shear surface of 39.4 cm^2. Tests were run with dry samples of mafic and felsic ashes, and quartz grains of a sand-to-silt fraction. Initial dry bulk densities were calculated from the sample weight filling the box volume. Volume reduction together with an increase in bulk density from shearing results from the contractancy (negative dilatancy) of materials.

[36] Tests were done using sizes ranging between 63 and 125 μm, and 125–250 μm corresponding to the first and second most abundant fraction in the SAT layer. Mafic and felsic ashes with 63–125 μm grain size have initial dry bulk densities of 1.06 g cm^{-3} and 1.2 g cm^{-3}, respectively. The quartz grains of the same fraction have initial dry bulk densities of about 1.6 g cm^{-3} indicating that rounded particles initially build up a denser grain framework. (These results are not caused by the material densities: Quartz has a material density of 2.65 g cm^{-3}, mafic glass has the highest material density of 2.75 g cm^{-3} and felsic glass the lowest material density of 2.45 g cm^{-3}.)

[37] Figure 11 shows that ashes have higher contractancy than the reference rounded quartz grains,

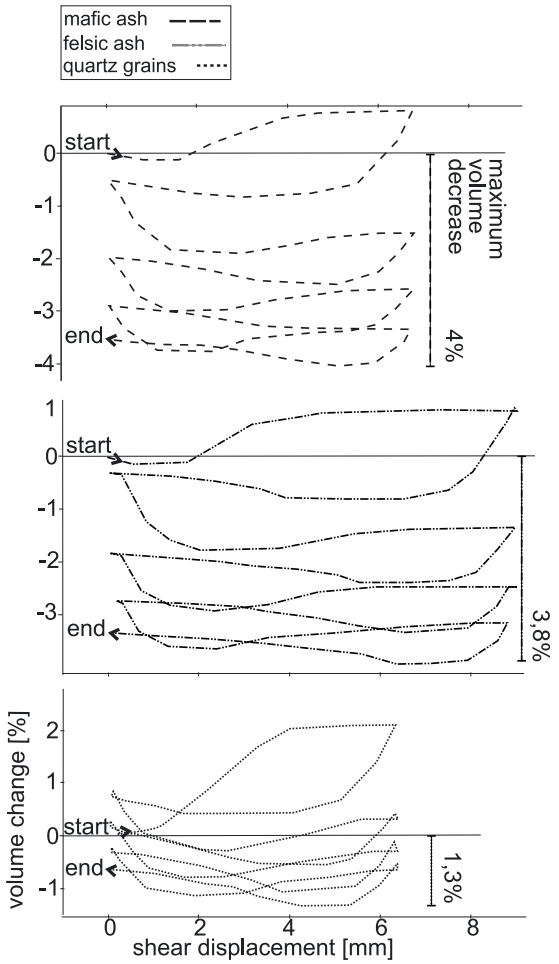

Figure 11. Cyclic direct shear tests showing total volume change in % of mafic and felsic ashes and quartz grains of 0.063–0.125 mm grain size. Shearing went from left to right, continued until no further volume changes were recorded, and sheared back to the left (arrows). For each sample four cycles of shearing were conducted (effective vertical stress is 40 kPa ~7 m below seafloor, and shear velocity is 0.5 mm/min).

as could be expected from their initial lower bulk densities. Tests using the most abundant ash grain size (63–125 μm silt to fine sand) show a volume reduction 3 times higher than for quartz grains (Figure 11). Tests using the second most abundant grain size (125–250 μm, fine to middle sand) show a volume reduction 8.5 times larger than for quartz grains. A rearrangement of subvertically orientated laminar ash shards into subhorizontal attitudes would explain the much higher rates of volume reduction compared to rounded particles of the quartz sand. Thus, tests indicate that ash layers may undergo an anomalously high volume reduction of their grain skeleton compared to any other typical slope sediment, including quartz-rich terrigenous sand or silt layers discretely interbedded within clay. Although our tests did not include tests with pressure waves simulating earthquake shaking on the slope, we interpret that the differences in compaction of the samples will also occur during shaking on the slope by earthquakes.

3.6. High Hydraulic Conductivities of the SAT Layer

[38] Coarser tephra material sandwiched in between very fine grained clayey sediment of the continental slope should create layers of high permeability. Therefore, we estimated hydraulic conductivities of the SAT in the three cores by means of the grain size distribution curves after *Hazen* [1892]. This is a simple method to estimate the hydraulic conductivity, because it gives values similar compared to pump experiments, if the soil is not too inhomogeneous (U < 5, where U is the unconformity index given as the quotient of the grain sizes corresponding to the 60% and the 10% intersection with the cumulative grain size curve). Because of its simplicity and reliability, this method is still routinely applied in hydrogeology [*Hoelting and Coldewey,* 2009] (for details of equation see caption of Figure 10). Following, hydraulic conductivities (k_f value) for the SAT layer were calculated: in core M66/151 it has a $k_f \sim 2.6 \times 10^{-5}$ m s^{-1} (due to the very little amount of tephra within core M66/151 this is only an indication), in core M66/167 it has a $k_f = 1.75 \times 10^{-5}$ m s^{-1}, and in core M54/11 it has a $k_f = 3.4 \times 10^{-5}$ m s^{-1} (Figure 10). All values are in the range of 10^{-5} m s^{-1}, which is consistent with published values for permeable coarse silt to middle sand [*Deutsches Institut für Normung,* 2003].

[39] Since the SAT layer is normally graded we also estimated k_f values for the lower, coarser part of the layer, and for the upper, finer part (for cores M66/167 and M54/11-2). We estimated a k_f of 6.6×10^{-4} m s^{-1} for the coarser part of sample M54/11-2, within the grain size range of 1000–250 μm, (making up 48% of the entire layer) (Figure 12). A similar value of $k_f = 3.6 \times 10^{-4}$ m s^{-1} for the grain size range 1000–176.7 μm, (making up 15.53% of the entire layer) was estimated for sample M66/167 (Figure 12). These k_f values are about one magnitude higher than the values estimated for the entire layer, which implies a much higher permeability in the coarser basal part of the ash layer.

[40] The finer parts of both samples have k_f values of magnitude 10^{-5}; 3.07×10^{-5} m s^{-1} for sample M54/11-2 within the grain size range 176.7–0.69 μm (constituting 51.53% of the ash layer (Figure 13)

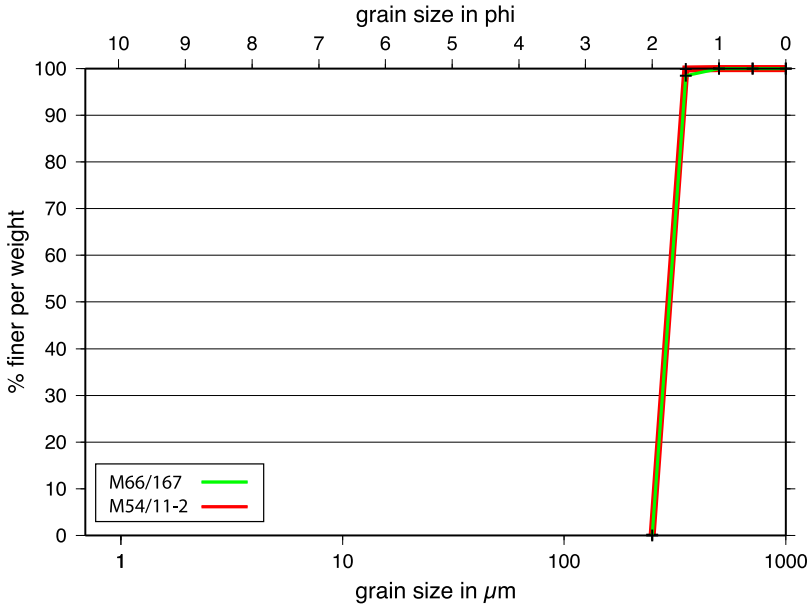

Figure 12. Cumulative grain size distribution of the coarser part of the SAT layer from cores M66/167 and M54/11-2, using the same method for k_f calculation described in Figure 10.

and for M66/167 $k_f = 1.16 \times 10^{-5}$ m s^{-1} for the grain size range of 125–0.69 μm (making up 84% of the layer) (Figure 13). Therefore, the hydraulic conductivity values of the SAT calculated from the grain size distribution suggest that the layer is highly permeable in comparison to other slope sediment, with higher permeability in its coarser basal lower part. These k_f values are similar to values of onshore aquifers [*Hoelting and Coldewey*, 2009].

3.7. Tephra Layers as Slide Planes: Conceptual Model

[41] Tephra layers contain disc-shaped ash particles that have accumulated by a different settling behavior than terrigenous clay sediments of the slope. After a volcanic eruption the ash is transported by winds and settles through the water column producing well-sorted deposits in just hours to a few days [*Fisher,* 1965; *Carey,* 1997]. Ash particles reach the seafloor in convective plumes that build dense particle-rich currents that move at least one order of magnitude faster than predicted by Stokes's law [*Carey,* 1997]. Therefore, the resulting deposit is not only well sorted, but also it bears the characteristics of random orientation of the disc-shaped volcanic shards. The resulting tephra is built by a rigid skeleton and large water-filled pore spaces, resulting in a hydraulically conductive layer. Such highly porous, highly conductive, 1–15 cm thick ash layers are intercalated within ~1 m thick clay units in the cores retrieved from the slides. In contrast, the clay-rich material, dominant on the slope, forms a water-retaining unit due to its low hydraulic conductivity.

[42] Shearing of ashes causes a high volume contraction that is produced by the rearrangement of the disc-shaped grain particles. We hypothesize that a significant difference in the rearrangement of particles along a shear plane may be expected during seismically induced shaking. Such a difference in rearrangement may cause proportionally different volumetric changes depending on the composition of single layers or may even occur within specific layers, with ash layers undergoing the largest contractancy.

[43] Shaking by large magnitude earthquakes of may force ash layers with noncohesive properties to undergo a sudden major grain rearrangement. The high hydraulic conductivity and relatively low bulk density of ashes, compared to the embedded terrigenous silt-sand, allow this process to occur under undrained conditions. Volume reduction will change the vertical profile of the shear strength of the ash layer: Grains settle toward the bottom of the layer where porosity rapidly decreases, and would be replaced by water in the middle to upper portion of the layer (Figure 14). The shear strength in the upper portion of the ash layer will suddenly decrease promoting the creation of a weak detachment plane. In extreme cases a water interlayer may be formed beneath the less permeable material.

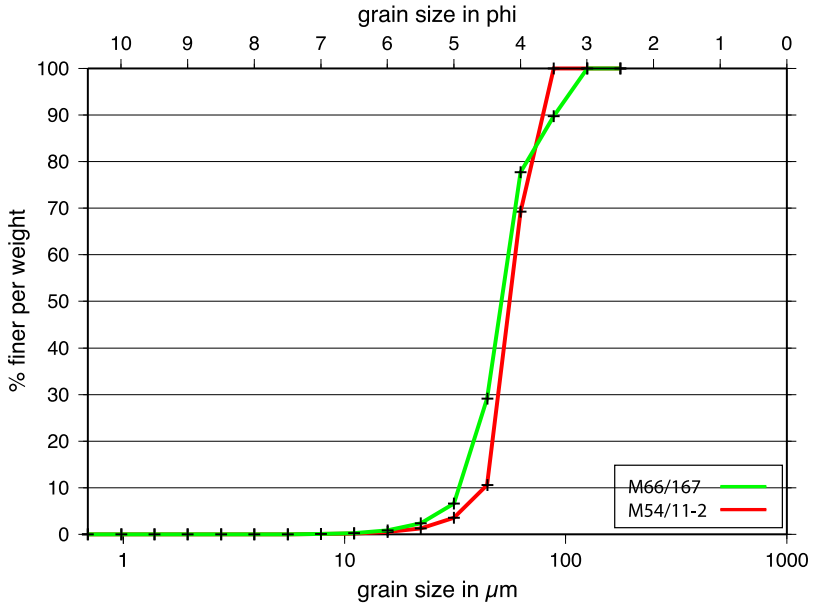

Figure 13. Cumulative grain size distribution of the finer part of the SAT layer from cores M66/167 and M54/11-2, using the same method for k_f calculation described in Figure 10.

Since the water interlayer would have zero shear strength a failure could easily occur.

4. Slides and Seismicity

[44] In addition to the contractancy and shear strength loss that could initiate sliding according to our hypothesis, individual tephra layer properties including thickness, lateral continuity and specific grain properties such as grain size, grain shape, degree of alteration, etc. may also influence the magnitude of the loss of shear strength during shaking. Our hypothesis is that the mafic ash layer of core M66/151 underwent liquefaction similar to the onshore NRC Mechanism B [*NRC*, 1985] inducing flow failure under undrained conditions.

[45] Comparing the number of large translational slides with the occurrence of large earthquakes offshore Costa Rica and Nicaragua (~15 earthquakes of Ms > 7 in last ~100 years, after *Ambraseys and Adams* [1996]), and considering the amount of time that the hemipelagic sediment accumulation rates of 30–40 cm kyr^{-1} [*Kutterolf et al.*, 2008c] require to fill tens of meters high slide scarps, it becomes clear that not each large earthquake causes a large slide. The largest headwall thickness at Masaya slide (Figures 1 and 3) is around 160 m. Applying sedimentation rates of 30–40 cm kyr^{-1} such a scarp would be filled in a time period of ~450,000 years. Therefore, we propose that the large Masaya and neighboring slides are less than ~450,000 years old, and in the case where sediment has not in filled the scars noticeably they are probably much younger. Large earthquakes (>7 Ms) occur along each segment of the margin with a 50–100 year recurrence time [*Ambraseys and Adams,* 1996], indicating that each area goes

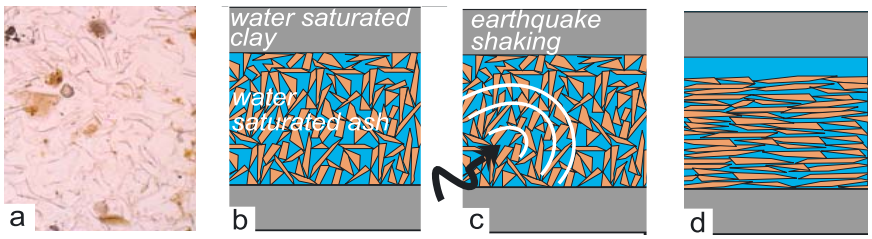

Figure 14. (a) Microscope photography of horizontally spread felsic ash shards (grain size is 63–125 μm). (b) Cartoon of a vertical cut through fresh deposited ash before an earthquake. (c) Earthquake shaking cancels grain-to-grain contact, which decreases the shear strength of the ash layer. (d) In the end-member case an interlayer may form during shaking.

through many earthquake cycles before sliding in a large event. This observation may indicate that besides the presence of ash layers the initiation of large-scale sliding is controlled by several conditions within the slope sediment, for instance the depth of penetration and the lateral extent of fault scarps within the slope, where many headwalls of the slides appear to initiate. However, core M66/151 recovered sediments indicative for a small-scale event, which is not visible with the resolution of our data. Hence, we interpret that small-scale slumping is more common than large-scale slumping. According to the estimated accumulation rates, the weak layer was less than 1 m depth below the seafloor. Accumulation rates can considerably change along slope, depending on the precise location and the corresponding environmental conditions on the slope. For example, higher accumulation rates must occur at the mouth of a canyon. And we speculate that the cored event removed sediment that was thicker than calculated by accumulation rates, because it is located in front of a canyon (Figures 1 and 2).

[46] Because failure occurs after several earthquake cycles, it is clear that the sediment undergoes several shaking event close to failure. This is important, because silty clays (normal marine sediment) undergoing repeated, nonfailure, seismic events can actually consolidate the sediment column through extrusion of excess pore water during earthquakes [*Locat and Lee,* 2002]. If rearrangement of grains in the ash layer happens abruptly, rather than being a gradual process, the ash layers do not undergo the same sediment strengthening during burial, and the slope strata is formed by layers of strengthened silty clays alternating with weakened ash layers. Thus, in our view the shear strength of clays and ashes follow opposed trends during repeated earthquake shaking.

[47] The behavior of the ash shards may perhaps be comparable to that of siliceous oozes, where the fragile framework of rigid skeletons of diatoms and radiolarians can be easily dissolved or being broken by overburden exceeding a certain threshold, and hence cause sudden porosity reduction and overpressuring of pore water [*Volpi et al.*, 2003, and references therein].

5. Conclusion

[48] Evidence from MSCL-density profiles, physical index properties, and pore water geochemistry indicate that tephra layers may act as weak layers in continental slope sediment and precondition the slope for instability. Our manuscript is based on observations of shallow slumps offshore Central America, where the base of the slide plane is parallel to the surrounding seafloor and the shallow stratigraphy. The proposed slip plane consists of a regionally well-mapped San Antonio tephra layer. Based on the precise age information about the deposition of the tephra and the accumulation rate we calculated the minimum of thickness of material that was removed by the slide. Grain size analysis shows, that the ash is highly conductive to water. Simple shear tests on the ash indicated high compaction rates during shear, leading us to the hypotheses that a sudden compaction due to rearrangement of the grains could produce peak pore pressures and liquefaction of the layer.

[49] The new model proposes that discrete tephra layers of the slope may have a distinct mechanical behavior compared to the more ubiquitous terrigenous slope sediment. The model proposes that the grain framework collapse of highly permeable ash layers during earthquake shaking creates a weak layer that serves as detachment plane for translational sliding.

[50] This scenario is applicable to all convergent margins with active volcanic arcs in geological settings similar to Central America, that occur around the Circum-Pacific, and Indian Ocean subduction zones and perhaps in the Mediterranean sea. Eruptions producing widespread submarine tephra layers also occur on volcanic islands (e.g., Hawaii, Canaries, Azores, Reunion, Cape Verde islands). Similar environments may exist onshore where large arc volcanoes occur within lakes such as in Kamchatka, Mexico, and Central America.

Acknowledgments

[51] This research was supported by the Deutsche Forschungsgemeinschaft as part of the SFB 574 (Sonderforschungsbereich). We thank the crew and captain of the *Meteor* and participants of cruise M66-3 for their help in collecting the cores and onboard measurements. This publication is contribution 136 of the Sonderforschungsbereich 574 “Volatiles and Fluids in Subduction Zones” at Kiel University. We thank C. R. Ranero and U. ten Brink for comments on a previous version of the manuscript and A. Wetzel for discussion. We are also thankful to the journal referees D. Orange and A. Camerlenghi for their constructive reviews.

References

Ambraseys, N. N., and R. D. Adams (1996), Large-magnitude Central American earthquakes, 1898–1994, *Geophys. J. Int.*, *127*, 665–692, doi:10.1111/j.1365-246X.1996.tb04046.x.

Blum, P. (1997), Physical properties handbook: A guide to the ship board measurement of physical properties of deep-sea cores, *Tech. Note, 26*, Ocean Drill. Program, College Station, Tex. (Available at http://www-odp.tamu.edu/publications/tnotes/tn26/INDEX.HTM)

Caress, D. W., and D. N. Chayes (1996), Improved processing of Hydrosweep DS multibeam data on the R/V *Maurice Ewing*, *Mar. Geophys. Res.*, *18*, 631–650, doi:10.1007/BF00313878.

Carey, S. (1997), Influence of convective sedimentation on the formation of widespread tephra fall layers in the deep sea, *Geology*, *25*(9), 839–842, doi:10.1130/0091-7613(1997)025<0839:IOCSOT>2.3.CO;2.

Castro, G. (1969), *Liquefaction of Sands*, *Harvard Soil Mech. Ser.*, vol. 87, Harvard Univ., Cambridge, Mass.

Deutsches Institut für Normung (2002), Soil, investigation and testing—Determination of shear strength—Part 3: Direct shear test, *Rep. DIN 18137-3*, Berlin.

Deutsches Institut für Normung (2003), Soil, investigation and testing—Determination of the coefficient of water permeability—Part 2: Field tests, *Rep. DIN 18130-1*, Berlin.

Field, M. E., J. V. Gardner, A. E. Jennings, and B. D. Edwards (1982), Earthquake induced sediment failures on a 0.258 slope, Klamath River delta, Calif. *Geol.*, *10*, 542–546.

Fisher, R. V. (1965), Settling velocity of glass shards, *Deep Sea Res.*, *12*, 345–353.

Graham, J. (1984), Methods of stability analysis, in *Slope Instability*, edited by B. Brunsdan and D. B Prior, pp. 171–215, John Wiley, New York.

Hampton, M. A., and H. J. Lee (1996), Submarine landslides, *Rev. Geophys.*, *34*, 33–59, doi:10.1029/95RG03287.

Hansbo, S. (1957), A new approach to the determination of the shear strength of clay by the fall-cone test, *Proc. R. Swed. Geotech. Inst.*, *14*, 5–47.

Hazen, A. (1892), Some physical properties of sand and gravels with special reference to their use in filtration, *Annu. Rep.*, 24, pp. 541–556, Mass. State Board of Health, Boston.

Hensen, C., M. Zabel, K. Pfeifer, T. Schwenk, S. Kasten, N. Riedinger, H. D. Schluz, and A. Boetius (2003), Control of sulfate pore-water profiles by sedimentary events and the significance of anaerobic oxidation of methane for the burial of sulfur in marine sediments, *Geochim. Cosmochim. Acta*, *67*(14), 2631–2647, doi:10.1016/S0016-7037(03)00199-6.

Hoelting, B., and W. G. Coldewey (2009), *Hydrogeologie-Einfuehrung in die allgemeine und angewandte Hydrogeologie*, 7th ed., 383 pp., Spektrum Akad., Heidelberg, Germany.

Houlsby, G. T. (1982), Theoretical analysis of the fall cone test, *Geotechnique*, *32*, 111–118, doi:10.1680/geot.1982.32.2.111.

Karlsrud, K., and L. Edgers (1982), Some aspects of submarine slope stability, in *Marine Slides and Other Mass Movements*, *NATO Conf. Ser. IV, Mar. Sci.*, vol. 6, edited by S. Saxov and J. K. Nieuwenhuis, pp. 68–81, Plenum, New York.

Kokusho, T. (2003), Current state of research on flow failure considering void redistribution in liquefied deposits, *Soil. Dyn. Earthquake Eng.*, *23*, 585–603, doi:10.1016/S0267-7261(03)00067-8.

Kutterolf, S., U. Schacht, H. Wehrmann, A. Freundt, and T. Moerz (2007a), Onshore to offshore tephrostratigraphy and marine ash layer diagenesis in Central America, in *Central America Geology, Resources and Hazards*, vol. 2, edited by J. Buntschuh and G. E. Alvarado, pp. 395–423, A. A. Balkema, Lisse, Netherlands.

Kutterolf, S., A. Freundt, W. Peréz, H. Wehrmann, and H. U. Schmincke (2007b), Late Pleistocene to Holocene, temporal succession and magnitudes of highly explosive volcanic eruptions in west-central Nicaragua, *J. Volcanol. Geotherm. Res.*, *163*, 55–82, doi:10.1016/j.jvolgeores.2007.02.006.

Kutterolf, S., A. Freundt, W. Perèz, T. Moerz, U. Schacht, H. Wehrmann, and H. -U. Schmincke (2008a), Pacific offshore record of plinian arc volcanism in Central America: 1. Along-arc correlations, *Geochem. Geophys. Geosyst.*, *9*, Q02S01, doi:10.1029/2007GC001631.

Kutterolf, S., A. Freundt, and W. Peréz (2008b), Pacific offshore record of plinian arc volcanism in Central America: 2. Tephra volumes and erupted masses, *Geochem. Geophys. Geosyst.*, *9*, Q02S02, doi:10.1029/2007GC001791.

Kutterolf, S., A. Freundt, U. Schacht, D. Buerk, R. Harders, T. Moerz, and W. Perèz (2008c), Pacific offshore record of plinian arc volcanism in Central America: 3. Application to forearc geology, *Geochem. Geophys. Geosyst.*, *9*, Q02S03, doi:10.1029/2007GC001826.

Kutterolf, S., V. Liebetrau, T. Mörz, A. Freundt, T. Hammerich, and D. Garbe-Schönberg (2008d), Lifetime and cyclicity of fluid venting at fore arc mound structures determined by tephrostratigraphy and radiometric dating of authigenic carbonates, *Geology*, *36*(9), 707–710, doi:10.1130/G24806A.1.

Locat, J., and H. J. Lee (2002), Submarine landslides: Advances and challenges, *Can. Geotech. J.*, *39*, 193–212, doi:10.1139/t01-089.

McIntosh, K. D., E. A. Silver, I. Ahmed, A. Berhorst, C. R. Ranero, R. K. Kelly, and E. R. Flueh (2007), The Nicaragua convergent margin: Seismic reflection imaging of the source of a tsunami earthquake, Costa Rica, in *The Seismogenic Zone of Subduction Thrust Faults*, edited by T. Dixon and J. C. Moore, pp. 257–287, Columbia Univ. Press, New York.

Mulder, T., and P. Cochonat (1996), Classification of offshore mass movements, *J. Sediment. Res.*, *66*, 34–57.

National Research Council (NRC) (1985), *Liquefaction of Soils During Earthquakes*, 240 pp., Natl. Acad. Press, Washington, D. C.

Peréz, W., and A. Freundt (2006), The youngest highly explosive basaltic eruptions from Masaya caldera (Nicaragua): Stratigraphy and hazard assessment, in *Volcanic Hazards in Central America*, edited by W. I. Rose et al., *Spec. Pap. Geol. Soc. Soc. Am.*, *412*, 189–207.

Ranero, C. R., and R. von Huene (2000), Subduction erosion along the Middle America convergent margin, *Nature*, *404*, 748–752, doi:10.1038/35008046.

Ranero, C. R., I. Grevemeyer, H. Sahling, U. Barckhausen, C. Hensen, K. Wallmann, W. Weinrebe, P. Vannucchi, R. von Huene, and K. McIntosh (2008), Hydrogeological system of erosional convergent margins and its influence on tectonics and interplate seismogenesis, *Geochem. Geophys. Geosyst.*, *9*, Q03S04, doi:10.1029/2007GC001679.

Riedinger, N., K. Pfeifer, S. Kasten, J. F. K. Garming, C. Vogt, and C. Hensen (2005), Diagenetic alteration of magnetic signals by anaerobic oxidation of methane related to a change in sedimentation rate, *Geochim. Cosmochim. Acta*, *69*, 4117–4126, doi:10.1016/j.gca.2005.02.004.

Sahling, H., D. G. Masson, C. R. Ranero, V. Hühnerbach, W. Weinrebe, I. Klaucke, D. Bürk, W. Brückmann, and E. Suess (2008), Fluid seepage at the continental margin offshore Costa Rica and southern Nicaragua, *Geochem. Geophys. Geosyst.*, *9*, Q05S05, doi:10.1029/2008GC001978.

Skempton, A. W., and J. N. Hutchinson (1969), Stability of natural slopes and embankment foundations: State-of-the-art report, *Proc. Int. Conf. Soil Mech. Found. Eng. 7th*, *2*, 291–335.

Spangenberg, T. (2002), Erdbeben-Hangrutschungen-Tsunami: Beitraege zum Verstaendnis zur Subduktion vor Nicaragua und zu den komplexen Beziehungen zwischen Erdbeben, gravitativen Massenverlagerungen und Tsunamigenerierung, Ph.D. thesis, 233 pp., Ernst-Moritz-Arndt Univ. Greifswald, Greifswald, Germany.

Thomson, J., T. R. S. Wilson, F. Culkin, and D. J. Hydes (1984), Non-steady state diagenetic record in eastern equatorial Atlantic sediments, *Earth Planet. Sci. Lett.*, *71*, 23–30, doi:10.1016/0012-821X(84)90049-9.

Volpi, V., A. Camerlenghi, C. -D. Hillebrand, M. Rebesco, and R. Ivaldi (2003), Effects of biogenic silica on sediment compaction and slope stability on the Pacific margin of the Antarctic Peninsula, *Basin Res.*, *15*, 339–363, doi:10.1046/j.1365-2117.2003.00210.x.

von Huene, R., C. R. Ranero, and W. Weinrebe (2000), Quaternary convergent margin tectonics of Costa Rica, segmentation of the Cocos Plate, and Central American volcanism, *Tectonics*, *19*, 314–334, doi:10.1029/1999TC001143.

von Huene, R., C. R. Ranero, and P. Watts (2004), Tsunamigenic slope failure along the Middle America Trench in two tectonic settings, *Mar. Geol.*, *203*, 303–317, doi:10.1016/S0025-3227(03)00312-8.

Wessel, P., and W. H. F. Smith (1998), New improved version of generic mapping tools released, *Eos Trans. AGU*, *79*, 579, doi:10.1029/98EO00426.

Wijewickreme, D., S. Sriskandakumar, and P. Byrne (2005), Cyclic loading response of loose air-pluviated Fraser River sand for validation of numerical models simulating centrifuge tests, *Can. Geotech. J.*, *42*, 550–561, doi:10.1139/t04-119.

Wilson, T. R. S., J. Thomson, D. J. Hydes, S. Colley, F. Culkin, and J. Sørensen (1986), Oxidation fronts in pelagic sediments: Diagenetic formation of metal-rich layers, *Science*, *232*, 972–975, doi:10.1126/science.232.4753.972.

Zabel, M., and H. D. Schulz (2001), Importance of submarine landslides for non-steady state conditions in pore-water systems—Lower Zaire (Congo) deep-sea fan, *Mar. Geol.*, *176*, 87–99, doi:10.1016/S0025-3227(01)00164-5.

Chapter 6

Retrospect & Outlook

This PhD work represents the first extensive study on submarine mass wasting processes along a convergent margin from a subduction zone that is dominated by tectonic erosion processes. The work has been focused on the Middle America Trench, but most of the conclusions are probably applicable to other convergent margins dominated by tectonic erosion processes, which represent about 50% of all subduction zones.

The PhD work initiated with the participation on two cruises, the first at the MAT in Fall 2005 and the second offshore Chile in spring 2006 to collect some of the data later analyzed, or data with similar scientific goals that have been analyzed by other groups within the SFB 574. To study the MAT margin we analyzed multibeam bathymetry, sidescan sonar imagery, seismic data, and sediment cores. The database is large, covering - with un-even distribution - much of the MAT continental slope, which has enabled to map an inventory of close to 150- mostly previously unreported - slope failures. The variety of structures and their distribution is complex, and potential preconditioning and triggering mechanisms related to variations in tectonic processes along the subduction system have been postulated. A selection of representative failures has been analyzed in greater detail, including their deformation patterns and sediment structures. Through sedimentological and geotechnical analysis of core sediment from the MAT slope we investigated in further detail possible preconditioning factors and trigger mechanisms for translational sliding. Finally, a preliminary interpretation of the nature of the failure and mass transport (e.g. catastrophic collapse) for as many as possible structures has been proposed. The goal has been to make the first regional assessment of natural hazards associated to slope failures along the MAT.

Therefore, a major contribution of this work is that it provides the first overview on submarine mass wasting at the MAT and describes those processes at a convergent margin dominated by subduction erosion, which has previously been largely neglected in slope stability studies. Our research has clearly shown that much basic research can be carried out using the tools available to the scientific community. However, intrinsic

to this achievement is that some of the novel topics have been only preliminarily developed and their understanding will require considerable further additional research on a number of issues at the MAT and at other margins dominated by tectonic erosion around the world (e.g. segments of Chile, where IFM-GEOMAR has abundant data, and perhaps Tonga, where IFM-GEOMAR has also collected data).

In the following, I would summarize the results of chapters 3-6 and present a brief outlook for future research that should expand and complete the work developed here. Based on my findings and experiences within this work I would suggest further research with existing data, and some experiments to collect new data with –in retrospect- improved sampling strategies over the experiments I have participated.

Chapter 3

Submarine slope failures along the convergent continental margin of the Middle America Trench

- The high-resolution bathymetry data used along the MAT enabled to map 147 submarine landslide structures. Offshore Costa Rica and part of Nicaragua failures and deposits were mapped with additional deep-towed side scan sonar, which permitted a detailed analysis of the structures. However, offshore Guatemala, El Salvador, and parts of Nicaragua mapping of the slope only with bathymetry makes it more difficult to understand slope processes. Somewhat surprisingly, slope deformation features such as fractures and faults cutting the sediment and slides appear regionally rather different. To better understand and compare these structures additional deep-towed sidescan sonar data would be needed. The additional resolution of sidescan sonar imagery, and acoustic impedance information of the seafloor could significantly help to understand the relations between fault structures and landsliding.
- In this PhD work only a limited amount of seismic data have been used. The data used were easily available and already processed by previous members of the project so that they could be readily integrated in the analysis. Unfortunately, those data are not of a resolution adequate to analyze slope-failure structures, even though they give useful information on the geometry of the entire overriding plate and subducting-plate morphology. Further, those available data were collected before high-resolution seafloor maps existed and thus are not optimally located.

Higher resolution, carefully located seismic reflection images would provide an information that could help to advance the understanding of the relations of landsliding to slope stratigraphy and tectonic structures like faults. The images could provide information on the sediment successions above and below the slip plane, the location and geometry of the slip planes and potential slip planes for future failures.

Sub-bottom profiling should be available along some of the structures because it has been collected along with bathymetry is numerous cruises. The information may locally be interesting, but in principle the images are grossly inadequate because the slope along the MAT are commonly steep (> 5º and often > 10º) and the locus of landsliding - particularly headwalls - are typically steep, so that images are poor. The Parasound profile shot across the headwall of "Hermosa" slide, shown in chapter 5, shows the difficulty to image steep environments. Likewise, penetration is in most cases not adequate for the goals described above. However, sub-bottom profiler could provide very valuable information on debris avalanche geometry, perhaps their stratigraphy, and of post-events overlaying pelagic sedimentation that could hardly be obtained by other means. Although such data have not been analyzed here due to time constrains, they could be analyzed in the future.

- Seismic data would also be needed to carefully estimate volumes involved in the mass transport deposits along the MAT. This would give quantitative information about sediment dynamics compared to other margins and other tectonic settings.

Chapter 4

An overview of the role of long-term tectonics and incoming plate structure on segmentation of submarine mass wasting phenomena along the Middle America Trench

- The chapter addresses the relationships between long-term tectonics and mass wasting processes. The goal was to investigate for the first time the connection between tectonic erosion processes and mass wasting at the scale of a large system like the MAT. In this chapter it is shown that long-term tectonic processes and mass wasting phenomena differ along the margin, so that they change across clear segments along slope. It is also shown that there is a resembling segmentation in the character of the incoming plate relief and structure. However, many important questions are still open and require of further study. Here we list a few:

- The distribution of tectonic erosion processes with depth along the plate boundary are not well understood yet and need to be addressed in more detail to further integrate long-term tectonics and their effect on preconditioning and triggering mechanisms of slope failures.
- Further, along- and across- slope erosion rates would be required to quantify their influence on the locus and abundance of mass wasting and to compare it to other margins and other tectonic settings. The tectonic erosion processes that lead to slope over-steepening, interpreted as one major preconditioning factor for mass wasting, should be investigated in greater detail. The volume of material removal from the underside of the overriding continental plate, which is supposed to trigger the subsidence and oversteepening of the entire slope should be quantified in form of a rate of material loss across the slope and along the margin.
- Conceivably, numerical modelling of the long-term tectonic erosion effects on slope evolution, taking into account rock properties (basement and sediment) would help to understand the dynamics of this setting and to integrate in a conceptual framework the observations from other data like seismic, bathymetry and sidescan sonar data.

Chapter 5

Tephra layers: A controlling factor on submarine translational sliding?

- The chapter investigates the effect on slope stability of intercalated discrete tephra layers on the otherwise rather monotonous slope stratigraphy of the MAT. The analysis of the sedimentological and geotechnical properties of cored sediment support that tephra layers could act as weak zones and promote failure of translational slides. The effect of tephra layers on slope stability has been recently tested by drilling in the Nankai Trough and preliminary results indicate that several slides have such a layer at the location of the slip plane.
- To further test this hypothesis, similar geotechnical investigations at other slide locations along the Middle America slope have to be conducted. For this purpose it would be essential to recover cores that enable to penetrate through the slide deposits and slip planes and into the sediments below. During the Meteor-54 cruise in 2005 it became clear after some testing that the best core positions for that purpose were right

below the headwalls. There, deposits are probably the thinnest and the slide plane may even be exposed to the surface, which optimizes the core recovery. To find the best position below the headwall in detail, parasound data should be shot simultaneously and the stratigraphy monitored. If gravity cores are used, an error of positioning of about a radius of 250m from the planned position must be calculated due to the low rope tension at great water depths of 1000-4000m. This might be a large error leading to imprecise results. The gravity coring devices used were also rather short (which in our cruise provided sediment cores no longer than 9m), forcing us to sample only small slides. Longer coring devices that can be better positioned should be used, so that they would permit to sample large slides to test whether the tephra layer hypothesis is valid for larger structures.

- To perform accurate geotechnical measurements it is essential that the recovered cores are not opened for description before geotechnical measurements are conducted. Undisturbed cores have to be put in a cold lab to protect the sediment from any further disturbance before they are sampled for geotechnical measurements. Specific layering, density of the sediment and the natural anisotropy due to the sedimentation history of the sediment should not be disturbed before measurements. Pore water contents should be preserved, since water loss would change the sediment structure.
- Due to fairly disturbed samples and limited sample material in our cores, the hydraulic conductivity of ash layers and marine clays had yet to be more accurately estimated. For further similar investigations it would be important to conduct laboratory tests of hydraulic conductivity direct on the different specimen.
- It would be important to conduct triaxial shear tests under saturated conditions on a specimen containing the relevant 3 layers (clay-ash-clay) and to use a device that is also able to simulate seismic loading. This would possibly give realistic values of pore pressure rise within or above the ash layer and in an ideal case it may result in a similar failure than it was hypothesized.

I Appendix

Pacific offshore record of plinian arc volcanism in Central America: 3. Application to fore arc geology

S. Kutterolf, A. Freundt, U. Schacht, D. Bürk, R. Harders, T. Moerz, W. Peréz

Published in G^3, Volume 9, No 2, February 2008, Q02S03, doi:10.1029/2007GC001826
ISSN: 1525-2027

Geochemistry Geophysics Geosystems G3
AN ELECTRONIC JOURNAL OF THE EARTH SCIENCES
Published by AGU and the Geochemical Society

Article
Volume 9, Number 2
8 February 2008
Q02S03, doi:10.1029/2007GC001826
ISSN: 1525-2027

Click Here for Full Article

Pacific offshore record of plinian arc volcanism in Central America: 3. Application to forearc geology

S. Kutterolf
SFB574 at Kiel University/IFM-GEOMAR, Wischhofstrasse 1-3, D-24148 Kiel, Germany (skutterolf@ifm-geomar.de)

A. Freundt
SFB574 at Kiel University/IFM-GEOMAR, Wischhofstrasse 1-3, D-24148 Kiel, Germany

IFM-GEOMAR, Wischhofstrasse 1-3, D-24148 Kiel, Germany

U. Schacht
SFB574 at Kiel University/IFM-GEOMAR, Wischhofstrasse 1-3, D-24148 Kiel, Germany

CO2CRC, Australian School of Petroleum, University of Adelaide, Adelaide, South Australia 5005, Australia

D. Bürk and R. Harders
SFB574 at Kiel University/IFM-GEOMAR, Wischhofstrasse 1-3, D-24148 Kiel, Germany

T. Mörz
MARUM, Leobener Strasse, D-28359 Bremen, Germany

W. Peréz
SFB574 at Kiel University/IFM-GEOMAR, Wischhofstrasse 1-3, D-24148 Kiel, Germany

[1] Sediment gravity cores collected on the Pacific slope and incoming plate offshore Central America reach up to 400 ka back in time and contain numerous ash layers from plinian eruptions at the Central American Volcanic Arc. The compositionally distinct widespread ash layers form a framework of marker horizons that allow us to stratigraphically correlate the sediment successions along and across the Middle America Trench. Moreover, ash layers correlated with 26 known eruptions on land provide absolute time lines through these successions. Having demonstrated the correlations in part 1, we here investigate implications for submarine sedimentary processes. Average accumulation rates of pelagic sediment packages constrained by bracketing tephras of known age range from ~1–6 cm/ka on the incoming plate to 30–40 cm/ka on the continental slope. There are time intervals in which the apparent pelagic sedimentation rates significantly vary laterally both on the forearc and on the incoming plate where steady conditions are usually expected. A period of unsteadiness at 17–25 ka on the forearc coincides with a period of intense erosion on land probably triggered by tectonic processes. Unsteady conditions on the incoming plate are attributed to bend faulting across the outer rise triggering erosion and resedimentation. Extremely low apparent sedimentation rates at time intervals >50–80 ka suggest stronger tectonic activity than during younger times and indicate bend faulting is unsteady on a longer timescale. Submarine landslides are often associated with ash layers forming structurally weak zones used for detachment. Ash beds constrain ages of >60 ka, ~19 ka, and <6 ka for three landslides offshore Nicaragua. Phases of intense fluid venting at mud mounds produce typical sediments around the mound that become covered by normal

pelagic sediment during phases of weak or no activity. Using intercalated ash layers, we determine for the first time the durations (several hundred to 9000 years) of highly active periods in the multistage growth history of mud mounds offshore Central America, which is essential to understand general mud-mound dynamics.

Components: 7470 words, 7 figures, 1 table.

Keywords: marine tephrostratigraphy; plinian volcanism; forearc geology; submarine slides; mound structures; Central America.

Index Terms: 8455 Volcanology: Tephrochronology (1145); 8428 Volcanology: Explosive volcanism; 4219 Oceanography: General: Continental shelf and slope processes (3002).

Received 13 September 2007; **Revised** 15 October 2007; **Accepted** 23 October 2007; **Published** 8 February 2008.

Kutterolf, S., A. Freundt, U. Schacht, D. Bürk, R. Harders, T. Mörz, and W. Peréz (2008), Pacific offshore record of plinian arc volcanism in Central America: 3. Application to forearc geology, *Geochem. Geophys. Geosyst.*, *9*, Q02S03, doi:10.1029/2007GC001826.

Theme: Central American Subduction System
Guest Editors: G. Alvarado, K. Hoernle, and E. Silver

1. Introduction

[2] Ash from numerous plinian, phreatoplinian and ignimbrite-forming eruptions from volcanic complexes along the Central American Volcanic Arc (CAVA) was dispersed far westward across the Pacific to form widespread ash layers extending >400 km from vent across 10^6 km^2 [*Kutterolf et al.*, 2007b, 2008a]. The 56 gravity cores of up to 11 m length we have drilled along the Middle America Trench on both the forearc and the incoming plate (Figure 1) contain the record of tephras and intercalated sediments reaching back to 400 ka. Distinct compositional characteristics of the ash layers allow their correlation between cores and with tephras exposed on land as shown in part 1 [*Kutterolf et al.*, 2008a], where we have identified the distal ashes of 26 large eruptions at the CAVA and constrained the ages of 10 previously undated eruptions from the marine record. In part 2 we have used these correlations to determine the distribution characteristics of the tephras and their erupted magma masses which we combined with published data to derive long-term magma discharge rates for the individual volcanic systems as well as the whole CAVA [*Kutterolf et al.*, 2008b]. Here we use the tephra record to constrain geological processes on the Pacific seafloor.

[3] The Central American Pacific forearc is characterized by the tectonics of subduction erosion, by numerous sites of localized fluid venting (Figure 1), and by submarine landslides triggered by gas hydrate dissolution or seamount subduction. During recent years these structures have been imaged in great detail by high resolution bathymetry and seismic profiling accompanied by geochemical analyses of vent fluids and biogeochemical studies of vent fauna. However, these methods do not determine the ages of such structures and their formation events. Ash layer provide a tool to determine sedimentation rates and formation ages, which we here use to date failures of the continental slope and to determine the "life cycle" of mud mounds. Such temporal constraints are essential to understand the dynamic processes and to identify forcing mechanisms and external controls.

2. Geological Setting

[4] The Central American Volcanic Arc (CAVA) extends from Panama in the south to Guatemala in the north and results from the subduction of the Cocos plate beneath the Caribbean plate [e.g., *Mann et al.*, 2007]. The CAVA is one of the most volcanically active regions in the world and produced numerous plinian eruptions in the last several hundred thousand years, which deposited tephra layers in the Pacific Ocean. Variations in the nature of the incoming plate [*Hoernle et al.*, 2002], in crustal thickness and composition [*Carr*, 1984] and in geophysical subduction parameters [*Syracuse and Abers*, 2006; *von Huene et al.*, 2000], caused systematic along-arc variations in

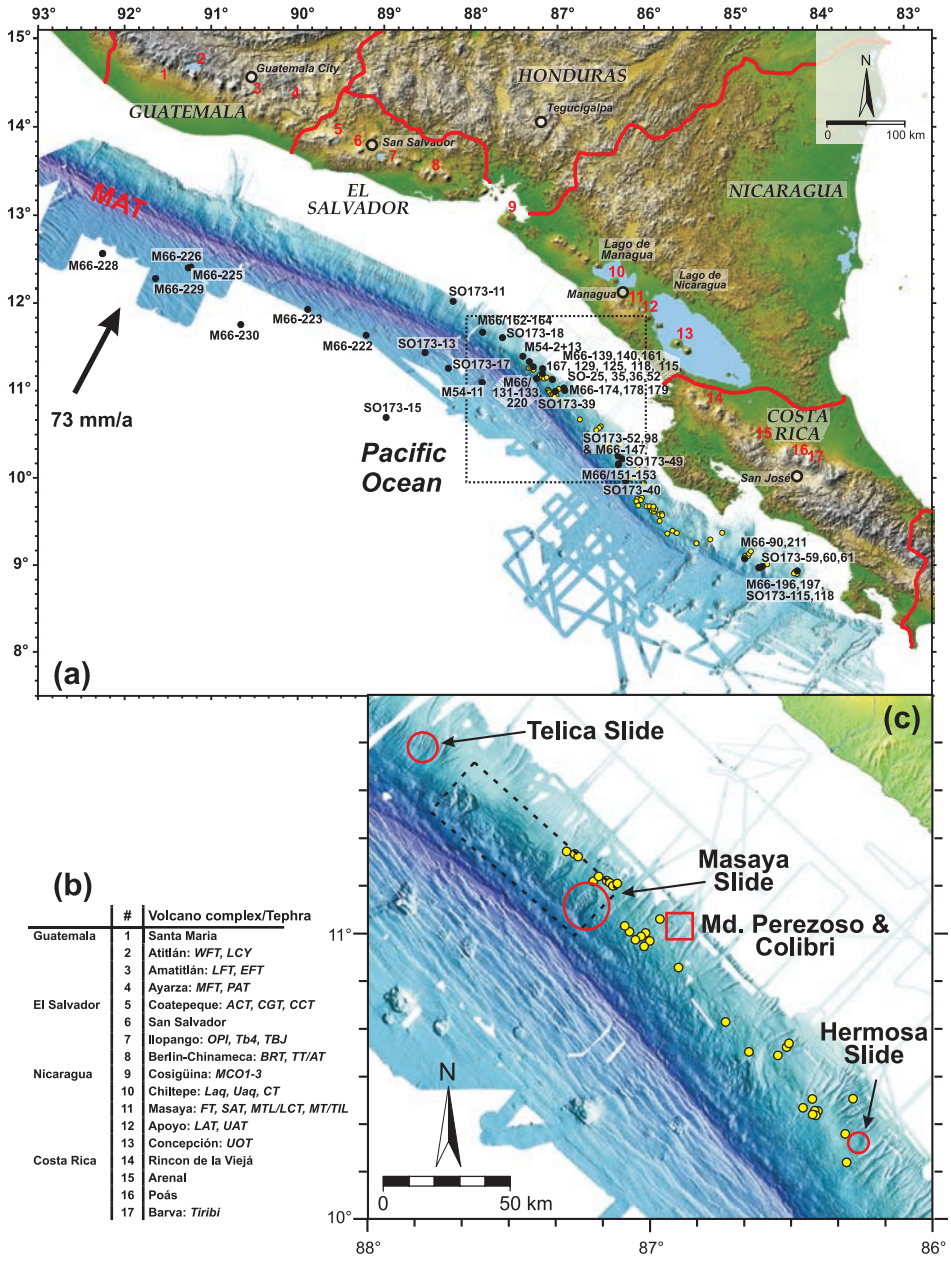

Figure 1. (a) Shaded and colored SRTM elevation model of Central America (NASA/JPL/NGA, 2000) and high-resolution bathymetry along the Middle America Trench (MAT) from *Ranero et al.* [2005]. The line of Central American arc volcanoes runs through the two large Nicaraguan lakes and parallel to the trench at 150–210 km distance. Black dots show core positions of R/V *METEOR* cruises M66 and M54 and R/V *SONNE* cruise SO173 along and across the trench. Yellow dots show distribution of methane seeps associated with mound and scar structures mapped at the slope offshore Costa Rica and Nicaragua by *Ranero et al.* [2008]. (b) Names of numbered volcanoes and major tephras: WFT, W-fall Tephra; LCY, Los Chocoyos Tephra; LFT, L-fall Tephra; EFT, E-fall Tephra; MFT, Mixta Tephra; PAT, Pinos Altos Tephra; ACT, Arce Tephra; CGT, Congo Tephra; CCT, Conacaste Tephra; OPI, Older pumice Ilopango; TB4, Terra Blanca 4 Tephra; TBJ, Terra Blanca Joven Tephra; BRT, Blanca Rosa Tephra; TT/AT, Twins/A-fall Tephra; MCO1-3, Mafic Cosigüina tephras; Laq, Lower Apoyeque Tephra; Uaq, Upper Apoyeque Tephra; CT, Chiltepe Tephra; FT, Fontana Tephra; SAT, San Antonio Tephra; MTL/LCT, Masaya Triple Layer/La Concepción Tephra; MT/TIL, Masaya Tuff/Ticuantepe Lapilli; LAT, Lower Apoyo Tephra; UAT, Upper Apoyo Tephra; UOT, Upper Ometepe Tephra. (c) Enlarged map section indicating landslides (red circles) and mud mounds (yellow dots) on the continental slope. Red rectangle gives position of Figure 5; black dashed rectangle gives position of Figure 3.

the composition of the volcanic rocks [*Carr et al.*, 2003, 2007; *Carr*, 1984; *Feigenson and Carr*, 1986; *Feigenson et al.*, 2004; *Hoernle et al.*, 2002; *Patino et al.*, 1997, 2000] that are very useful for geochemical correlations [*Kutterolf et al.*, 2008a].

[5] While bending into the subduction zone, the Cocos plate forms an outer rise in front of the trench along which it become dissected by numerous, deep-reaching bend faults [*Ranero et al.*, 2003]. Anomalous heat flow and seismic velocities indicate substantial hydration of crust and uppermost mantle by seawater invading the faults [*Grevemeyer et al.*, 2005], which is thought to be a major process to carry water into the subduction zone to ultimately generate melting in the mantle wedge [*Rüpke et al.*, 2002]. As the Cocos plate subducts beneath the Caribbean plate, the forearc is tectonically eroded [*Clift et al.*, 2005; *Ranero and von Huene*, 2000; *Vannucchi et al.*, 2004; *von Huene et al.*, 2004a]. Subduction erosion controls the structure of the forearc and causes oversteepening and destabilization of the continental slope particularly where seamounts are subducted [*von Huene et al.*, 2004b]. Parallel to the trench at intermediate water depths, the Middle American forearc is straddled with numerous fluid venting structures (Figure 1) believed to be fed by fluids expelled from subducted sediments by compaction and ascending along faults [*Hensen et al.*, 2004; *Moerz et al.*, 2005a, 2005b]. These include mud and carbonate mounds as well as vents at landslide scarps formed either by seamount subduction or by gas hydrate dissolution.

2.1. Mud and Carbonate Mounds

[6] Mud or carbonate mounds offshore Central America have diameters in the range of 100–2000 m and elevations above the surrounding seafloor of 20–200 m. They are composed of over-consolidated mud clasts, liquefied mudflows as well as highly variable authigenic carbonates. Mounds are mostly covered by massive carbonate crusts and boulders formed by the anaerobic oxidation of methane at the seafloor and in the extruded sediments [*Moerz et al.*, 2005b]. Seismic profiles show that the mounds visible at the surface cap are diatreme structures dissecting the gas hydrate layer (visible as Bottom Simulating Reflector, BSR) and extending at least several hundred meters deep into the forearc [*Talukder et al.*, 2007]. Fluid-chemical (Cl-depleted pore waters, C-isotopes) and petrographic evidence (MORB fragments, over-consolidated clay clasts) show that the fluids probably derive from dewatering of subducted sediments at 10–15 km depth, using permeable forearc faults created by tectonic erosion [*Ranero et al.*, 2008] to ascend to the surface [*Grevemeyer et al.*, 2004; *Hensen et al.*, 2004; *Mau et al.*, 2006, 2007; *Moerz et al.*, 2005a, 2005b]. The methane output flux at vent structures is temporally variable [*Mau et al.*, 2006]. Typically mixed sediments occur around mound structures that are thought to have been ejected during phases of intense activity [*Moerz et al.*, 2005b]. Their intercalation with background pelagic sediments demonstrates that mound activity is not steady but periodic. However, the lifetime of mud mounds and the age and duration of active periods are presently unknown.

2.2. Submarine Slides

[7] The sedimentary architecture of active and passive continental margins is frequently modified by submarine slope failures, which can occur on larger scales than known from terrestrial mass wasting events. Volumes of up to 20000 km^3 (e.g., Agulhas slide [*Hampton et al.*, 1996]) are mobilized, probably in a catastrophic manner, and are therefore a potential trigger mechanism for tsunamis that can devastate coastal areas [*Tappin et al.*, 2001]. The formation of gas hydrates cements and stabilizes the slope sediments but also prevents further compaction and build-up of shear strength [*Reston and Bialas*, 2002]. Partial dissolution of gas hydrates thus favors the formation of submarine landslides that may be triggered by earthquakes, particularly on continental slopes steepened by subduction erosion [*Harders et al.*, 2006]. Two different types of slope failure have been identified on the continental slope off Costa Rica and Nicaragua: rotational slumps and translational slides. Rotational slumps appear to be triggered by seamount subduction [*von Huene et al.*, 2000, 2004b]. In contrast, the formation of translational slides appears to be related to layers of low shear strength in the sediment succession [*Harders et al.*, 2006].

3. Marine Sediment Cores

3.1. Marine Core Sampling

[8] During R/V *METEOR* cruises M54/2 and M66/3 as well as R/V *SONNE* cruise SO173/3, 56 sediment gravity cores have been collected offshore Central America. The locations (9°12′N/

84°39′E and 12°45′N/92°30′E) of the cores are on the oceanic plate and the continental slope in 1200–4000 m water depth and distances of 150–370 km from the CAVA (Figure 1). The cores contain 213 ash horizons including primary ash layers and slightly reworked ash that retained its compositional integrity and stratigraphic position and therefore can be used as marker beds. Criteria identifying primary and variably reworked ash horizons, and the methods employed to correlate them with deposits on land are described and discussed in part 1 [*Kutterolf et al.*, 2008a]. In the following we focus on the intercalated sediments and on cores from sites that have been specifically targeted to penetrate sediments at mound structures, landslide deposits, and landslide detachment planes.

3.2. General Description of Cores

[9] The 56 cores collected from offshore Central America contain a total of 213 ash bearing horizons, including 133 distinct ash layers. Of these, 69 are light gray to white felsic ashes, 24 are gray layers of intermediate composition and 40 are black mafic layers. The ash layers and their components are described in more detail in part 1 of this contribution [*Kutterolf et al.*, 2008a].

[10] Pelagic silty to sandy clay sediment is commonly dark olive green but changes to lighter shades of green deeper in the cores. The pelagic sediment is mixed with terrigeneous input from the volcanic arc and its basement. The modal composition is typically 10 to 20% total quartz, 40 to 60% of clay (mainly smectite), 20 to 30% feldspar, and fresh to incipiently altered volcanic glass shards and rock fragments of various compositions (reworked sediments, basalts, carbonates). Additionally, <10% pyrite, 10 to 20% biogenic material including foraminifers, diatoms, some radiolarians and occasionally slope detritus like shells and corals can be found in the cores. Accessory chlorite clasts (<2%) occur in nearly every examined sample.

[11] In the upper part of core M66-228, M54-11, SO173-17, lower part of SO173-15, 18 and M54-13, and the entire sections of M66 cores 222 and 229, the pelagic sediment is compositionally and structurally completely monotonous indicating continuous sedimentation at constant rates. In other cores and core sections, however, there are abundant structural indications of small-scale slumping and mingling events interrupting the background clay sedimentation, even in cores from the incoming plate at considerable distance from the trench axis. This local small-scale reworking, however, did not significantly affect the stratigraphic order of the ash horizons.

[12] Sediment successions at the carbonate and mud mounds differ by including layers compositionally dominated by the products of these structures. Color changes from dark-olive-green to light-olive-gray of the fine grained matrix reflect increasing abundance of carbonate mud derived from the active mound. The clast components in the lighter layers are dominated by carbonate and/or mud detritus including over-consolidated "scaly" clay clasts that originated from deeper levels. Such layers are interpreted as mudflow deposits emitted by mud volcanoes [*Moerz et al.*, 2005a, 2005b]. During inactive phases of the mounds, the background clay sedimentation continues. At the intermediate depths on the slope, these sediments are heterogeneous and include abundant detritus from the shelf such as fragments of oysters, corals, and wood.

4. Applications of Tephrostratigraphy to Continental Slope Geology

[13] We focus on the Pacific region offshore Nicaragua. Table 1 summarizes a subset of 22 of the tephras correlated in part 1 that are relevant for the determination of ages and rates of the geological processes discussed in the following. These 22 tephras have well-constrained ages, characteristic compositions and form distinct distal marine ash beds.

4.1. Sedimentation Rates

[14] Time marks given by dated ash layers allow us to calculate average apparent sedimentation rates of the intercalated pelagic sediment (Figure 2, Figure S1[1], and Table 1). In these calculations, the thickness of the intercalated sediment interval is reduced by the intervening undated ash beds to obtain the pelagic sediment thickness. However, the pelagic clay is often mixed to variable extent with volcanic ash particles, which contribute to the sedimentation rate but are not corrected for. Sediment-petrographic studies underway will further refine sedimentation rates. Some core sections show intense bioturbation and the addition of organic matter may have increased the sediment

[1] Auxiliary materials are available in the HTML. doi:10.1029/2007GC001826.

Table 1. Summary of 22 Onshore Tephras Correlated in Part 1 That Are Relevant for the Determination of Ages and Rates of the Geological Processes[a]

Tephra Name	Tephra Acronym	Correlated Ash Layers	Age, ka	Source Volcano	Country	Max. Observed Ash Dispersal From the Source, km
Tierra Blanca Joven Tephra	TBJ	C1	1.6	Ilopango Caldera	El Salvador	390
Masaya Tuff/Ticuantepe Lapilli	MT/TIL	C2	1.8	Masaya Caldera	Nicaragua	200
Chiltepe Tephra	CT	C3	1.9	Chiletepe complex	Nicaragua	570
Masaya Triple Layer/ La Concepción Tephra	MTL/LCT	C4	2.1	Masaya Caldera	Nicaragua	170
San Antonio Tephra	SAT	C5	6	Masaya Caldera	Nicaragua	330
Upper Apoyeque Tephra	UAq	C6	12.4	Chiletepe complex	Nicaragua	300
Lower Apoyeque Tephra	LAq	C7	17	Chiletepe complex	Nicaragua	210
Upper Ometepe Tephra	UOT	C8	19	Concepción volcano	Nicaragua	280
Mafic Cosigüina Tephras	MCO	C9	21–23	Cosigüina volcano	Nicaragua	220
Upper Apoyo Tephra	UAT	C10	24.5	Apoyo Caldera	Nicaragua	530
Lower Apoyo Tephra	LAT	C11	24.8	Apoyo Caldera	Nicaragua	270
Tierra Blanca 4 Tephra	TB4	C12	36	Ilopango Caldera	El Salvador	380
Mixta Fall Tephra	MFT	C13	39	Ayarza Caldera	Guatemala	340
Conacaste Tephra	CCT	C14	51	Coatepeque Caldera	El Salvador	320
Congo Tephra	CGT	C15	53	Coatepeque Caldera	El Salvador	320
Fontana Tephra	FT	C16	~60	Las Nubes Caldera	Nicaragua	330
Twins/A-Fall Tephra	TT/AT	C17	60	Berlin-Pacayal-Volcan group	El Salvador	270
Arce tephra	ACT	C18	75	Coatepeque Caldera	El Salvador	320
Older Ilopango Pumice	OPI	C20	75–84	Ilopango Caldera	El Salvador	470
Los Chocoyos tephra	LCY	C21	84	Atitlán Caldera	Guatemala	1900
W-Fall Tephra	WFT	C22	158	Atitlán Caldera	Guatemala	560
L-Fall Tephra	LFT	C23	191	Amatitlán Caldera	Guatemala	810

[a] Ash layers (C#) were correlated by *Kutterolf et al.* [2008a].

thickness. Also, we typically obtain higher apparent sedimentation rates for the upper few decimeters of the cores than for deeper levels due to incomplete compaction near the seafloor. Since we do not attempt to correct for compaction, this must be considered when comparing apparent sedimentation rates for different age intervals.

[15] In general, we observe pelagic sedimentation rates of ~1–6 cm/ka on the incoming plate and up to 30–40 cm/ka on the continental slope. However, the apparent sedimentation rates vary with depth in the cores and between cores, both at the continental slope and on the incoming plate. In core SO173-15 at a position farthest away from the trench on the incoming plate (Figure 1), the apparent sedimentation rate gradually decreases with depth (Figure 2a). The high value of 27.5 cm/ka near the top reflects the poor compaction of the sediment. Below ~60 cm bsf, the sedimentation rate rapidly decreases to 5.7 cm/ka, similar to the 5.4 cm/ka estimated by *Bowles et al.* [1973]; this may be taken as a representative value of monotonous sedimentation on the Cocos plate offshore Nicaragua.

4.2. Sedimentation and Bend Faulting

[16] Sedimentation was not monotonous everywhere on the incoming plate. In core M66-222 (Figure 1; see Figure 10 in part 1), ash layers C10 (distal ash of the 24.5 ka Upper Apoyo Tephra, UAT) and C15 (53 ka Congo Tephra, CGT) are separated by ~188 cm of pelagic sediment indicating an average accumulation rate of 6.7 cm/ka. In contrast, ash bed C10 immediately follows atop ash pods of C15 in core M66-230; apparently some erosive event has removed sediment accumulated above C15 prior to emplacement of C10. Another example is core SO173-17 on the incoming plate offshore Nicaragua (Figure S1) where ash layers C10 (UAT) and C11, the distal ash of the Lower (LAT) Apoyo tephra, are separated by 15 cm sediment such that the sedimentation rate of 2 cm/ka determined by other ash beds implies a time period of ~7 ka between these eruptions. Geological evidence on land and overlapping radiocarbon ages [*Kutterolf et al.*, 2007a] demonstrate these eruptions occurred within a few hundred years at around 25 ka. Moreover, LAT and UAT are separated by 7 cm sediment on the continental slope

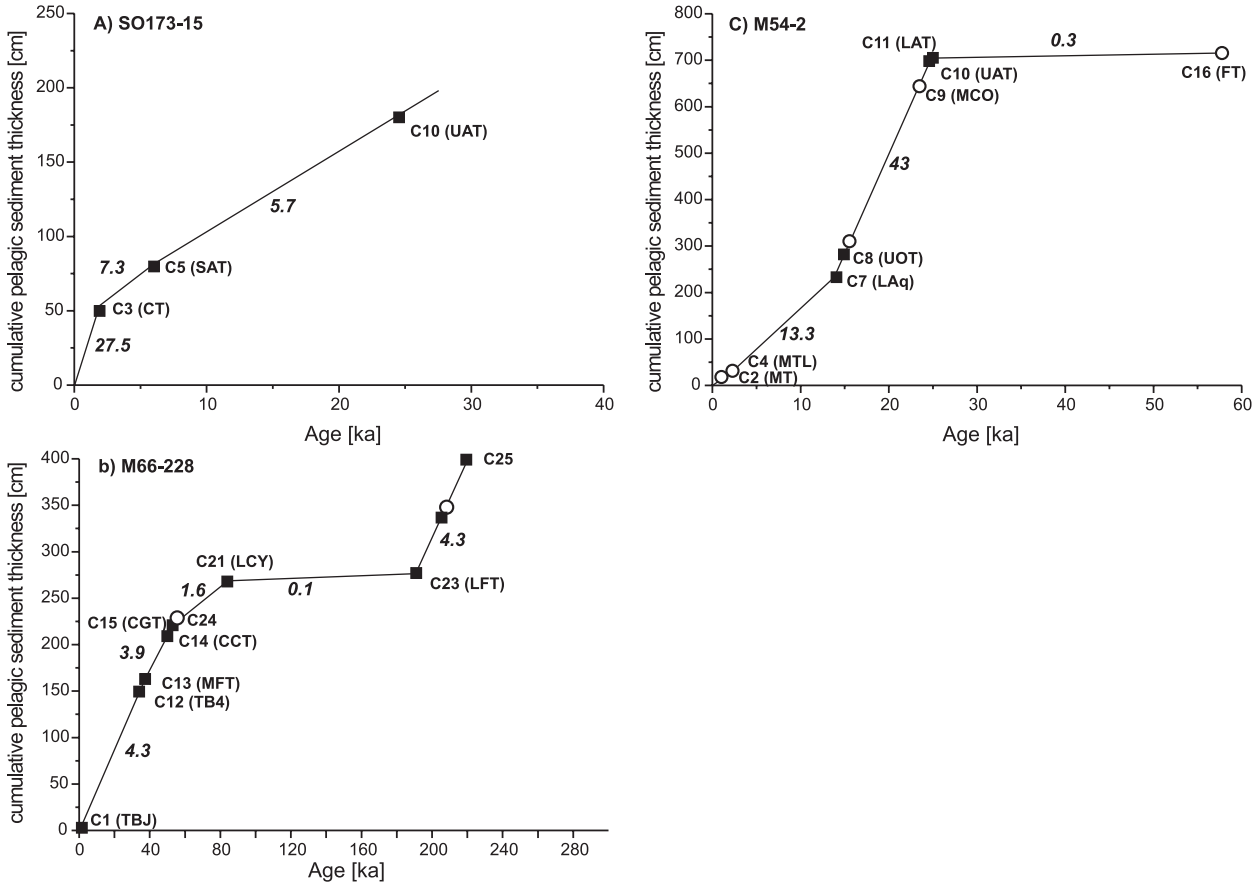

Figure 2. Cumulative thickness of pelagic sediment versus age for selected cores. (a) Core SO173-15 on incoming plate ~200 km distance from the trench. (b) Core M66-228 on incoming plate close to the trench; C25 only correlated to marine cores, not to tephras on land. (c) Core M54-2 on the middle continental slope. Filled squares show felsic ash layers and white circles show mafic ash layers correlated to field tephras (see Figure 1 for acronyms) of known age after *Kutterolf et al.* [2008a]. The slopes of line segments between tephras yield average apparent accumulation rates (numbers in cm/ka). Respective diagrams for other cores are shown in auxiliary material Figure S1.

(core M54-2; Figure 2c), where accumulation at 43 cm/ka suggests a time interval of ~200 years. The sediment interval in core SO173-17 contains small ash lenses of underlying LAT ash indicating that its excess thickness is due to reworking.

[17] Anomalously low apparent sedimentation rates of mostly <1 cm/ka mark the time intervals of 50–190 ka in core M66-223, 60–160 ka in core M66-230, 90–190 ka in cores M66-226 and M66-228 (Figure 2b), and to lesser extent at 60–70 ka in core M66-229 (Figure S1). Lower apparent sedimentation rates are also found at around 200 cm depths, or at >80 ka age, in cores SO173-17 and M54-11 closer to the trench offshore Nicaragua (Figure S1). These dramatic reductions in apparent sedimentation rate are not related to compaction because they occur at a similar age range but at different depths in the cores, e.g., beginning at 60 cm depth bsf in cores M66-223 and M66-226 but at 270 cm depth in core M66-229. Moreover, pore water analyses and strength measurements as well as core-logging data did not reveal significant differences in the state of sediment compaction (T. Mörz, personal communication, 2006). Structures such as clay lenses (see Figure 3e in part 1) and tilted ash pods rather suggest that the low apparent sedimentation rates result from repeated small-scale erosive events that occurred on the incoming plate. Although some turbidity currents from the continental slope may have reached the drill sites on the incoming plate, these were probably no longer erosive after crossing the trench and climbing the outer rise. We rather interpret that these local events of erosion and reworking were related to tectonic activity at the numerous bend faults that dissect the incoming plate on the outer rise and

have offsets increasing toward the trench (Figure 1) [*Ranero et al.*, 2005]. During the time span represented by the cores, core positions moved about 30 km along the subduction vector but remained within the zone of bend faulting. Across <50 ka sections of the cores, sedimentation rates are higher but laterally variable. Apparent sedimentation rates of 4–7.5 cm/ka in cores M66-228 and M66-229 farther away from the trench contrast with 0.6 and 1.1 cm/ka in cores M66-226 and M66-223 closer to the trench where fault offsets are larger. This suggests a tendency for stronger sediment reworking where fault offsets are larger. On the other hand, core M66-222 with 6.7 cm/ka is also close to the trench while core M66-230 with only 4.2 cm/ka lies farther away. Hence the local sedimentation and erosion of the younger core sections is controlled by both distance from trench (magnitude of fault offset) and proximity to the local faults (unknown due to insufficient resolution of core positioning and bathymetry). The apparent sedimentation rates of the older core sections are significantly lower but much more uniform between cores. A possible explanation may be that one or more intense tectonic events occurred between 80–190 ka that caused dramatic regional erosion irrespective of the detailed core position. An implication of this interpretation is that bend faulting is not continuous but proceeds by sporadic bursts that are separated by periods of less intense activity lasting on the order of 10^4 years.

4.3. Sedimentation on the Continental Slope

[18] Cores from the continental slope offshore Nicaragua reveal large differences in apparent sedimentation rates at comparable time intervals. For example, the core M54-2 (Figure 2c) has ~4 m sediment between ash layers C7 (LAq) and C10 (UAT), yielding accumulation at 35 cm/ka, while this interval is condensed to only ~0.2 m (2.2 cm/ka) in neighboring core M54–13 (Figure 1). The sediment thickness between layer C4 (2.1 ka MTL) and C7 is more than halved from core SO173-18 to M54-2. The top section above C2 (1.8 ka MT) likewise reduces from 1.5 m to 10 cm (rate from 90 to 13.3 cm/ka). The accumulated sediment of the past 6 ka is strongly reduced (1.1 cm/ka sedimentation rate) at the top of M54-13. These comparisons show that there are large local and temporal deviations from the "normal" accumulation rate of 30–40 cm/ka estimated from other, more monotonous cores (Figure S1). We interpret that these variations in apparent accumulation rates reflect laterally and temporally variable phases of excess sediment delivery and erosion probably by turbidity currents descending the slope. For example, excess accumulation rate of ~90 cm/ka across the upper 1.5 m of core SO173-18, which was taken from the rim of a submarine canyon on the Nicaraguan slope (Figure 1), can be explained by accumulation of turbidite overbank sediments from currents passing through the canyon.

[19] On land in Nicaragua we have identified major periods of erosion that occurred around 17–25 ka and 2–6 ka (unconformities U1 and U2-4 [*Kutterolf et al.*, 2007a]). Increased turbidity current activity on the continental slope causing lateral changes in apparent accumulation rates is probably linked to these erosive phases on land which appear to be related to tectonic activity (U1) and changing climatic conditions (U2-4) [*Kutterolf et al.*, 2007a]. There is no evidence on land correlating with erosion on the continental slope during the past <2 ka seen in some cores; this seems to be controlled by conditions at the slope only. We note that this is a preliminary interpretation because detailed petrographic studies of the sediments still need to be done. The absence of sharp unconformities in condensed sections can be explained by reworking of the soft sediments in an unconsolidated state.

4.4. Submarine Landslides and Ash Layers

[20] Fast, erosive subduction of the rough Cocos Plate beneath the Caribbean Plate leads to an oversteepening of the Nicaraguan continental slope [*Ranero and von Huene*, 2000; *von Huene et al.*, 2004b] on which sediment packages become unstable and collapse as submarine landslides [*Harders et al.*, 2006]. Large failures are abundant on the middle slope offshore Nicaragua (Figure 3) and increase the tsunami hazard. Detachment planes of landslides typically form in sediment layers of low shear strength. Drilling through two exposed slide planes offshore Costa Rica (SO173-59) and Nicaragua (M66/3-151) showed that detachment occurred at the level of ash layers. We use core M66/3-151 from the Hermosa slide as an illustrative example. An unconformity at 1.5 m bsf separates overlying undisturbed massive homogeneous pelagic clay from underlying, <10-cm-thick reworked mélange containing rounded intraclasts of consolidated clay in an unconsolidated clay matrix mixed with ash. This is underlain by a mafic ash layer that has an eroded top and high

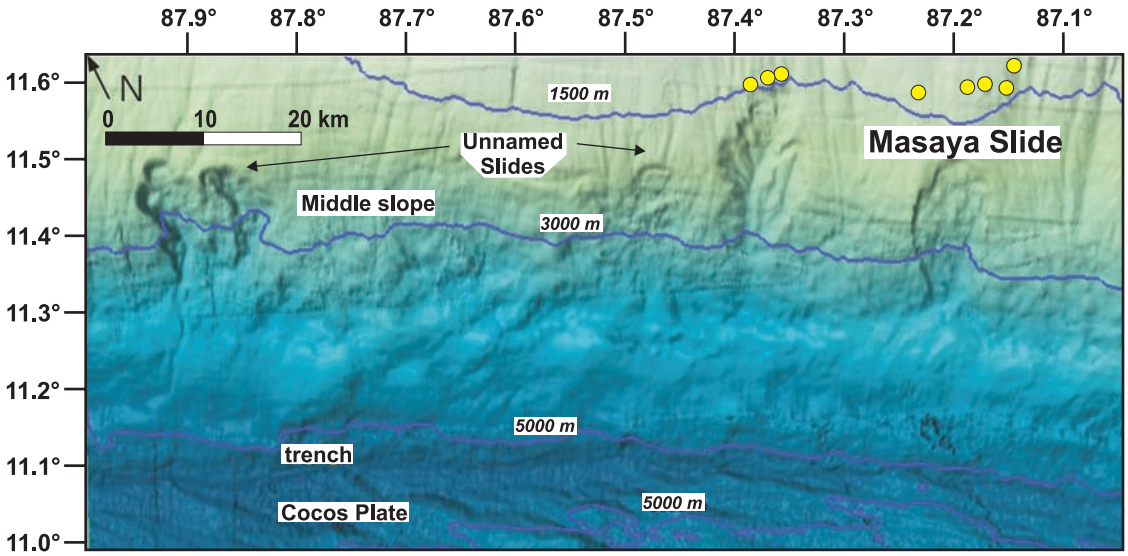

Figure 3. Bathymetric map of the middle slope offshore central Nicaragua (see Figure 1c) showing slide scarps that have dimensions from several kilometers up to tens of kilometers, and headwalls up to 100 m high. Yellow circles show fluid vents above the Masaya Slide.

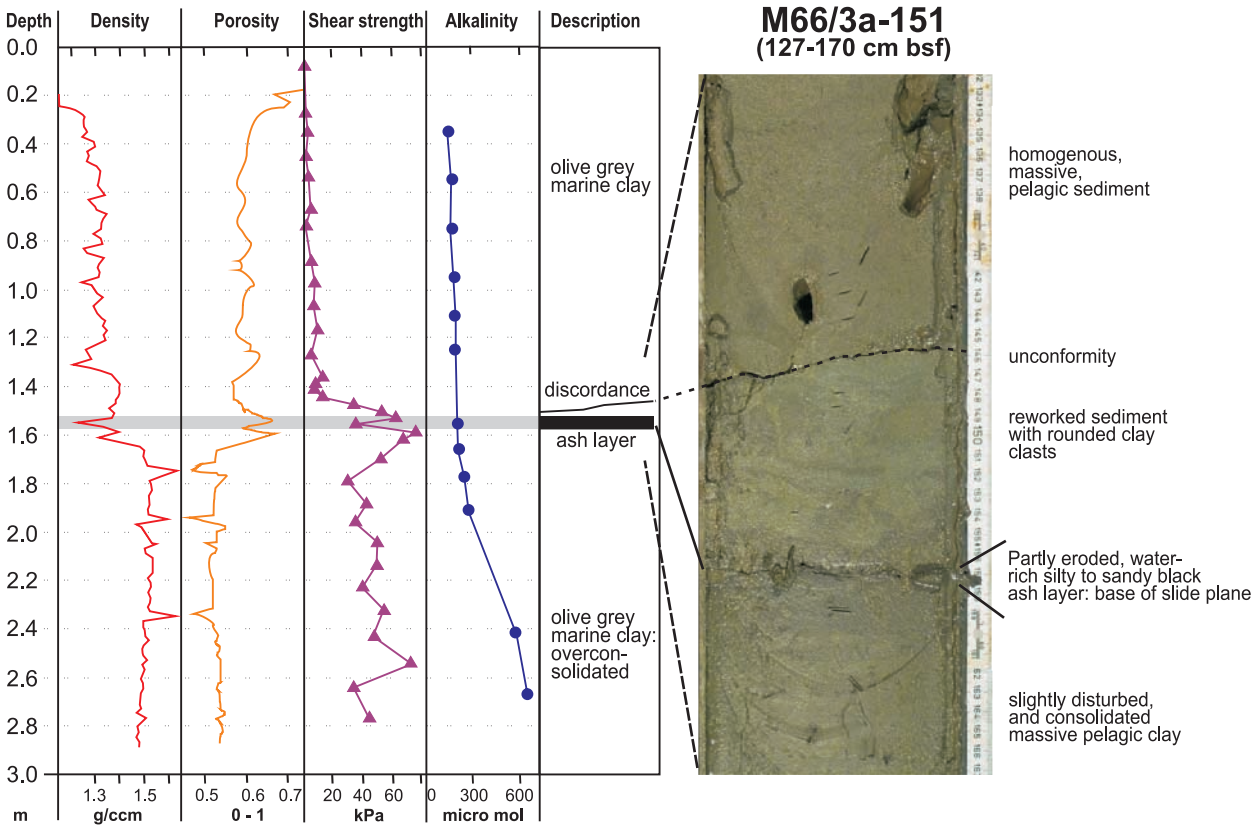

Figure 4. Physical and geochemical logging parameters of core M66/151 drilled through the detachment plane of the Hermosa slide (Figure 1c). The core section photograph shows the slide plane covered by a mafic ash layer of low shear strength that is overlain by 10 cm of clay mélange which is capped by the upper detachment unconformity.

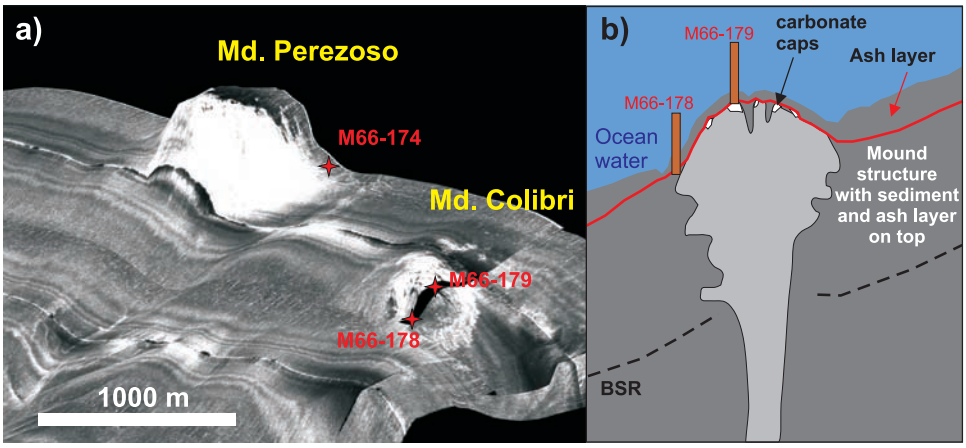

Figure 5. (a) Side-scan sonar backscatter image of Mounds Colibri and Perezoso with gravity core positions (red diamonds and labels); 3 times vertical exaggeration. The dimensions (height/length/width) of the structures are 130/940/780 m for Perezoso and 30/620/588 m for Colibri. (b) Schematic cross section of a mound structure overlain by an ash layer (modified after *Moerz et al.* [2005a]) showing the core positions M66-178 on the lower flank and M66/179 on the top. BSR is Bottom Simulating Reflector, marking the base of the gas hydrate layer interrupted by mud diapirism.

porosity and low density in the core logging data (Figure 4). The massive clay below the ash layer is slightly deformed near the top. Low porosity, high density and high pore water alkalinity show that this lower clay package is significantly more compacted and older than the clay package above the unconformity. Measured shear strength decreases steeply from high values in the underlying clay to low values in the clay overlying the unconformity (Figure 4). The steep gradients in physical properties and residence time (alkalinity) and the deformation structures strongly suggest that a significant sediment package has been removed from this level by sliding prior to renewed pelagic sedimentation above the unconformity. The shear zone of detachment reaches from the unconformity to the ash layer but minor shear also affected the top of the underlying clay. Within the steep shear strength gradient across this zone, the ash layer marks an excursion to about half the strength value. Moreover, the high porosity of the well-sorted ash and its being sealed by impermeable clay at top and bottom suggests that high pore pressure would have been generated in the ash layer during compaction, further reducing its strength. Ash layers thus are predestined to form structurally weak horizons on which sediment packages begin to slide when triggered by processes such as steepening of the slope.

[21] The mafic ash layer in the detachment zone of the Hermosa slide correlates with the ~6 ka old San Antonio Tephra erupted from Masaya Caldera [*Kutterolf et al.*, 2007a; *Pérez and Freundt*, 2006]. The slide detachment thus occurred less than 6 ka ago. Core M66/3-162 penetrated the detachment plane of the Telica slide, which is overlain by the distal ash of the ~60 ka Fontana Tephra at 57–59 cm bsf such that the landslide occurred more than 60 ka ago. The Masaya slide, the largest known landslide offshore Nicaragua, occurred ~19 ka ago because its detachment plane is immediately overlain by distal ashes of the ~17 ka Lower Apoyeque and ~19 ka Upper Ometepe tephras in cores M66/3-132 and 220. These examples illustrate how useful marine ash layers are to constrain ages of submarine landslides provided they can be correlated to tephras of known age or otherwise dated.

4.5. Dating Mud-Mound Activity by Ash Layers

[22] Mud-mound formation processes are discussed in detail by [*Moerz et al.*, 2005a, 2005b]. Mud mounds evolve unsteadily and their surrounding sediments provide a record of alternating active and inactive phases. We use Mound Colibri offshore central Nicaragua (Figure 1) as an illustrative example. The side-scan sonar backscatter image (Figure 5a) shows Mound Colibri and adjacent Mound Perezosa rising above the seafloor and capped by highly reflective carbonate. These structures have dimensions typical of mounds offshore Nicaragua which range from several tens of meters to hundreds of meters height and from 0.2 to

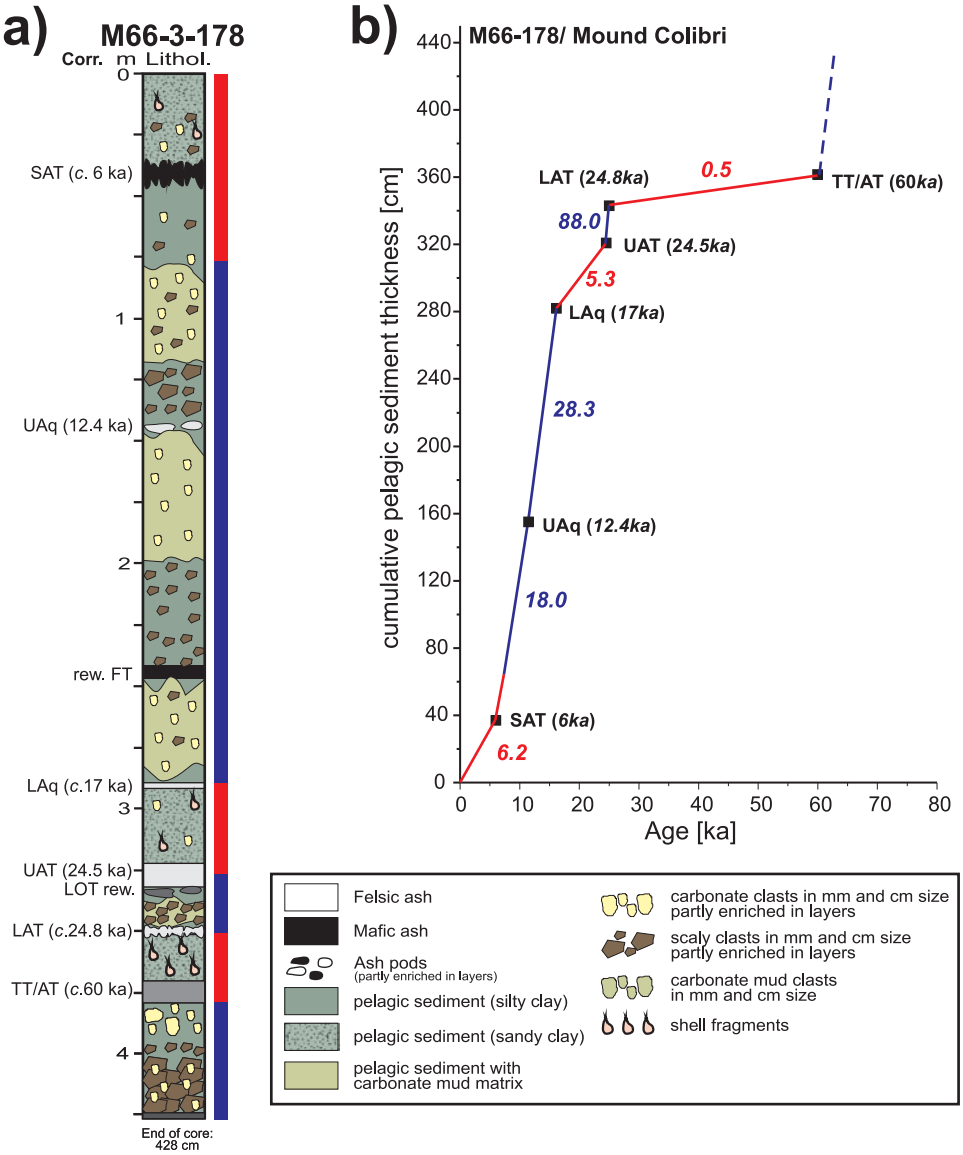

Figure 6. (a) Lithologic section of core M66-178 with correlated ash layers. SAT, 6 ka San Antonio Tephra; UAq, 12.4 ka Upper Apoyeque Tephra; LAq, ~17 ka Lower Apoyeque Tephra; UAT, 24.5 ka Upper Upoyo Tephra; LAT, 24.8 ka Lower Apoyo Tephra; TT/AT, ~60 ka Twins/A-fall Tephra. Blue bars along section mark intervals of mound sediments; red bars mark pelagic background sediments. (b) Cumulative pelagic sediment thickness versus age. Squares mark correlated ash layers of known age. Line slopes give apparent sedimentation rates (numbers in cm/ka) varying along the core. Blue line segments mark mud-mound activity; red line sections mark phases of relative inactivity.

>1.0 km^2 basal area. Such visible dimensions, however, have no relation to the age of the cold seep structures (D. Bürk, personal communication, 2007). Core M66/3-178, drilled through the flank of Mound Colibri, contains two major types of sediment (Figure 6a): (1) rounded clay and carbonate clasts, ash lenses and shelf-derived fossils dispersed in a matrix of sandy clay and (2) a bimodal population of angular scaly clay and carbonate clasts in a fine-grained matrix of clay or carbonate mud. The inventory of sediment (2) is the typical material ejected by mound structures during phases of strong venting activity [*Moerz et al.*, 2005b]. The heterolithologic sediment (1) typical of the background sedimentation on the middle slope receiving input from the shelf is emplaced while the adjacent mound was relatively inactive. The sediments in core M66/3-178

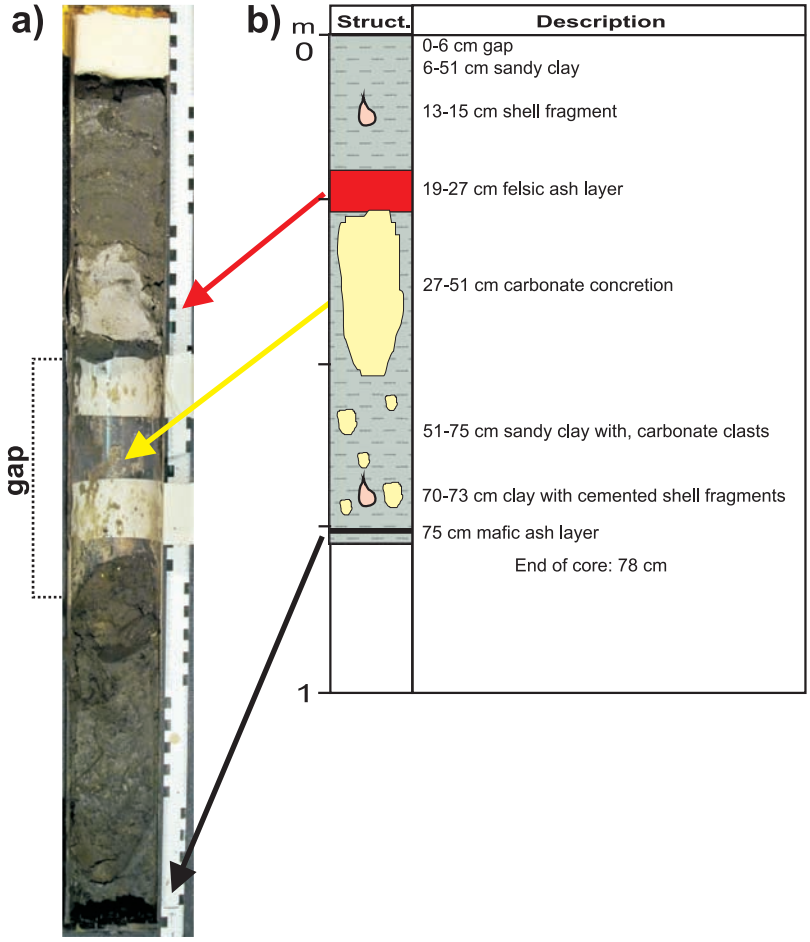

Figure 7. (a) Core M66-179 section 0–100 cm bsf obtained by vibrocorer shows a white marine ash layer (24.5 ka UAT) atop a carbonate concretion at the top of Mound Colibri. The carbonate section of 30 cm thickness was removed to facilitate opening of the core. (b) Description of the core section shown in Figure 7a.

are intercalated with ash layers that we correlate with dated tephras on land. These time constraints show that apparent sedimentation rates are strongly elevated above background levels at intervals composed of type-2 mound sediments (Figure 6b). The ash layers show that Mound Colibri had at least three phases of high venting activity at >60 ka, a short phase at 24.5–24.8 ka, and an extended phase from 17 to ~8 ka.

[23] Core M66/3-179 drilled on the top of Mound Colibri contains distal ash of the 25 ka Upper Apoyo Tephra above the carbonate cap and overlain by pelagic sediment type-1 (Figure 7). This would suggest mound activity terminated >25 ka ago in contrast to the above results from core M66/3-178 from the mound flank. This discrepancy may be due to erosion at the mound top or to lateral shifting of vents across the mound; in any case, this example suggests that flank cores are more useful to decipher an extended history of mound activity. These preliminary results, which for the first time provide absolute ages for active mud mound phases, demonstrate the power of marine tephrostratigraphy in understanding the periodic dynamic evolution of mud mounds.

5. Conclusions

[24] Apart from helping to reconstruct the history of arc volcanism, offshore tephrostratigraphy also delivers important data for understanding geological processes operating at the continental slope and on the incoming plate. Apparent pelagic sedimentation rates derived from dated ash layers identify periods of erosion and enhanced accumulation both at the continental slope, where they seem to be related to climatic and possibly tectonic conditions on land, and on the incoming plate,

where they are related to bend faulting of the plate across the outer rise.

[25] Dated ash layers also constrain the times at which submarine landslides detached from the continental slope; such slides often used ash beds as low-strength shear planes. Moreover, using correlated ash layers, we were able for the first time to determine the age and duration of repeated phases of high venting activity alternating with periods of low or no activity of mud mounds.

Acknowledgments

[26] We especially thank all members of the scientific parties of R/V *METEOR* cruises M66/3 and M54/2 and R/V *SONNE* cruise SO173/3 for the good and successful working atmosphere. Eric Steen and Mark Schmidt did the coring. We also thank Oliver Bardtoff, Cosima Burkert, Kristina Bernoth, Emelina Cordero, Joana Deppe, Yann Lahaye, Julia Mahlke, Dagmar Rau, and Mario Thöner, who assisted sampling on board, sample preparation, and analytical work. W.P. acknowledges a Ph.D. stipend by the Deutscher Akademischer Austauschdienst (DAAD). We also appreciate the helpful comments and suggestions of Vincent Salters, Stephen Blake, Mike Carr, Phil Shane, and Tom Vogel, who reviewed an earlier version of this paper. This publication is contribution 106 of the Sonderforschungsbereich 574 "Volatiles and Fluids in Subduction Zones" at Kiel University. R/V *METEOR* and R/V *SONNE* cruises were funded by the Deutsche Forschungsgemeinschaft (DFG).

References

Bowles, F. A., R. N. Jack, and I. S. E. Carmichael (1973), Investigation of deep-sea volcanic ash layers from equatorial Pacific cores, *Geol. Soc. Am. Bull.*, *84*, 2371–2388.

Carr, M., M. D. Feigenson, L. C. Patino, and J. A. Walker (2003), Volcanism and geochemistry in Central America: Progress and problems, in *Inside the Subduction Factory*, *Geophys. Monogr. Ser.*, vol. 138, edited by J. Eiler, pp. 153–174, AGU, Washington, D. C.

Carr, M. J. (1984), Symmetrical and segmented variation of physical and geochemical characteristics of the Central American Volcanic Front, *J. Volcanol. Geotherm. Res.*, *20*, 231–252.

Carr, M. J., L. C. Patino, and M. D. Feigenson (2007), Petrology and geochemistry of lavas, in *Central America—Geology, Resources and Hazards*, vol. 2, edited by J. Buntschuh and G. E. Alvarado, pp. 565–590, A. A. Balkema, Rotterdam, Netherlands.

Clift, P. D., L.-H. Chan, J. Blusztajn, G. D. Layne, M. Kastner, and R. K. Kelly (2005), Pulsed subduction accretion and tectonic erosion reconstructed since 2.5 Ma from the tephra record offshore Costa Rica, *Geochem. Geophys. Geosyst.*, *6*, Q09016, doi:10.1029/2005GC000963.

Feigenson, M. D., and M. J. Carr (1986), Positively correlated Nd and Sr isotope ratios of lavas from the Central American volcanic front, *Geology*, *14*, 79–82.

Feigenson, M. D., M. J. Carr, S. V. Maharaj, S. Juliano, and L. L. Bolge (2004), Lead isotope composition of Central American volcanoes: Influence of the Galapagos plume, *Geochem. Geophys. Geosyst.*, *5*, Q06001, doi:10.1029/2003GC000621.

Grevemeyer, I., A. Kopf, N. Fekete, N. Kaul, M. Heesemann, H.-H. Gennerich, M. Müller, V. Spiess, K. Wallmann, and W. Weinrebe (2004), Fluid flow trough active mud dome Mound Culebra offshore Nicoya Peninsula, Costa Rica: Evidence from heat flow surveying, *Mar. Geol.*, *207*(1–4), 145–157.

Grevemeyer, I., N. Kaul, J. L. Diaz-Naveas, H. W. Villinger, C. R. Ranero, and C. Reichert (2005), Heat flow and bending-related faulting at subduction trenches: Case studies offshore of Nicaragua and central Chile, *Earth Planet. Sci. Lett.*, *236*, 238–248.

Hampton, M. E., H. J. Lee, and J. Locat (1996), Submarine landslides, *Rev. Geophys.*, *34*, 33–59.

Harders, R., W. Brückmann, V. Feeser, C. Hensen, and S. Kutterolf (2006), Ash layers: The controlling factor on translational sliding offshore Central America?, *Eos Trans. AGU*, *87*(52), Fall Meet. Suppl., Abstract OS43C-0666.

Hensen, C., K. Wallmann, M. Schmidt, C. R. Ranero, and E. Suess (2004), Fluid expulsion related to mud extrusion off Costa Rica continental margin—A window to the subducting slab, *Geology*, *32*, 201–204.

Hoernle, K., P. van den Bogaard, R. Werner, B. Lissinna, G. E. Alvarado, and D. C.-Garbe-Schönberg (2002), Missing history (16–71 Ma) of the Galapagos hotspot: Implications for the tectonic and biological evolution of the Americas, *Geology*, *30*(9), 795–798.

Kutterolf, S., A. Freundt, W. Peréz, H. Wehrmann, and H.-U. Schmincke (2007a), Late Pleistocene to Holocene temporal succession and magnitudes of highly-explosive volcanic eruptions in west-central Nicaragua, *J. Volcanol. Geotherm. Res.*, *163*, 55–82.

Kutterolf, S., U. Schacht, H. Wehrmann, A. Freundt, and T. Mörz (2007b), Onshore to offshore tephrostratigraphy and marine ash layer diagenesis in Central America, in *Central America—Geology, Resources and Hazards*, vol. 2, edited by J. Buntschuh and G. E. Alvarado, pp. 395–423, A. A. Balkema, Lisse, Netherlands.

Kutterolf, S., A. Freundt, W. Peréz, T. Mörz, U. Schacht, H. Wehrmann, and H.-U. Schmincke (2008a), Pacific offshore record of plinian arc volcanism in Central America: 1. Along-arc correlations, *Geochem. Geophys. Geosyst.*, doi:10.1029/2007GC001631, in press.

Kutterolf, S., A. Freundt, and W. Peréz (2008b), Pacific offshore record of plinian arc volcanism in Central America: 2. Tephra volumes and erupted masses, *Geochem. Geophys. Geosyst.*, doi:10.1029/2007GC001791, in press.

Mann, P., R. D. Rogers, and L. Gahagan (2007), Overview of plate tectonic history and its unresolved tectonic problems, in *Central America—Geology, Resources and Hazards*, vol. 2, edited by J. Buntschuh and G. E. Alvarado, pp. 201–238, A. A. Balkema, Lisse, Netherlands.

Mau, S., H. Sahling, G. Rehder, E. Suess, P. Linke, and E. Soeding (2006), Estimates of methane output from mud extrusions at the erosive convergent margin off Costa Rica, *Mar. Geol.*, *225*, 129–144.

Mau, S., G. Rehder, I. G. Arroyo, J. Gossler, and E. Suess (2007), Indications of a link between seismotectonics and CH4 release from seeps off Costa Rica, *Geochem. Geophys. Geosyst.*, *8*, Q04003, doi:10.1029/2006GC001326.

Moerz, T., et al. (2005a), Styles and productivity of diapirism along the Middle America margin, Part II: Mound Culebra and Mounds 11, and 12, in *Mud Volcanoes, Geodynamics and Seismicity*, *NATO Sci. Ser., Ser. IV*, vol. 51, edited by G. Martinelli and B. Panahi, Springer, Dordrecht, Germany.

Moerz, T., A. Kopf, W. Brueckmann, H. Sahling, N. Fekete, V. Hühnerbach, D. Masson, D. A. Hepp, and E. Suess (2005b), Styles and productivity of diapirism along the Middle America margin, Part I: Margin evolution, segmentation, dewatering and mud diapirism, in *Mud Volcanoes, Geodynamics and Seismicity*, *NATO Sci. Ser., Ser. IV*, vol. 51, edited by G. Martinelli and B. Panahi, pp. 35–48, Springer, Dordrecht, Germany.

Patino, L. C., M. Carr, and M. D. Feigenson (1997), Cross-arc geochemical variations in volcanic fields in Honduras C. A.: Progressive changes in source with distance from the volcanic front, *Contrib. Mineral. Petrol.*, *129*, 341–351.

Patino, L. C., M. Carr, and M. D. Feigenson (2000), Local and regional variations in Central American arc lavas controlled by variations in subducted sediment input, *Contrib. Mineral. Petrol.*, *138*, 256–283.

Pérez, W. and A. Freundt (2006), The youngest highly explosive basaltic eruptions from Masaya Caldera (Nicaragua): Stratigraphy and hazard assessment, in *Volcanic Hazards in Central America*, edited by W. I. Rose et al., *Spec. Pap. Geol. Soc. Am.*, *412*, 189–207.

Ranero, C., and R. von Huene (2000), Subduction erosion along the Middle of America convergent margin, *Nature*, *404*, 748–752.

Ranero, C. R., J. Phipps Morgan, K. McIntosh, and C. Reichert (2003), Bending-related faulting and mantle serpentinization at the Middle America trench, *Nature*, *425*, 367–373.

Ranero, C. R., A. Villaseñor, J. Phipps Morgan, and W. Weinrebe (2005), Relationship between bend-faulting at trenches and intermediate-depth seismicity, *Geochem. Geophys. Geosyst.*, *6*, Q12002, doi:10.1029/2005GC000997.

Ranero, C. R., I. Grevemeyer, H. Sahling, U. Barckhausen, C. Hensen, K. Wallmann, W. Weinrebe, P. Vannucchi, R. von Huene, and K. McIntosh (2008), Hydrogeological system of erosional convergent margins and its influence on tectonics and interplate seismogenesis, *Geochem. Geophys. Geosyst.*, doi:10.1029/2007GC001679, in press.

Reston, T. and J. Bialas (2002), RV SONNE, Cruise Report SO162, INGGAS-Test, Chile and Peru, *GEOMAR Rep. 103*, 114 pp., IFM-GEOMAR, Kiel, Germany.

Rüpke, L. H., J. P. Morgan, M. Hort, and J. A. D. Connolly (2002), Are the regional variations in Central American arc lavas due to differing basaltic versus peridotitic slab sources of fluids?, *Geology*, *30*, 1035–1038.

Syracuse, E. M., and G. A. Abers (2006), Global compilation of variations in slab depth beneath arc volcanoes and implications, *Geochem. Geophys. Geosyst.*, *7*, Q05017, doi:10.1029/2005GC001045.

Talukder, A. R., J. Bialas, D. Klaeschen, D. Buerk, W. Brueckmann, T. Reston, and M. Breitzke (2007), High-resolution, deep tow, multichannel seismic and sidescan sonar survey of the submarine mounds and associated BSR off Nicaragua Pacific margin, *Mar. Geol.*, *241*(1–4), 33–43.

Tappin, D. R., P. Watts, G. M. McMurtry, Y. Lafoy, and T. Matsumoto (2001), The Sissano, Papua New Guinea tsunami of July 1998: Offshore evidence on the source mechanism, *Mar. Geol.*, *175*, 1–23.

Vannucchi, P., S. Galeotti, P. Clift, C. Ranero, and R. von Huene (2004), Longterm subduction erosion along the Guatemalan margin of the Middle America Trench, *Geology*, *32*, 617–620.

von Huene, R., C. R. Ranero, and W. Weinrebe (2000), Quaternary convergent margin tectonics of Costa Rica, segmentation of the Cocos plate, and Central American volcanism, *Tectonics*, *19*, 314–334.

von Huene, R., C. Ranero, and P. Vannucchi (2004a), Generic model of subduction erosion, *Geology*, *32*(10), 913–916.

von Huene, R., C. R. Ranero, and P. Watts (2004b), Tsunamigenic slope failure along the Middle America Trench in two tectonic settings, *Mar. Geol.*, *203*, 303–317.

Danksagung

Für die Vergabe der Arbeit möchte ich mich bei Dr. Warner Brückmann bedanken, der durch seine stets positive und motivierende Einstellung für diese Arbeit in ihrem Werden alle Türen offen hielt und mir so besonders im geotechnischen Bereich einen großen Freiraum ließ.

Ich bedanke mich sehr bei Dr. Wilhelm Weinrebe für die Gewinnung der bathymetrischen,- und seitensichtsonar- Daten, sowie für die aufwendige Aufbereitungsarbeit und die Bereitstellung.

Bedanken möchte ich mich auch herzlich bei Dr. Steffen Kutterolf für seine immer große Hilfsbereitschaft und Offenheit. Ob es um das Lösen von Computerproblemen ging oder um Formalitäten, um Spekulationen über das mechanische Verhalten von Tephra, Versuchsaufbauten oder allgemeine Fragen, hier fand stets ein reger und kreativer Austausch statt.

Für die entscheidende Hilfe bei der Planung und Durchführung der Kernentnahme und Beprobung während der Ausfahrt Meteor 66/3 möchte ich mich bei Dr. Steffen Kutterolf und Dr. Christian Hensen bedanken, ohne deren Ratschläge eine erfolgreiche Beprobung der sehr großen Strukturen nicht möglich gewesen wäre.

Mein Dank gilt auch Dr. Tobias Mörz, von dessen Ideenreichtum und Vorstellungskraft diese Arbeit insbesondere im geotechnischen Bereich sehr profitiert hat.

Ausserdem bedanke ich mich bei der gesamten Besatzung der Ausfahrt Meteor 66/ 3 für ihren unermüdlichen Einsatz beim Schwerelotkernen und der Bergung der Proben. Für die Hilfe bei der Kernbeschreibung und den sedimentologischen Arbeiten an Bord bedanke ich mich bei Dr. Mark Schmidt, Dr. Steffen Kutterolf und den studentischen Hilfskräften Julia Mahlke, Florian Leis und Joana Deppe.

Für das unermüdliche Produzieren von unersetzlichen Seekarten mit GMT und das bei stets guter Laune bedanke ich mich ganz herzlich bei Tanja Fromm.

Erik Steen gilt mein Dank für die Durchführung und Überwachung der Schwerelotkernung sowie für seine Informationen über die Funktion und Eigenschaften der Anlage.

Ich bedanke mich bei Prof. Volker Feeser für die Bereitstellung der geotechnischen

Geräte, sowie für seine Ratschläge bei den Messungen.

Für die Einweisung in das Labor und technische Hilfe bedanke ich mich bei den Mitarbeitern der Arbeitsgruppe Ingenieurgeologie.

An dieser Stelle bedanke ich mich natürlich auch bei meinen lieben Eltern für ihre finanzielle Unterstützung während des Studiums, ihr Interesse an meiner Arbeit und ihr immer grosses Vertrauen in mich und meine Vorhaben. Ich danke Ihnen auch für ihre ganz direkte Hilfe mit meinen Kindern und ihr Verständnis für die besonders zeitintensive Arbeit am Schreibtisch, insbesondere im letzten Jahr. Gleiches gilt meinen lieben Geschwistern Venna und Immo und meinen geduldigen Freunden!

Letztlich möchte ich mich ganz besonders und vor allem bei meinem lieben Mann César für seine Geduld und Hilfe bedanken. Ohne seinen Beistand im familiären -, wie auch im fachlichen Bereich wäre die Fertigstellung dieser Arbeit nebst Kinderbrei und langen Nächten entweder viel später oder gar nicht möglich gewesen.

Für die Betreuung dieser Arbeit in ihrer letzten Phase möchte ich mich bei Prof. Dr. Jan Hinrich Behrmann bedanken.

Curriculum Vitae:

Name:	Rieka Karoline Harders
Date of birth:	21.12.1976
Place of birh:	Eckernförde/ Schleswig-Holstein
Citizenship:	German

Education:

05/ 1997	Abitur at "Wirtschaftsgymnasium am Ravensberg Kiel"
09-12/ 1997	Stay abroad for English studies in London/ England
09/ 1997	Matriculation at "Christian-Albrechts-Universität zu Kiel" (CAU) for undergraduate studies of Geology and Palaeontology
08-11/ 1998	Student research assistant at the institut of Geology and Palaeontology of the CAU
01-03/ 2001	Student research assistant at GEOMAR (Fb2)
07/ 2001	Intermediate Examination
02-08/ 2002	Job training to become a Scientific Diver and succesfull final examination
09-12/ 2002	Practical course and stay abroad in the USA, Massachusetts at Woods Hole Oceanographic Institution as student research assistant at the Departement of Marine Chemistry & Geochemistry
09/ 2003-2004	Diploma thesis and geological mapping; Title: Quartärgeologische Großkartierung in der Lübecker Bucht mittels hydroakustischen Methoden und Sondierungen bei Pelzerhaken
09/ 2004- 04/ 2005	Studies of Journalism: Geomedien 1a
03/ 2005	Final examination in Geology with majors in marine Geology and Applied Hydrogeology
04-07/ 2005	Studies of Geo-Journalism: Geomedien 1b, Geomedien 2a, 2b at University of Kiel
06-08/ 2005	First Author publication: Harders, R.; Dehde, B.; Diesing, M.; Gelhart, M.; Schwarzer, K. (2005): Postglacial development of the Neustadt Bay, Meyniana, v. 57. Kiel"
09/ 2005- 07/ 2007	PhD student at SFB 574
07/ 2007-06/ 2008	Maternity leave and parental leave, birth of first child in August 2007

02/ 2008	Co-Author in: Kutterolf, S., Freundt, A., Schacht, U., Bürk, D., Harders, R., Mörz, T., Peréz, W., Pacific offshore record of plinian arc volcanism in Central America: 3. Application to forearc geology, published in G^3 Q02S03, doi:10.1029/2007GC001826
07/ 2008-02/2009	PhD student at IFM-GEOMAR
03/ 2009-04/ 2009	PhD student at Univerity of Kiel
05/ 2009-08/ 2009	PhD student at IFM-GEOMAR
09/ 2009-08/ 2011	PhD student at University of Kiel, birth of second child in November 2011
05/ 2010	First-author-publication in G^3, Title: Tephra layers: A controlling factor on submarine translational sliding?, see Chapter 5 of this thesis
06/ 2011	First-author-publication in G^3, Title: Submarine slope failures along the convergent continental margin of the Middle America Trench, see Chapter 3, of this thesis